Coupling kinetic models and advection-diffusion equations to model vascular transport in plants, applied to sucrose accumulation in sugarcane

Lafras Uys
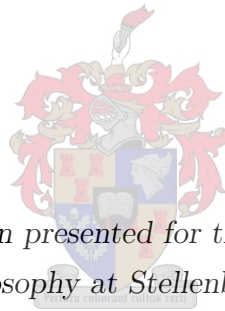
Dissertation presented for the degree of
Doctor of Philosophy at Stellenbosch University

Promotor:

Prof J.M. Rohwer

Co-promotor:

Prof J.-H.S. Hofmeyr

December 2009

By submitting this dissertation electronically, I declare that the entirety of the work contained therein is my own, original work, that I am the owner of the copyright thereof (unless to the extent explicitly otherwise stated) and that I have not previously in its entirety or in part submitted it for obtaining any qualification.

Signature: . . . .

Date: . . . .

Summary

The sugarcane stalk, besides being the main structural component of the plant, is also the major storage organ for carbohydrates. Sucrose forms the bulk of stored carbohydrates. Previous studies have modelled the sucrose accumulation pathway in the internodal storage parenchyma of sugarcane using kinetic models cast as systems of ordinary differential equations. Typically, results were analysed with methods such as metabolic control analysis. The present study extends those original models within an advection-diffusion-reaction framework, requiring the use of partial differential equations to model sucrose metabolism coupled to phloem translocation.

Let $\mathbf{N}$ be a stoichiometric matrix, $\mathbf{v}$ a vector of reaction rates, $\mathbf{s}$ a vector of species concentrations and ∇ the gradient operator. Consider a coupled network of chemical reactions where the species may be advected with velocities, $\mathbf{U}$, or diffuse with coefficients, $\mathbf{D}$, or both. We propose the use of the dynamic system,

$$\dot{\mathbf{s}} + \nabla \bullet (\mathbf{Us}) + \nabla \bullet (\mathbf{D}\nabla\mathbf{s}) = \mathbf{Nv},$$

for a kinetic model where species can exist in different compartments and can be transported over long distances in a fluid medium, or involved in chemical reactions, or both. Darcy's law is used to model fluid flow and allows a simplified, phenomenological approach to be applied to translocation in the phloem. Similarly, generic reversible Hill equations are used to model biochemical reaction rates. These are also phenomenological equations, where all the parameters have operationally defined interpretations.

Numerical solutions to this formulation are demonstrated with time-courses of two toy models. The first model uses a simple "linear" pathway definition to study the impact of the system geometry on the solutions. Although this is an elementary model, it is able to demonstrate the up-regulation of photosynthesis in response to a change in sink demand. The second model elaborates on the reaction pathway while keeping the same geometry definition as the first. This pathway is designed to be an abstracted model of sucrose metabolism. Finally, a realistic model of sucrose translocation, metabolism and accumulation is presented, spanning eight internodes and four compartments. Most of the parameters and species concentrations used as initial values were obtained from experimental measurements.

To analyse the models, a method of sensitivity analysis called the Fourier Amplitude Sensitivity Test (FAST) is employed. FAST calculates the contribution of the possible variation in a parameter to the total variation in the output from the model, i.e. the species concentrations and reaction rates.

The model predicted that the most important factors affecting sucrose accumulation are the synthesis and breakdown of sucrose in futile cycles and the rate of cross-membrane transport of sucrose. The models also showed that sucrose moves down a concentration gradient from the leaves to the symplast, where it is transported against a concentration gradient into the vacuole. There was a net gain in carbohydrate accumulation in the realistic model, despite an increase in futile cycling with internode maturity.

The model presented provides a very comprehensive description of sucrose accumulation and is a rigorous, quantitative framework for future modelling and experimental design.

Opsomming

Benewens sy strukturele belang, is die suikerrietstingel ook die primêre bergingsorgaan vir kool-hidrate. Die oorgrote meerderheid van hierdie koolhidrate word as sukrose opgeberg. Studies tot dusver het die metabolisme rondom sukroseberging in die parenchiem van die onderskeie stingellitte as stelsels gewone differensiaalvergelykings gemodelleer. Die resultate is onder-meer met metaboliese kontrole-analise geanaliseer. Hierdie studie brei uit op die oorspronklike modelle, deur gebruik te maak van 'n stromings-diffusie-reaksie-raamwerk. Parsiële differensi-aalvergelykings is geformuleer om die metabolisme van sukrose te koppel aan die vloei in die floëem.

Gestel $\mathbf{N}$ is 'n stoichiometriese matriks, $\mathbf{v}$ 'n vektor van reaksiesnelhede, $\mathbf{s}$ 'n vektor van spesie-konsentrasies en ∇ die differensiaalvektoroperator. Beskou 'n netwerk van gekoppelde reaksies waar die onderskeie spesies stroom met snelhede $\mathbf{U}$, of diffundeer met koëffisiënte $\mathbf{D}$, of onderhewig is aan beide prosesse. Dit word voorgestel dat die dinamiese stelsel,

$$\dot{\mathbf{s}} + \nabla \bullet (\mathbf{U}\mathbf{s}) + \nabla \bullet (\mathbf{D}\nabla\mathbf{s}) = \mathbf{N}\mathbf{v},$$

gebruik kan word vir 'n kinetiese model waar spesies in verskeie kompartemente kan voorkom en vervoer kan word oor lang afstande saam met 'n vloeier, of kan deelneem aan chemiese reaksies, of albei. Darcy se wet word gebruik om die vloeier te modelleer en maak dit moontlik om 'n eenvoudige, fenomenologiese benadering toe te pas op floëem-vervoer. Eweneens word generiese, omkeerbare Hill-vergelykings gebruik om biochemiese reaksiesnelhede te modelleer. Hierdie vergelykings is ook fenomenologies van aard en beskik oor parameters met 'n duidelike fisiese betekenis.

Hierdie omvattende raamwerk is ondermeer gedemonstreer met behulp van numeriese oploss-ings van twee vereenvoudigde modelle as voorbeelde. Die eerste model het bestaan uit 'n lineêre reaksienetwerk en is gebruik om die geometrie van die stelsel te bestudeer. Alhoewel hierdie 'n eenvoudige model is, kon dit die toename in fotosintese as gevolg van 'n verander-ing in metaboliese aanvraag verklaar. Die tweede model het uitgebrei op die reaksieskema van die eerste, terwyl dieselfde stelselgeometrie behou is. Hierdie skema is ontwerp as 'n ab-strakte weergawe van sukrosemetabolisme. Ten slotte is 'n realistiese model van sukrosevervoer,

metabolisme en berging ontwikkel wat agt stingellitte en vier kompartemente omvat. Die meeste parameters en konsentrasies van biochemiese spesies wat as aanvanklike waardes in die model gebruik is, is direk vanaf eksperimentele metings verkry.

Die Fourier Amplitude Sensitiwiteits-Toets (FAST) is gebruik om die modelle te analiseer. FAST maak dit moontlik om die bydrae van parameters tot variasie in modeluitsette soos reaksiesnelhede en die konsentrasies van chemiese spesies te bepaal.

Die model het voorspel dat sintese en afbraak van sukrose in 'n futiele siklus, asook trans-membraan sukrosevervoer, die belangrikste faktore is wat sukrose-berging beïnvloed. Die model het ook getoon dat sukrose saam met 'n konsentrasiegradiënt beweeg vanaf die blare tot by die stingelparenchiem-sitoplasma, van waar dit teen 'n konsentrasiegradiënt na die vogselholte (vakuool) vervoer word. Volgens die realistiese model was daar 'n netto toename in die totale hoeveelheid koolhidrate, ten spyte van 'n toename in die futile siklus van sukrose in die ouer stingellitte.

Die model wat in hierdie proefskrif voorgestel word verskaf 'n uitgebreide, omvattende beskrywing van sukroseberging. Voorts stel dit 'n rigiede kwantitatiewe raamwerk daar vir toekomstige modellering en eksperimentele ontwerp.

Contents

List of Figures

List of Tables

Abbreviations

so   Source

ph   Phloem

ap   Apoplast

sk   Symplast

vc   Vacuole

S   Sucrose

F   Fructose

G   Glucose

H   Protons, Chapter 3

       Hexose phosphates, Chapter 4

T   Triose phosphates

S^P Sucrose-6-phophate

G^U UDP-Glucose

G^{1P} Glucose-1-phophate

G^{6P} Glucose-6-phophate

F^{6P} Frucose-6-phophate

F^P_P Frucose-1,6-*bis*phophate

ASI   Acid-soluble invertase

AWI   Acid-wall invertase

NI   Neutral invertase

SS   Sucrose synthase

SPS   Sucrose phosphate synthetase

SP   Sucrose phosphatase

HKG   Hexokinase (Glucose as substrate)

FRK   Fructokinase

PFP   Phosphofructophosphatase

PFK   Phosphofructokinase

ALD   Aldolase

UGD   UDP-Glucose Dehydrogenase

Notation

a	Cross-sectional area
b	Loading rate
c	Boundary condition
	Stoichiometric coefficient
$\mathrm{cdf}(\,\cdot\,)$	Cumulative density function
C	Control coefficient
$\mathbf{C}$	Control coefficient matrix
D	Diffusion coefficient
$\mathbf{D}$	Diffusion coefficient matrix, not to be confused with a diffusion tensor
$\mathbf{e}$	Vector of enzyme concentrations
$\mathbf{E}$	Matrix of structural properties
$E(\,\cdot\,)$	Expected value
f	Function
g	Function
i	An arbitrary index
$\mathbf{i}$, $\mathbf{j}$, $\mathbf{k}$	Unit vectors
$\mathbf{I}$	Identity matrix
$\mathrm{Im}(\,\cdot\,)$	Imaginary part of a complex number
j	Axial solution flux
J	Steady-state flux
k	Permeability
k_a, k_x	Michaelis-Menten constants
$\mathbf{K}$	Kernel of the stoichiometric matrix (nullspace)
$\mathbf{L}$	Link matrix
K_{eq}	Equilibrium constant
m	Modifier concentration scaled by $M_{0.5}$
M	Modifier amount
$M_{0.5}$	Half-saturation constant for modifier M

$\mathbf{N}$	Stoichiometric matrix
$\mathcal{N}(\,\cdot\,,\,\cdot\,)$	Normal distribution
O	Control volume boundary surface
p	Product concentration scaled by $P_{0.5}$
	Parameter
p_k	k^{th}-parameter
p^*	Parameter search value
$\mathbf{p}$	Parameter vector
$\mathrm{pdf}(\,\cdot\,)$	Probability density function
P	Pressure
	Product amount
P_0	Reference pressure
$P_{0.5}$	Half-saturation constant for product P
q	Equilibrium constant in §4.5
r	Position
R	Gas constant
$\mathbf{R_p^y}$	Response coefficient matrix
$\mathrm{Re}(\,\cdot\,)$	Real part of a complex number
s	Substrate concentration scaled by $S_{0.5}$
S	Species amount
$S_{0.5}$	Half-saturation constant
t	Time
T	Temperature
$\vec{u}$	Intrinsic phase average velocity
$\mathbf{U}$	Diagonal matrix of phase average velocities
v_i	Reaction rate
V_f	Maximal activity
$\mathrm{Var}(\,\cdot\,)$	Variance
w	Passive membrane water flux
x	Variable
$\mathbf{x}$	Vector
$\mathbf{X}$	Matrix
α	K-effect
$\alpha_{\pm k}$	Fourier coefficients
γ	V-effect
Γ	Mass-action ratio

∂_i	Partial derivative with respect to i
ϵ_{s_i}	Concentration elasticity
ϵ_{p_k}	Parameter elasticity
ε	Concentration elasticity matrix
Θ	Control volume
κ	Hydraulic conductivity
Λ	Fourier spectrum
μ	Viscosity
Π	Osmotic potential
ρ	Set of reactions
σ	Set of species
τ	Set of transporters
ϕ	Variable to be solved for in a PDE
Φ	Set-point concentration
ω_p	Frequency assigned to parameter p
Ω	Search function
χ	Set of physiological and subcellular compartments, set of reaction volumes
∇	Gradient operator—defined on page 16
∇^2	Laplace operator

For Theo

Acknowledgements

- The first person on this list can only be my promotor, Prof Johann Rohwer. My infinite thanks for...well, everything. I am a much better scientist for having been your student. Thanks for taking a chance on me all those years ago and for having the faith to let me follow my own, sometimes weird, path(s).

- Prof Jannie Hofmeyr—thank you for helping with the original ADR formulation, also for many interesting discussions in foreign countries, introducing me to good design and absolute perfectionism.

- Prof Prieur du Plessis gave me the idea for using Darcy's law to model fluid flow and, probably does not realise it, but made all this work seem possible.

- Dr Brett Olivier, thanks for much rock solid advice and speculative discussion fuelled by coffee and/or beer.

- To my parents, for giving me an unsatiable love of reading and learning.

- The National Bioinformatics Network (ZA) for funding.

Chapter 1

Mathematical modelling and sugarcane

A model is an arbitrary statement about how the world works. To test the veracity of the model we compare it, or some logical consequence thereof, to the world around us. The natural language in which to express a model is mathematics. When studying large, complex problems it is often the only language in which to do so. Problems in biology definitely qualify as large and complex—biological systems contain many components, many interactions and are often highly parametrised. This has led to the advent of fields such as high-throughput biology and computational systems biology [1].

This dissertation is about modelling and plants, or more specifically, partial differential equations and sugarcane. It is the hope that modelling can point out why sucrose accumulation in sugarcane is such an efficient process. This chapter gives a brief and general introduction to modelling and sugarcane.

1.1   Modelling in general

Mathematical modelling assumes that physical phenomena have mathematical counterparts. Observation (experiment) leads to hypothesis (model), which in turn leads to verification (prediction). The following figure illustrates a number of terms synonymous with modelling:
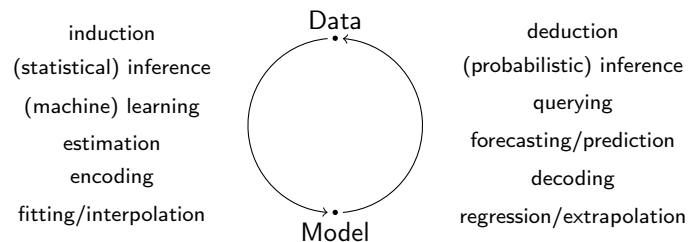
There are various flavours of mathematical modelling. Statistical modelling assumes that data are described by some family of probability distributions or densities. Stochastic modelling is

applied to noisy data. Unlike statistical modelling, the actual physical process is stochastic and noise in the data is not simply due to measurement error. For example, protein expression in a single cell is stochastic. Discrete modelling, such as with Boolean networks, is used to model finite state processes, e.g. signal transduction pathways can be treated as systems of logic gates. Topological, or structural modelling as it is often called in the flux balance analysis literature, is concerned with the connectivities in networks [2]. Deterministic modelling often uses differential equations, such as ordinary/partial differential or differential-algebraic equations. Data are not just statistically correlated, but the underlying mechanism is understood to some degree. Differential equations can be used to model systems of chemical reactions, as in the kinetic modelling of biochemical pathways [3].

1.2 Kinetic modelling

Reactions in a cell are all connected, if not directly then by a chain of intermediate reactants forming a network [2, 4]. Consider the following hypothetical reaction scheme as an example. Terminal reactants are indicated by X, intermediate reactants by S, moiety conserved reactants by M and enzymes by a number in a box.
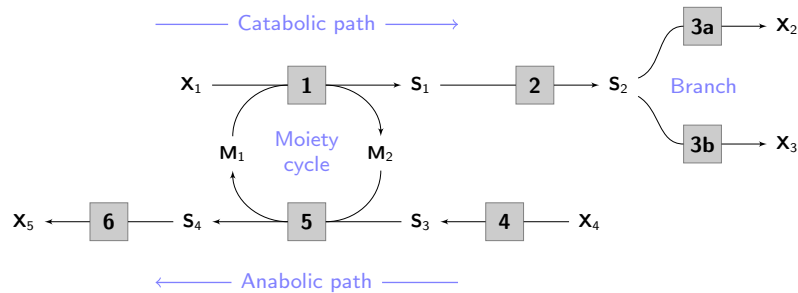
Connections can be expressed as integer amounts, the stoichiometry, and a system of reactions by the stoichiometry matrix, $\mathbf{N}$. For the pathway above the stoichiometry matrix is shown here.

	1	2	3a	3b	4	5	6
M_1	-1	0	0	0	0	1	0
M_2	1	0	0	0	0	-1	0
S_1	1	-1	0	0	0	0	0
S_2	0	1	-1	-1	0	0	0
S_3	0	0	0	0	1	-1	0
S_4	0	0	0	0	0	1	-1

The stoichiometry matrix maps each reactant to a reaction and gives the number of each consumed $(-)$ or produced $(+)$. If $\mathbf{s}$ is a vector of species concentrations (or mole amounts) and $\mathbf{v}$ a vector of rates, then a kinetic model can be written as,

$$\dot{\mathbf{s}} = \mathbf{Nv}. \qquad (1.1)$$

This formulation is a set of time dependent Ordinary Differential Equations (ODEs) governing the movement of mass through a pathway [3–5].

Every reaction has an associated rate equation. This is a function of one or more reactant concentrations and parameters that specify how fast a reaction will proceed. Rate equations try to capture all the kinetic and thermodynamic properties of a reaction. Appropriate terms in the rate equations account for allostery and cooperativity. Cornish-Bowden [6] gives a good introduction to enzyme kinetics. Examples of generic rate equations can be found in §2.4 and §4.4.

If enzyme translation is included in a model, then enzyme concentrations become variables and the necessary differential equations are added to the system of equations. Covalent modification of enzymes, for example phosphorylation, can be accounted for by treating each phosphorylated enzyme species as a variable. Genetic regulation and signal transduction networks could also be accounted for. Hofmeyr & Westerhoff [7] give a framework for modelling multi-level hierarchical networks.

Time course simulations   A possible solution to Equation 1.1 when applied to the example pathway is shown in Figure 1.1. The model uses reversible Michaelis-Menten rate equations with arbitrary parameters and initial conditions. The change in concentration and reaction rates with time (50 steps) is plotted. Note how the trajectories for both the concentrations and rates reach a plateau. In other words, the variables do not change with time anymore and a steady-state has been reached.

Steady-state and Metabolic control analysis   The advantage to modelling is that "What if?" questions can be answered, for example, by changing parameters to values outside the range that were considered in an experiment. A model that replicates an experiment gives a concise, encapsulated description, but otherwise does not tell one much. A model should be able to predict behaviour to be valid. It is for this reason that methods to interrogate models are necessary.

The framework of using ODEs to model systems of reactions, and analysis techniques such as steady-state analysis are well developed [3, 4]. Steady-state analysis considers solutions to
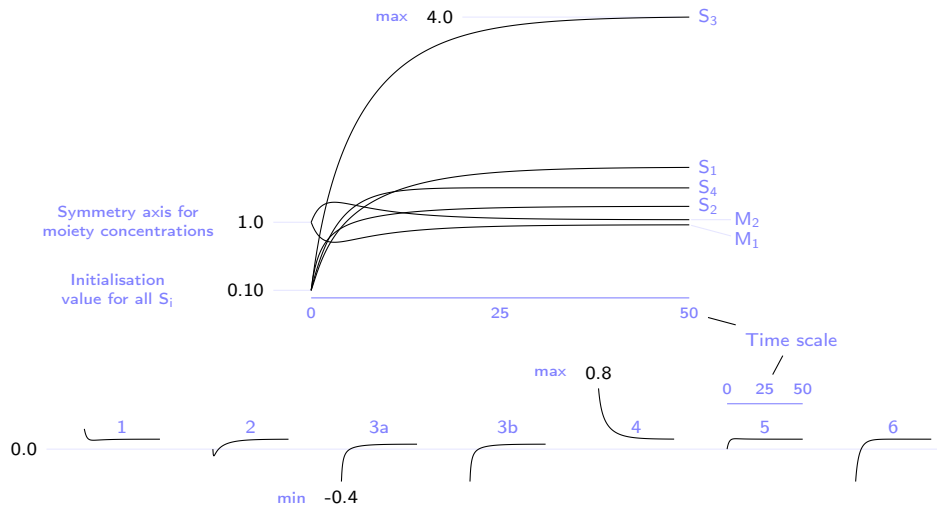
Figure 1.1: An example of a time course simulation. Concentrations are shown on top and reaction rates in the row at the bottom.
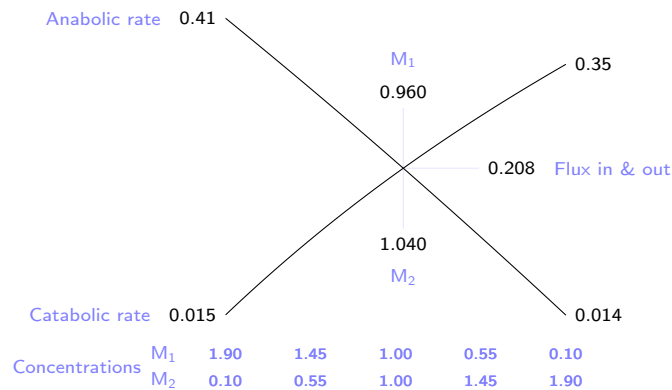
Figure 1.2: A supply-demand analysis of the example pathway. The independent axis shows m_1/m_2 and the dependent axis shows the reaction rates through the anabolic and catabolic pathways. The steady-state for the system is at the point where the catabolic and anabolic rate trajectories cross. Analysing the local neighbourhood around the intersection provides more information about how the system behaves.

the equation,

$$\dot{\mathbf{s}} = \mathbf{N}\mathbf{v} = \mathbf{0}, \tag{1.2}$$

in other words, when the concentrations in a system remain constant with time. Supply-demand analysis is an example of steady-state analysis [8]. Figure 1.2 shows a rate characteristic for the example scheme.

When the steady-state assumption holds, the distribution of control amongst all the reactions in the system can be quantified. This is known as Metabolic Control Analysis (MCA)

[4, 9, 10] and can be neatly summarised in the following equation,

$$\begin{bmatrix} \mathbf{C^{J_i}} \\ \mathbf{C^{s_i}} \end{bmatrix} [\mathbf{K} - \boldsymbol{\varepsilon_s}\mathbf{L}] = \mathbf{I}, \tag{1.3}$$

where $\mathbf{C^{J_i}}$ and $\mathbf{C^{s_i}}$ are control coefficient matrices, $\mathbf{K}$ is the kernel (nullspace of the stoichiometric matrix), $\boldsymbol{\varepsilon_s}$ is the concentration elasticity matrix and $\mathbf{L}$ is the link matrix. Equation 1.3 is known as the control matrix equation [4] and can be abbreviated to $\mathbf{C^i E} = \mathbf{I}$. The definition of an elasticity coefficient is given by [3],

$$\epsilon_{s_i}^{v_j} = \partial \ln v_j / \partial \ln s_i, \tag{1.4}$$

$$\epsilon_{p_k}^{v_j} = \partial \ln v_j / \partial \ln p_k, \tag{1.5}$$

where v_j is a reaction rate, s_i is a species and p_k is a parameter. Note that it is Equation 1.4 that appears in the control matrix equation. The definition of a control coefficient is given by,

$$C_k^{s_i} = \partial \ln s_i / \partial \ln v_k, \tag{1.6}$$

$$C_k^{J_j} = \partial \ln J_j / \partial \ln v_k, \tag{1.7}$$

where J is the flux. The response of a variable can be related to a perturbation in any parameter of the system by calculating the matrix of response coefficients,

$$\mathbf{R_p^y} = \mathbf{C^y}\boldsymbol{\varepsilon_p}, \tag{1.8}$$

where y is either the flux (J) or concentration (s). The response coefficients show that MCA can be thought of as a type of sensitivity analysis. However, MCA, as outlined here, is only appropriate for kinetic models cast as systems of ODEs. It is not appropriate for the non-steady-state, PDE based models that are introduced in Chapter 2. MCA is only mentioned because it is ubiquitous in the kinetic modelling literature and as a contrast to the method of sensitivity analysis used in Chapter 3 and Chapter 4.

Kinetic modelling has been extensively used to study plants. A survey of kinetic modelling applied to plants can be found in [11, 12]. The next section gives a brief overview of sugarcane followed by an introduction to the kinetic modelling of sugarcane.

Table 1.1: Approximate amount of sugarcane harvested (metric tons) in 103 countries across the world for 2007. Data available from the Food and Agriculture Organisation of the United Nations (FAO) statistics website (`faostat.fao.org`).

Country	Amount	Country	Amount	Country	Amount
Brazil	514079729				
India	355520000	Guyana	3250000	Liberia	265000
China	106316000	Fiji	3200000	Gabon	220000
Thailand	64365682	Tanzania	2750000	Lao	220000
Pakistan	54752000	Madagascar	2700000	Niger	220000
Mexico	50680000	Mozambique	2650000	Martinique	215000
Colombia	40000000	Nepal	2599789	Somalia	215000
Australia	36000000	Malawi	2500000	Uruguay	190000
USA	27750600	Zambia	2500000	Burundi	180000
Philippines	25300000	Ethiopia	2470000	Cambodia	170000
Indonesia	25200000	Jamaica	2000000	Ghana	145000
South Africa	20500000	Uganda	2000000	Suriname	120000
Argentina	19200000	Reunion	1880000	St. Kitts & Nevis	105000
Guatemala	18800000	Panama	1800000	Central African Republic	90000
Egypt	16200000	DRC	1550000	Afghanistan	70000
Viet Nam	16000000	Cameroon	1430000	Rwanda	70000
Cuba	11100000	Japan	1275000	Sierra Leone	70000
Venezuela	9300000	Belize	1250000	Spain	60000
Peru	8246406	Cote d'Ivoire	1100000	Iraq	55000
Sudan	7500000	Nigeria	1029000	Benin	38000
Myanmar	7450000	Haiti	1000000	St. Vincent & Grenadines	20000
Ecuador	7300000	Morocco	900000	Cape Verde	15400
Bolivia	6200000	Senegal	836000	Bhutan	13300
Bangladesh	6000000	Guadeloupe	800000	Grenada	7200
Dominican Republic	5700000	Malaysia	800000	Bahamas	5800
Iran	5700000	Sri Lanka	782510	French Guiana	5500
El Salvador	5400000	Congo	550000	Guinea-Bissau	5500
Honduras	5000000	Trinidad and Tobago	475000	Portugal	5100
Swaziland	5000000	Burkina Faso	455000	Dominica	4800
Kenya	4950000	Papua New Guinea	450000	French Polynesia	3000
Nicaragua	4875000	Barbados	410000	Oman	550
Mauritius	4400000	Chad	390000	Djibouti	52
Costa Rica	4300000	Angola	360000	American Samoa	28
Zimbabwe	3600000	Mali	350000	Wallis & Futuna Ils	20
Paraguay	3400000	Guinea	283000	Samoa	12

1.3 Sugarcane

Approximately 1.5 billion tons of sugarcane is harvested annually across the world. Table 1.1 gives a breakdown of the amount harvested for 2007 in most of the sugarcane producing countries.

Sugarcane is part of the family of grasses [13]. Unlike some of the other grass crops, like maize, sorghum and barley, it is the stalk (also called a culm) which acts as the primary assimilate sink [14]. The stalk is divided into alternating nodes and internodes, with a single leaf attached to a node. Sucrose is primarily synthesised in the leaves and loaded into the phloem, where it is transported up or down the stalk and unloaded in the storage parenchyma [15–17].

Sucrose is the most abundant soluble carbohydrate found in sugarcane and is actively
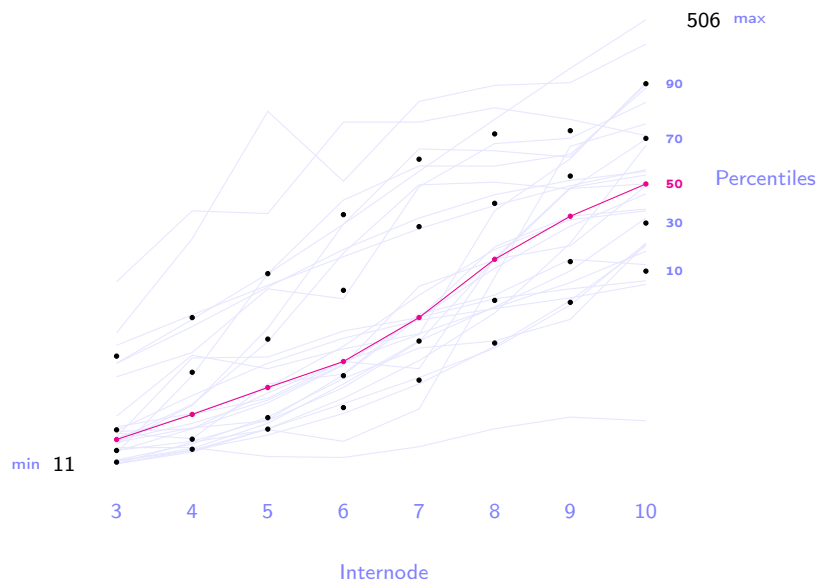
Figure 1.3: Sucrose concentrations (mM), from 27 different plant sources, as measured for internodes 3—10. Data for eight internodes are shown, 216 points in total. Lines connecting a series of points represent a single set of measurements. The red line is the sample median. The data was collected from the literature and collated in Uys [30].

accumulated to levels much higher than in most other plants [13, 18]. Figure 1.3 shows the range of sucrose concentrations found in various sugarcane cultivars.

A number of factors influence the amount and rate of sucrose accumulation. Environmental conditions, such as temperature, sunlight (or rather incident radiation), rainfall and soil types play a role [19, 20]. Agricultural practices such as fertilisation and chemical ripening can speed up accumulation [19, 20]. Biochemical factors, such as genetics [21], futile cycling [22–26] and membrane transporters [27–29] will limit the maximum accumulation possible.

1.4 Kinetic models of sucrose accumulation in sugarcane

Rohwer & Botha [26] used the pathway in Figure 1.4 to model sucrose accumulation in the sugarcane culm storage parenchyma. The model focused on the futile cycling of sucrose. They concluded that a decrease in futile cycling causes an increase in sucrose accumulation. A variation of the model was subsequently used by Schäfer et al. [31] to study the kinetics of sucrose synthase. Bosch [32] added the trehalose branch to the original model and concluded that partitioning to trehalose does not significantly impact sucrose accumulation.

Uys et al. [33] extended the Rohwer and Botha model by explicitly modelling the sucrose synthase and fructokinase isoforms, adding PFK, PFP and UDP-glucose dehydrogenase. The steady-state was calculated for eight different sets of maximal activity data, representing in-
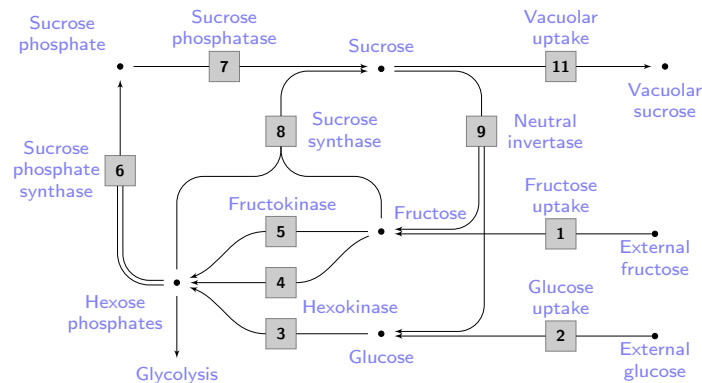
Figure 1.4: The sucrose accumulation pathway used by Rohwer & Botha [26] in their original model.

ternodes 3—10. The analysis is repeated in Appendix B of this dissertation for two sets of maximal activity data. The models so far only focused on the reactions around sucrose in the cytoplasmic space (symplast) to study the effect of sucrose breakdown and synthesis.

The Uys model showed overall, higher sucrose concentrations than the Rohwer and Botha model. However sucrose gradients did not come close to measured concentrations. This was because the vacuole, apoplast and phloem were not explicitly included in the model. The inclusion of the phloem changes the entire modelling approach because now geometry and sap flow becomes important.

1.5 Phloem

The phloem is a whole complex of cells. The sieve elements are arrayed end-to-end, separated from each other by a sieve plate, forming the sieve tube. The sieve tube in turn is surrounded by companion cells, one or more to each sieve element [35, 36]. Thompson [34] described phloem with three analogies. These are illustrated graphically in Figure 1.5.

> "A sieve tube is like dialysis tubing"

There is constant movement of solutes and water between the phloem and the surrounding tissue. Turgor pressure is regulated through changes in solute concentrations. If phloem loading and unloading were only to occur at the extremities of a phloem tube, pressure gradients would be difficult to control. The series of plots at the top of Figure 1.5 shows what happens if loading occurs across the first half of a tube and unloading in the second half. It is compared to loading and unloading at the ends only. If loading only occurs at the ends, rapid, local changes in pressure gradients become difficult to induce.
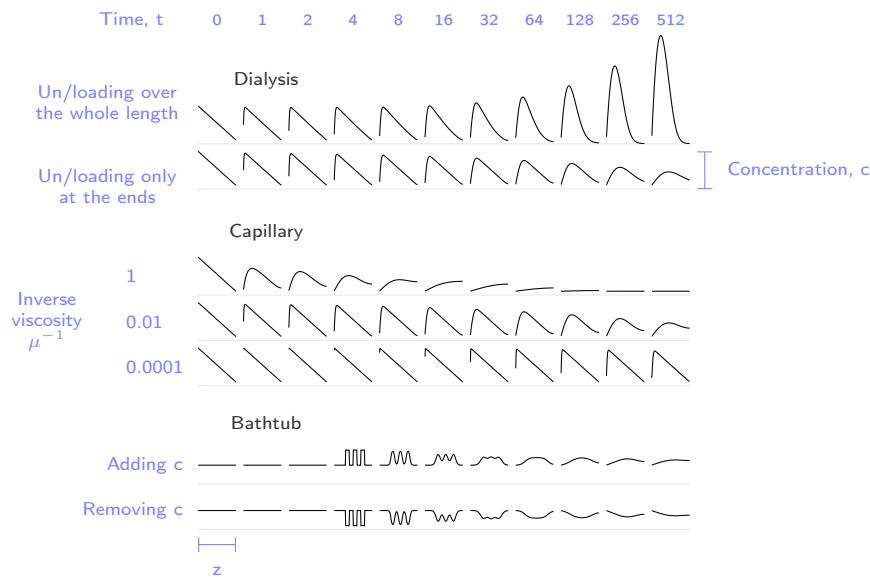
Figure 1.5: Three analogies that explain the factors affecting phloem flow [34]. Each small plot shows a concentration (c) gradient over a distance (z) at a particular time (t) point. A row of plots is a set of samples from a logarithmic time series. The details are discussed in the text. The plots were generated by solving the equation, $\partial_t c = a \cdot \partial_z^2 c + b(z)$, where a and b were manipulated to obtain the desired effect. The equation will be discussed in much more detail in Chapter 2 and its exact meaning should not be of concern here.

> *"A sieve tube is like a capillary"*

Phloem flow is dominated by shear forces rather than inertial forces. In other words, viscosity trumps momentum. As a consequence, pressure gradients develop as a result of energy dissipation. The centre plots in Figure 1.5 shows what happens to the flow of solute if viscosity increases (i.e. viscous forces begin dominating) and all other factors are kept constant. As the viscosity increases, the flow rate of solute decreases. It is important to note that a pressure-concentration wave can propagate faster than the actual velocity of the phloem sap [34, 37].

> *"A sieve tube is like a full bathtub"*

A change in the solute concentration at a local point along the phloem translates into a flux of solute, towards or away, from the surrounding sap. This ripple effect propagates along the phloem tube and becomes more diffuse as it moves further away from the source of the perturbation. The absolute magnitude of the flux is proportional to the solute concentration and also the gradient of the solute concentration. This is illustrated by the last two sets of plots in Figure 1.5.

Bieleski [38] points out four features of sugarcane that separates it from other plants.

1. The plant can be seen as a row of sinks all connected by the phloem.

2. Sinks with widely differing sugar content all "feed" off the same phloem strands.

3. Phloem unloading occurs along the entire length of the phloem tube. This is in contrast to other plants where the phloem has a well defined "terminus".

4. Any point along the phloem can act as a loading or unloading site.

1.6   Modelling phloem transport

The Münch hypothesis [39–41] is the premise for most modelling of fluid flow in xylem and phloem [42–44]. Fluid flow is driven by a pressure gradient generated by an osmotic potential. The effect was confirmed by Gould *et al.* [45]. Appendix A in [46] provides a concise review of phloem modelling based on Münch's hypothesis. The current definitive description of phloem flow is also given by Thompson & Holbrook [46]. They proposed the following two equations to model phloem flow and assimilate (sucrose) transport:

$$\frac{\partial}{\partial t} a = V_s b + w - \frac{\partial}{\partial z} j, \tag{1.9}$$

$$\frac{\partial}{\partial t} c_l = b - \frac{\partial}{\partial z} j_s. \tag{1.10}$$

The variables are defined as follows.

- a is the cross-sectional area of the sieve tube and may possibly vary due to pressure. This is because the sieve tube wall is elastic. After [46], it was subsequently shown in [37, 47] that elasticity may be safely ignored as the effect on phloem flow is negligible.

- V_s is the partial molal volume of sucrose and b is a piece-wise defined function describing the loading or unloading of sucrose. The model assumes loading and unloading at the end of the sieve tubes. This assumption is also made by Henton *et al.* [48] and Höltta *et al.* [44].

- w is the passive membrane water flux and is itself a function of the sieve tube cross section, plasma membrane permeability and pressure.

- j is the axial flux of the solution; it depends on the hydraulic conductivity and pressure gradient of a sieve tube, z is the distance along the length of the sieve tube,

- c_l is the length specific sucrose concentration, the product of the cross-sectional surface area and concentration, i.e. units of $mol \, m^{-1}$, and

- j_s is the axial molar flux rate of sucrose, a function of solute concentration and axial flux.

Equation 1.9 simply states that the volume is conserved. Equation 1.10 accounts for solute conservation. Amongst other findings the model predicted that a pressure front outpaces the solute front, that sieve tube wall elasticity is of little biological significance and that sieve plate resistance dominates phloem flow. In a series of follow-up articles, Thompson & Holbrook [47, 49] used dimensional analysis to study their approach to phloem modelling.

The assumption of equilibrium between phloem sap and apoplast water potential was shown to be plausible [47]. This is important for the modelling presented later, since this allows Equations 1.9 and 1.10 to be simplified [34]. Furthermore, a relatively small pressure drop would allow more accurate control of solute loading. Thompson & Holbrook [49] studied "information transmission" through the phloem. Under certain conditions it is possible for a local change in solute concentration or pressure to propagate through the phloem faster than the actual velocity of the phloem sap. The implication is that message passing along the phloem is possible in a reasonable amount of time.

1.7   Outline of this dissertation

Equation 1.2 assumes a steady-state. There is also a second implicit assumption, that is, that all components (metabolites and enzymes) in the system are well mixed and uniformly distributed. This is a reasonable approximation when all reactions are within the confines of a single cell or similar small volume. However, if reactions are separated in space, such that molecular travelling distance has to be accounted for before a species engages in a reaction, then the assumption of a well-mixed reaction fails. Furthermore, if the travelling time of a molecule is orders of magnitudes longer than the time a reaction takes, then the steady-state assumption has to be reconsidered, or dropped.

Equation 1.3 also needs to be reconsidered. This is because a perturbation in either source or sink will require time to effect a response in the other or the same type of tissue. During this time a perturbation may have its rippling effect fade out or possibly even become amplified.

The source/sink relationship in plants is an example where the well-mixed and steady-state assumptions do not readily apply. For example, Equation 1.1 is ill-suited to capturing delayed sink feedback on source reactions, where the delay is caused by the spatial separation of source and sink.

This dissertation is about addressing the above-mentioned shortcomings by formulating a new modelling approach that couples advection-diffusion processes in the phloem to kinetic models of metabolic processes in other cellular compartments.

Chapter 2 is about formulating an advection-diffusion-reaction (ADR) model, which accounts for phloem flow and reaction kinetic models. The model is cast as a set of partial differential equations. Examples of a "linear" pathway are given together with some variations. Chapter 3 introduces a stripped down toy model of sucrose accumulation in sugarcane. Since MCA cannot be used, a sensitivity analysis using the FAST algorithm is performed. Chapter 4 shows how a "real" model is cast as an ADR system and presents a sensitivity analysis on the maximal activities of the model. A general discussion and conclusion is given in Chapter 5.

Chapter 2

Vascular transport in plants: coupling kinetic models and advection-diffusion equations

2.1 Introduction

Consider a sugarcane stalk. Carbon dioxide is captured by the leaves, where sucrose is made, moved into the phloem and transported to the storage parenchyma [14, 19, 20]. There are many reactions, compartments and physical processes involved. A well established reaction kinetic model of sucrose accumulation in sugarcane exists [26, 33]. Likewise, the modelling of phloem has been thoroughly investigated by Thompson & Holbrook [46] (see also [34, 37, 47, 49]). This chapter lays the groundwork for combining phloem flow and reaction networks into a single model. Amongst other applications, it is expected that the development of concentration gradients along the sugarcane stalk could be better understood. Furthermore, factors that promote, or inhibit, the rapid accumulation of sucrose may be identified.

The processes involved in sucrose accumulation can be collectively referred to as advection-diffusion-reaction (ADR) behaviour. A framework is presented in which this behaviour can be modelled as a set of Partial Differential Equations (PDEs).

Transport phenomena ADR models are examples of a class of problems called *transport phenomena* [50]. The mathematics describing the movement of a measurable quantity turns out to be similar for a large range of phenomena. Central to any transport phenomenon is the principle of conservation. For an arbitrary variable, ϕ, a general conservation equation can be

written as follows:

$$\partial_t \phi + \nabla f (t, r, \phi, \nabla \phi) = g (t, r, \phi), \tag{2.1}$$

where t is time and ∇ is the gradient operator. f and g are functions of time, position (r), ϕ and the gradient of ϕ $(\nabla \phi)$. f and g are respectively called the flux and source. For example, the diffusion of heat or the diffusion of a solute through a liquid would both depend on the divergence of the gradient together with some, possibly constant, coefficient. Mathematically the expressions are identical even though two different physical properties are being modelled. The differences are the actual *values* and *units* of the variables and parameters. These are measured experimentally.

In §2.2 reaction kinetic models are coupled to phloem flow in an ADR framework. The framework is then populated by the necessary equations to model phloem flow and reactions.

Phenomenological equations   Modelling sometimes requires a decision to be made between using equations of state that are mechanistically complete or just behaviourally complete, the latter being a necessary condition for the former. In general, the definitive equation for modelling fluid flow would be the Navier-Stokes equations [50]. There are many difficulties in solving these equations and what is gained in the solution is not necessarily of any practical use. For example, the Navier-Stokes equations can account for turbulent flow, but one would not expect to see turbulence in plant phloem. In other words Reynolds numbers would be very low and flow would be laminar. Similarly, phloem sap is not really compressible. This would justify the use of simplified forms of Navier-Stokes, as was done in [48]. Similarly, the use of Equations 1.9 and 1.10 for modelling phloem, although not derived from Navier-Stokes, can be simplified [34].

The same reasoning applies to rate equations. Mechanistic rate equations can be used, but often the number of parameters required is greater than would be needed for phenomenological equations—parameters that have not necessarily been measured. As a further example, the order in which substrates bind to an enzyme may affect the rate of the reaction. If the rate can be calculated without knowing the binding order then there is no loss of generality in the model. It is for these reasons that a purely phenomenological approach is taken in the formulation presented in §2.2. In §2.3 it shown how the Darcy equation, for modelling flow in porous media [51], is used to model phloem flow and §2.4 gives the generic reversible Hill equations to find reaction rates. Solute flow and reactions are defined on certain compartments and sometimes also span a number of compartments.

Compartmental modelling   According to the Münch hypothesis, fluid flow is driven by a pressure gradient [39–41]. Pressure gradients are created by osmotic potentials, which in turn

are due to concentrations of solute. Likewise, reactions are driven by concentrations of solutes. Of course, solutes are called reactants when they are involved in reactions. When solutes are transported from one compartment to another the difference in compartment volume needs to be accounted for. A possible way to do this is to have volumes appear explicitly in the relevant equations, with solutes measured in amounts. Terms in the differential equations would then have units of amounts per unit time.

Outline In Section 2.2 it is shown that there is a natural extension to Equation 1.1 in §1.2 from the well-mixed to the heterogeneous case. We propose the use of a dynamic system for a kinetic model where species can be in different compartments, transported over long distances in a fluid medium and/or involved in chemical reactions. Section 2.5 demonstrates model building in the framework. As with most modelling, only idealised cases are considered. Simulation results are presented in Section 2.6. In a first scenario, the only regulation of phloem loading is through product inhibition of phloem solute. A normal time simulation is shown in Figure 2.4. In Figure 2.7 is shown a simulation where certain phloem loading sites are removed after a short interval. A second scenario allows for a model with allosteric feedback of leaf assimilate on source reactions and a third model with allosteric feedback of phloem solute on phloem loading (Figures 2.5 and 2.6). Section 2.7 discusses the relative merits of the formalism and results presented. This work prepares the way for studying sucrose metabolism and translocation of sucrose in sugarcane.

2.2 Conservation of mass

Suppose a molecule, S, with concentration, s, is found in a small *control volume*, Θ, bounded by a surface, O (See Figure 2.1). The number of S in Θ can change if the following occurs,

1. S is involved in a set of enzyme catalysed reactions, ρ, found in Θ with each reaction having *signed* stoichiometric coefficient, c, and rate, v,

2. or S crosses O because of,

    a) convection, e.g. advection, $\nabla \bullet (\vec{u}s)$, by a velocity vector field, $\vec{u}$,

    b) diffusion due to a concentration gradient, ∇s, with coefficient, D, such that the divergence of the concentration gradient is $\nabla \bullet (D\nabla s)$,

    c) facilitated or active transport due to a set of transporters, τ, with each transport step having *signed* stoichiometric coefficient, c, and a rate, v, as in the case of a reaction.

DIFFUSION

Molecules move over the control volume boundary due to a concentration gradient.

CONVECTION

A vector field, such as a flowing fluid, moves a molecule over the control volume boundary.

REACTIONS

Chemical reactions may change the type of a molecule, thereby changing the concentration.

CONTROL VOLUME, Θ

The control volume remains static with respect to a set of coordinate axes.

Figure 2.1: Possible changes in the *number* of a molecule, S, in a small control volume.

A conservation equation for s can then be written as,

$$\dot{s} + \nabla \bullet (\vec{u}s) + \nabla \bullet (D\nabla s) = \sum_{i \in \rho \cup \tau} c_i v_i. \tag{2.2}$$

Equation 2.2 can be generalised to account for multiple species in diverse physiological and subcellular compartments. However, some notation needs to be defined first.

Notation   The del operator notation will have two possible definitions. ∇ takes its cue from the object it is acting on. For example, a concentration gradient is given by

$$\nabla s = \left[\mathbf{i} \cdot \frac{\partial}{\partial x} + \mathbf{j} \cdot \frac{\partial}{\partial y} + \mathbf{k} \cdot \frac{\partial}{\partial z} \right] \cdot s.$$

Given a vector of concentrations, matters are slightly different, del becomes a diagonal matrix of gradient operators,

$$\nabla \mathbf{s} = \begin{bmatrix} \mathbf{i} \cdot \frac{\partial}{\partial x} + \mathbf{j} \cdot \frac{\partial}{\partial y} + \mathbf{k} \cdot \frac{\partial}{\partial z} & & \\ & \mathbf{i} \cdot \frac{\partial}{\partial x} + \mathbf{j} \cdot \frac{\partial}{\partial y} + \mathbf{k} \cdot \frac{\partial}{\partial z} & \\ & & \cdots \\ & & & \cdots \end{bmatrix} \begin{bmatrix} s_1 \\ s_2 \\ \vdots \end{bmatrix}.$$

The definition of ∇ should however be clear from the context. Note as well that x, y and z are taken to be in the same direction as the unit vectors $\mathbf{i}$, $\mathbf{j}$ and $\mathbf{k}$.

Let $\mathbf{N}$ be a stoichiometric matrix, $\mathbf{v}$ a vector of reaction rates and $\mathbf{s}$ a vector of species concentrations. Consider a multi-compartment, coupled network of chemical reactions where, depending on the compartment, the species may be advected and/or undergo diffusion. Equation 2.2 can then be written in matrix form as,

$$\dot{\mathbf{s}} + \nabla \bullet (\mathbf{U}\mathbf{s}) + \nabla \bullet (\mathbf{D}\nabla\mathbf{s}) = \mathbf{N}\mathbf{v}, \tag{2.3}$$

where the general rate vector, $\mathbf{v} = \mathbf{v}(\mathbf{s}, \mathbf{p}, \mathbf{r}, t)$ is a function of species concentrations, a parameter vector ($\mathbf{p}$), a position vector ($\mathbf{r}$) and time. $\mathbf{v}$ can be partitioned into reaction equations, ρ, and cross-membrane transport equations, τ. Let χ be a set of compartments. Then, $\mathbf{s}$ can be partitioned over χ into sets of species grouped by compartment. Furthermore, $\mathbf{U} = \mathbf{U}(\mathbf{s})$ is a matrix with compartment-specific phase average velocities on the diagonal. It follows that species found in the same compartment will be subject to the same velocity vector field and therefore some repetition will be expected. Similarly, $\mathbf{D} = \mathbf{D}(\mathbf{s})$ is a matrix with diffusion coefficients on the diagonal. Each species, however, has a unique diffusion coefficient. The diffusion matrix is not to be confused with a diffusion tensor and implicitly assumes isotropic diffusion for each individual species.

To solve Equation 2.3 for $\mathbf{s}$ the following need to be specified: the equations that govern reaction rates and phase average velocity, diffusion coefficients, the geometry and subsequent domain on which the variables are defined, the initial conditions and possible boundary conditions that may exist. Given sufficient initial conditions the *time-dependent* behaviour of the system can be modelled. As is, Equation 2.3, is a very broad framework in which a model needs to fit. Not all compartments will allow advection to occur, some species may diffuse quickly through a compartment to form a homogeneous concentration field, other compartments will allow some combination of advection, diffusion and reaction to occur.

The next section deals specifically with the simplifications that can be made to Equation 2.3 to model translocation of assimilate in the phloem.

2.3 "Solute driven advection"

Long-distance *assimilate* transport in plants occurs via the phloem [35, 38]. Since, all further modelling in this work will only have a single solute in the phloem, it suffices to consider only Equation 2.2,

$$\dot{s} + \nabla \bullet (\vec{u}s) + \nabla \bullet (D\nabla s) = \sum_{i \in \rho \cup \tau} c_i v_i.$$

The phase average velocity, $\vec{u}$, can be obtained from Darcy's law [51],

$$\vec{u} = -\kappa/\mu \cdot \nabla P, \tag{2.4}$$

where κ is the hydraulic conductivity (a constant measurable quantity [47]), μ is the viscosity, P is pressure and ∇P is the pressure gradient. By substituting Equation 2.4 into the second term of Equation 2.2 the following is obtained,

$$\nabla \bullet (\vec{u}s) = \nabla \bullet \left(s \cdot (-\kappa/\mu \cdot \nabla P)\right) \tag{2.5}$$

$$= -\kappa/\mu \cdot \nabla \bullet (s\nabla P). \tag{2.6}$$

This formulation casts advection in terms of a pressure gradient, which can in turn be solved by using the van't Hoff equation for dilute solutions [52],

$$P = \Pi + P_0 \tag{2.7}$$

$$= RTs + P_0 \tag{2.8}$$

$$\nabla P = RT \cdot \nabla s + 0, \tag{2.9}$$

where Π is the osmotic pressure and P_0 is the surrounding pressure from the apoplast. Substitution of Equation 2.9 into Equation 2.6 gives the following relation,

$$\nabla \bullet (\vec{u}s) = -\kappa/\mu \cdot \nabla \bullet \left(s \cdot (RT \cdot \nabla s)\right) \tag{2.10}$$

$$= -\kappa/\mu \cdot RT \cdot \nabla \bullet (s \cdot \nabla s). \tag{2.11}$$

For high osmotic pressure (large s) and small pressure changes (small ∇P implies small ∇s), s approaches Φ [34, 47]. By the product rule,

$$\nabla \bullet (s \cdot \nabla s) = \nabla s \bullet \nabla s + s \cdot \left(\nabla \bullet (\nabla s)\right) \tag{2.12}$$

$$\approx 0 + s \cdot \left(\nabla \bullet (\nabla s)\right) \tag{2.13}$$

$$\approx \Phi \cdot \left(\nabla \bullet (\nabla s)\right), \tag{2.14}$$

where Φ is called the set-point concentration. This is the concentration of s, at the end of the phloem tube, that the plant tries to maintain homoeostatically. Φ is a measurable quantity, hence making the treatment of phloem flow presented here completely phenomenological. Substitution of this approximation into Equation 2.11 yields,

$$\nabla \bullet (\vec{u}s) = -\kappa/\mu \cdot RT\Phi \cdot \nabla \bullet (\nabla s) \tag{2.15}$$

$$= -\kappa/\mu \cdot RT\Phi \cdot \nabla^2 s. \tag{2.16}$$

If one further assumes that the diffusion coefficient remains constant, this gives a conservation equation of the following form,

$$\dot{s} - \kappa/\mu \cdot RT\Phi \cdot \nabla^2 s + D \cdot \nabla^2 s = \sum_{i \in \rho \cup \tau} c_i v_i.$$

Furthermore, the contribution of the diffusion term to phloem translocation is typically two orders of magnitude smaller than the contribution from the advective term [47, 48], in other words,

$$D \ll |-\kappa/\mu \cdot RT\Phi|. \tag{2.17}$$

For the rest of this dissertation this assumption only applies to the phloem, not any of the other compartments. It allows phloem translocation to be modelled with the following approximation,

$$\dot{s} - \kappa/\mu \cdot RT\Phi \cdot \nabla^2 s = \sum_{i \in \rho \cup \tau} c_i v_i. \tag{2.18}$$

Thompson [34] called this "solute driven advection".

The next section describes the equations governing catalytic conversions and cross-membrane transport. In other words finding the rates to populate $\mathbf{v}$ in terms of metabolite concentrations and parameters.

2.4 Reactions and cross-membrane transport

The following generic rate equations [53–55] are used. For uni-uni reactions,

$$v = V_{\text{f}} \cdot \left(1 - \frac{\Gamma}{K_{\text{eq}}}\right) \cdot \frac{s}{1 + s + p}, \tag{2.19}$$

where

- V_{f} is the maximal forward reaction rate,

- Γ is the mass-action ratio,

- K_{eq} is the equilibrium constant,

- $(1 - \Gamma/K_{\text{eq}})$ therefore determines the direction of the reaction, and

- s and p are substrate and product concentrations scaled by their respective half-saturation constants.

Compartment volumes are modelled explicitly, therefore all s are actually defined as,

$$s = \frac{S}{V} \cdot \frac{1}{S_{0.5}} = \frac{\text{No. of moles of } S}{\text{Volume} \times \text{Half-saturation const.}} \tag{2.20}$$

and appear as such in the model.

Generic rate equations are used because they explicitly incorporate a thermodynamic term, thus implicitly satisfy the Haldane relationship, have all kinetic terms separated from thermodynamic terms, and possible allosteric terms are separated from mass action terms and finally all kinetic parameters are phenomenological, thus have an immediate experimental interpretation.

Two cases of allosteric feedback use the generic, non-cooperative, reversible Hill equation [53, 54],

$$v = V_{\mathrm{f}} \cdot \left(1 - \frac{\Gamma}{K_{\mathrm{eq}}}\right) \cdot \frac{s\,(1 + \gamma\alpha m)}{(1 + m) + (1 + \alpha m)\,(s + p)}, \tag{2.21}$$

where,

- m is the scaled modifier concentration, defined as for s and p,

- γ affects the rate by scaling V_{f}, known as a V-effect,

- and similar K-effects, scaling half saturation constants, are introduced through α.

- For α and γ: less than 1, rate attenuation or inhibition occurs; greater than 1, amplification, or activation; and equal to 1, no effect is seen.

If $\alpha = \gamma = 1$ then Equation 2.21 simplifies to Equation 2.19.

For the dynamic system as defined in Equation (2.3) enzymes are also subject to movement by advection-diffusion. This means that enzyme concentrations (call them $\mathbf{e}$) will change with position and therefore maximal activities will also change. Nothing prohibits setting, $\mathbf{s} \supset \mathbf{e}$, with appropriate equations for enzyme expression and degradation in $\mathbf{v}$. However for this work it is assumed that the enzyme concentration gradient remains constant, i.e. $\delta \nabla \mathbf{e} = 0$

2.5 Example of building a model

The first step in building the model is to describe the geometry. The geometry is divided into finite volumes or "meshed". Compartments are defined on these elements. A compartment can span a number of elements and compartments of the same type can be separated by a number of elements. A pathway or reaction network is defined across the compartments. Species concentration and reaction rates are variables that in turn are defined on the network. Note that the same chemical species found in two different compartments are *two separate* variables. Therefore each variable is only defined for its specific compartment and it cannot assume a value anywhere outside of it. This is known as the domain of the variable. Reaction rates are calculated from species concentrations and it follows that they cannot have values at positions where a species variable does not exist. The behaviour of the variables is governed

1D APPROXIMATION WITH LENGTH, L

DISCRETISE

The problem domain is divided ("meshed") into 50 finite volumes.

COMPARTMENTALISE

Compartments are defined on parts of the mesh.

VACUOLE

The vacuole size is the same as that of a finite volume. Facilitated transport into the vacuole can only occur from the symplast. No transport between neighbouring vacuoles and internal advection-diffusion can occur. Metabolites are not clamped.

INTERNODE   NODE

1   2   3   4   5

PHLOEM

The phloem is one long, continuous compartment. Metabolites may be loaded or unloaded from the source or the symplast. Metabolites can be advected.

SYMPLAST

The symplast is the bridging compartment between the phloem and the vacuoles.

SOURCE

External metabolites are clamped. Reactions may occur. Facilitated transport is only into the phloem. The size of the source compartment is the same as a finite volume element, i.e. it is a *point source*

Figure 2.2: Schematic of the problem domain for the toy model. Note that because the domain is treated as one-dimensional, the source elements "overlap" the symplast.

by a set of PDEs. With sufficient parameter values, initial conditions and boundary conditions a time course simulation can be performed. If a model formulation has proceeded this far, then appropriate software can be sought and programs written to analyse the model behaviour, which forms the topic of Section 2.6. Given the above hierarchy of modelling steps, we start with a straight line segment.

Geometry, domain and compartments

The problem domain is approximated by a 1D mesh (straight line segment), with arbitrary length, $L = 1.0$ and divided into 50 finite volumes. The phloem and symplast span all 50 elements, with leaves acting as source tissue feeding assimilate into the phloem at the nodes, and storage parenchyma in the internodes acting as sink tissues extracting assimilate from the phloem (see Figure 2.2). There are 5 sequential node and internode pairs, numbered from 1 to 5, where internode 1 is considered immature tissue and internode 5 is mature tissue. There

are 10 elements to a node/internode pair; the first element of each group of 10 is used for the
node, the remaining 9 for the internode. The only path out of a leaf element is into the phloem.
There are 4 possible paths for a molecule in the phloem, up, down, into the leaf or into the
symplast. Molecules in the symplast can move, up, down, into the phloem or into a vacuole.
A vacuole corresponds to one finite volume; consequently there are 50 vacuolar compartments
in the symplast. Molecules in a vacuole cannot move to another vacuole, they can only move
to the symplast.

The choice of $N = 50$ is the minimum number of finite volumes required to have five node
and internode pairs such that the length of an internode is 9 times longer than a node. The ratio
of 1:9 is an approximation of real internode lengths. To ensure that this level of granularity
suffices, we performed simulations with $N = 100$; these yielded plots indistinguishable from
Figure 2.4.

Pathway description

Previous models of phloem flow usually approximate the sieve tube as a cylinder with loading
of solute at the one end and unloading at the other [46, 48]. A few models have also considered
branched vascular bundles [56]. Some others have included general sink type demand, such
as "respiration" or "starch" [57]. To the best of our knowledge the combination of phloem
modelling, with un/loading along the entire length of the sieve tube, compartmentation and
detailed reaction kinetic modelling has not been done before.

Given a length, L, in the z-direction, we define a model (Figure 2.3) where X is converted
to S at certain sites (the source, so) on L. At the same sites S is transported (loaded) into
another compartment (the phloem, ph) where it is advected. S can be removed at all the sites
on L i.e. unloading sites (sinks, sk). In the sink S may undergo diffusion, with "constrictions"
at the nodes where a smaller diffusion coefficient is applied. We assume that the sink tissue is
symplastically linked for segments on L flanked on either side by a source segment. S may be
converted to P, which may similarly be diffused, which is then actively transported across a
membrane (a tonoplast perhaps) into another compartment (call it the vacuole). Once in the
vacuole there is no diffusion. The vacuole size also corresponds with a single finite volume.
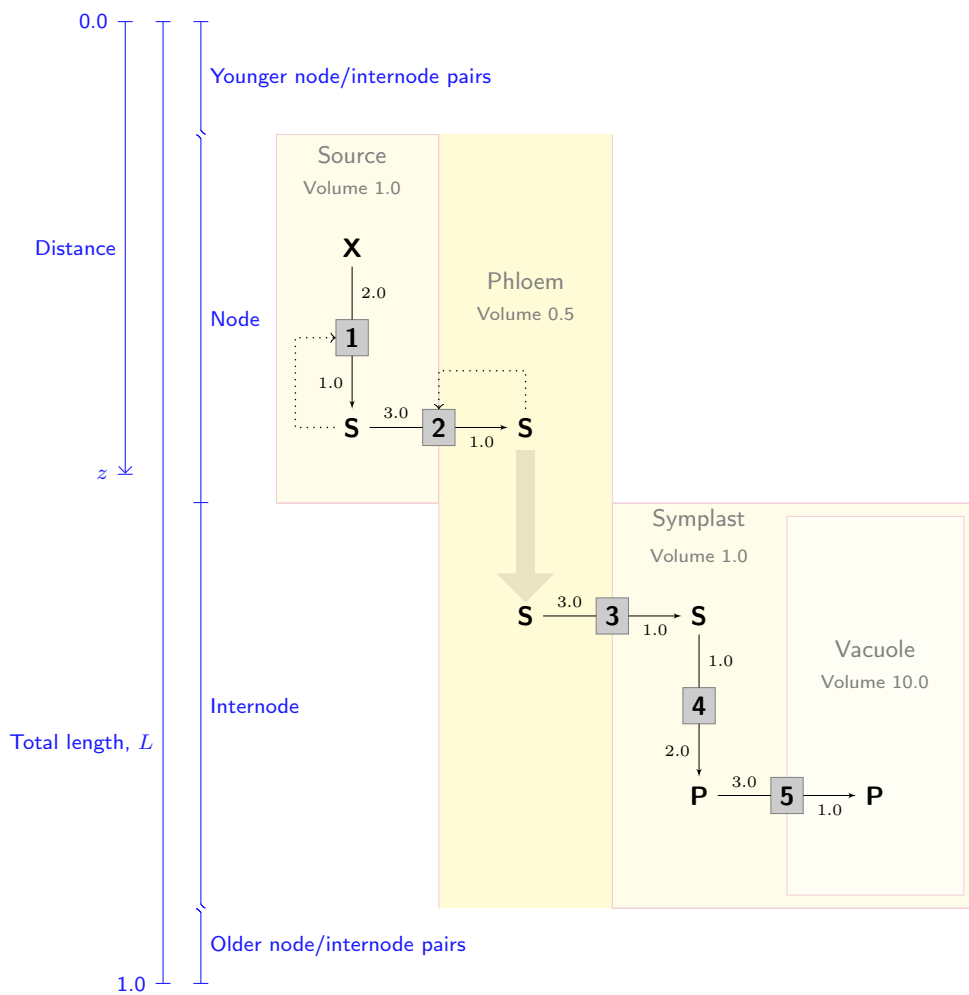
Figure 2.3: The toy model. A single node and internode pair are shown. X is a fixed amount of some reactant, which is converted to S in the "leaf". S can be transported into the phloem where it is advected either up or down, depending on ∇S in the phloem. Phloem unloading occurs into a "symplastic" space. A single reaction occurs in the symplast and P is accumulated in the "vacuole". Numbers between an enzyme (grey boxes) and a metabolite are the half saturation constants of the metabolite for that enzyme.

Partial differential equations

The following abbreviations are defined for convenience:

$$\partial_t x_i = \frac{\partial}{\partial t} x_i,$$

$$\partial_z^2 x_i = \frac{\partial^2}{\partial z^2} x_i,$$

$$\Delta x = \partial_t x + D_x \partial_z^2 x.$$

Mole amounts of a reactant is indicated by a X, S or P. The choice of units in this model is completely arbitrary.

X is constant,

$$\partial_t X_{so} = 0. \tag{2.22}$$

The change of S in the source is given by,

$$\partial_t S_{so} = v_1 - v_2. \tag{2.23}$$

Loading, unloading and transport of S in the phloem is given by,

$$\partial_t S_{ph} - \kappa/\mu \cdot RT\Phi \cdot \partial_z^2 S_{ph} = v_2 - v_3. \tag{2.24}$$

S in the sink symplastic space is given by,

$$\Delta S_{sk} = v_3 - v_4. \tag{2.25}$$

Similarly for P,

$$\Delta P_{sk} = v_4 - v_5. \tag{2.26}$$

And for P in the vacuolar space,

$$\partial_t P_{vc} = v_5. \tag{2.27}$$

Parameter values, constants, initialisation values and boundary conditions

Parameter values were chosen by trial and error. However there is some bias in the choices, that reflect roughly what occurs in sugarcane. The selected parameters are meant to exaggerate model behaviour.

Compartment volumes are set at the same value for each internode,

$$V_{so} = 1.0, \qquad\qquad V_{ph} = 0.5,$$

$$V_{sk} = 1.0, \qquad\qquad V_{vc} = 10.0.$$

Equilibrium constants are,

$$K_{\text{eq}}^{(1)} = 0.5, \qquad\qquad K_{\text{eq}}^{(2,3,5)} = 1.0, \qquad\qquad K_{\text{eq}}^{(4)} = 2.0.$$

The maximal velocities are defined as,

$$V_{\text{f}}^{(1)} = 1.0, \qquad\quad V_{\text{f}}^{(2)} = 3.0, \qquad\quad V_{\text{f}}^{(3,4,5)}(z) = m \cdot z + 1.0.$$

The maximal activities for the last three reaction equations increase *linearly* from 1.0 to 3.0 along L as a function of z, i.e. $m = 2.0$. Half-saturation constants are set according to the values shown in Figure 2.3.

The flow parameters in Equation 2.24 were estimated at a single coefficient,

$$\kappa/\mu \cdot RT\Phi = 1.0 \times 10^{-3}.$$

Diffusion coefficients for S_{sk} and P_{sk} in the symplast are set at,

$$D_{S_{sk}} = D_{P_{sk}} = \begin{cases} 10^{-7} & \text{if} \quad n \pmod{10} \equiv 0, \quad n = 0, 1, ..., N \\ 10^{-5} & \text{otherwise} \end{cases}, \qquad (2.28)$$

where n indexes the finite volumes. In other words, diffusion coefficients are set two orders of magnitude smaller at the nodes compared to the internodes. Even though molecular travelling in the symplast across the nodes may occur it will be slow. The nodes act as "constriction points" partially defining the internode symplast as a separate volume.

Feedback parameters are chosen to be,

$$\alpha = 0.1, \qquad\qquad \gamma = 0.1, \qquad\qquad M_{0.5} = 0.5.$$

where $M_{0.5}$ is the modifier half saturation constant.

Software

FiPy is a Partial Differential Equation (PDE) solver using finite volume methods [58, 59]. FiPy is written in Python. It provides an object-oriented interface to solving coupled sets of PDEs. Suppose a problem can be cast in the form of a general conservation equation,

$$\frac{\partial(\rho\phi)}{\partial t} = \nabla \cdot (\vec{u}\phi) + [\nabla \cdot (D_i\nabla)]^n \phi + S_\phi, \qquad (2.29)$$

where ρ is some coefficient, ϕ is the variable being solved, $\vec{u}$ is a vector coefficient (for example velocity), D_i is a generic coefficient of diffusion (for example heat or solute diffusion) and S_ϕ is a source term (i.e. a source of ϕ). If a PDE can be written in the form of Equation 2.29 then there is a natural way to program the equation in Python. It should be immediately clear that Equation 2.3 is amenable to this formalism.

2.6   Time simulation

Time-course simulation results for Equations 2.22 to 2.27 and parameter values given in Section 2.5 are shown in Figure 2.4. The results at every time step are not shown, rather an exponential scale is used on the time axis. This choice was made to emphasise the rapid changes that occur early in the simulation, $0 \leq t \lessapprox 32$. These changes would have been masked by a linear sample from the time course. Furthermore, as $\Delta \log_2 t$ becomes larger the detail from relatively slow kinetics at $t \gtrapprox 32$ is more readily discernible from the plot. The absence of any units does not allow one to comment on the time taken for the system to relax to equilibrium.

The S_{ph} concentration has a characteristic "saw-tooth" profile with peaks at the nodes. This means that solute is able to flow up or down the phloem away from the source tissue.

The model actively accumulates P_{vc}, with concentrations increasing faster in internode 1 than in internode 5. In other words the P_{vc} gradient profile shows "filling" behaviour.

After 2^{13} time units, metabolite concentrations, for all points where they are defined on z, decrease from source to sink. This distribution of concentrations is a direct result of the choice of equilibrium constants. Product concentrations, scaled by the respective equilibrium constants, are lower than the substrate concentrations. P_{sk} is higher than S_{sk} as consequence of the K_{eq} for reaction 3 being 2.

The model tends towards a quasi-steady-state in the short term, while generally approaching equilibrium. If the steady-state flux at a point in a node is compared to that of a point in an internode, then the fluxes in a node are much higher. However, the sum of rates over z in the source tissue (all the nodes) is very close to the sum of rates in the sink. There are fewer source points than accumulation points along the stalk, in other words the internodes are longer than the nodes. This means that reaction rates in the leaves, on average, need to be much higher than at any point in an internode to satisfy demand. This also means means reactions in the leaf need to be much faster than those in the parenchyma in order for a quasi-steady-state to be reached.

The conclusion is that assimilate accumulation behaviour along the length of a stalk is the process of moving towards equilibrium while maintaining a quasi-steady-state.

Comparison of feedback on source

There are two variations on the model (reference model or Model 0); the first (Model 1) allows allosteric inhibition of reaction 1 (synthesis) by its product, S_{so}, and the second (Model 2) of reaction 2 (phloem loading) by S_{ph}. The parameters α and γ were both set to 0.1, first for the synthesis and then the phloem loading versions. Results are shown in Figures 2.5 and 2.6.

Both feedback models showed decreased rates of accumulation, in other words the tendency
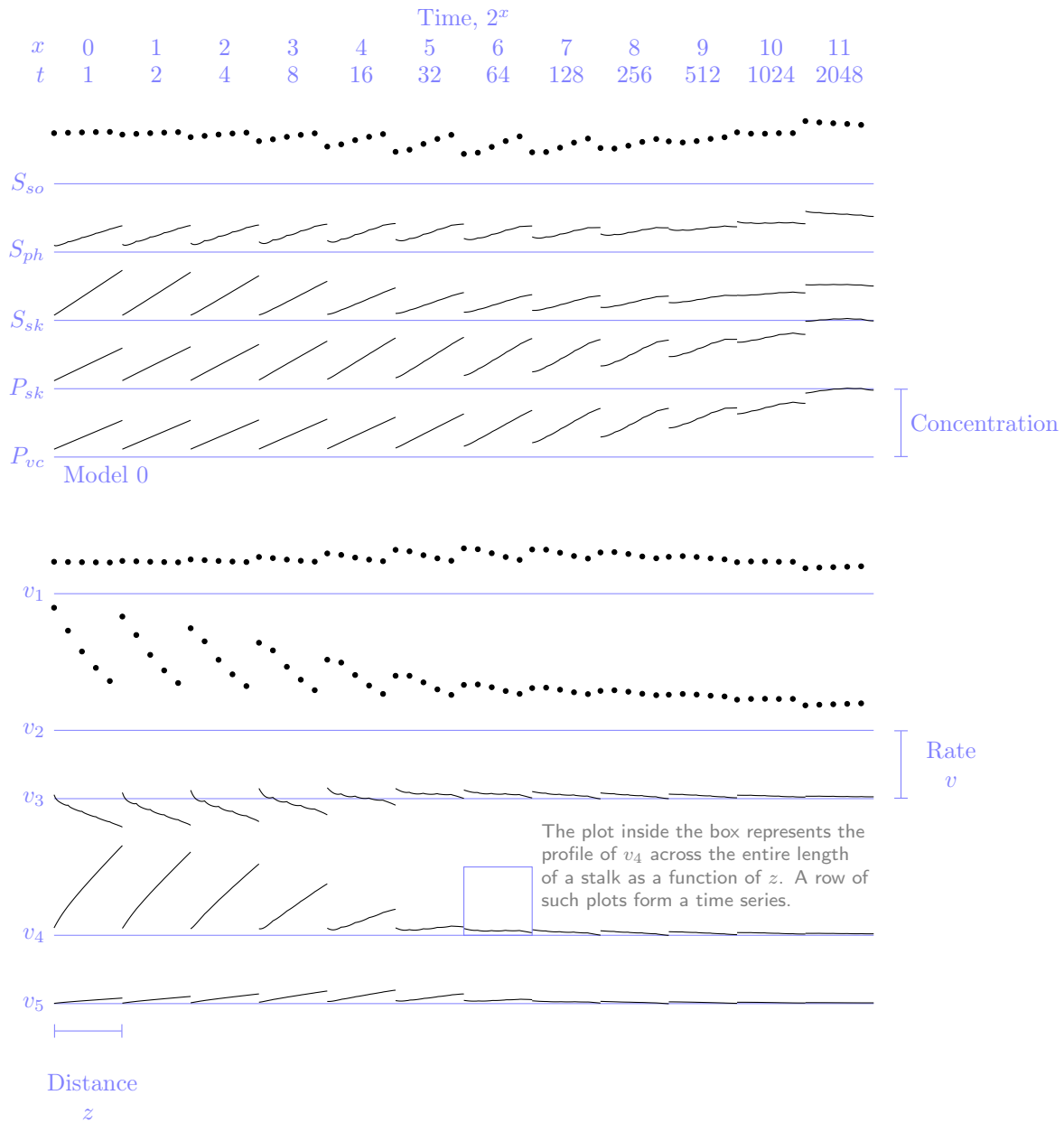
Figure 2.4: Metabolite concentrations and reaction rates for the toy model presented in Figure 2.3. Concentrations and rates are given on the y-axis, gradients along z are given in single columns and changes from column to column indicate changes with time. Variables plotted as dots are only defined at the nodes, for example S_{so} does not exist in the internode. Note that time scales are in exponential form (t) or logarithmic (x). The results are discussed in the text (see §2.6). This time simulation is the reference model (Model 0) for the rest of the chapter.
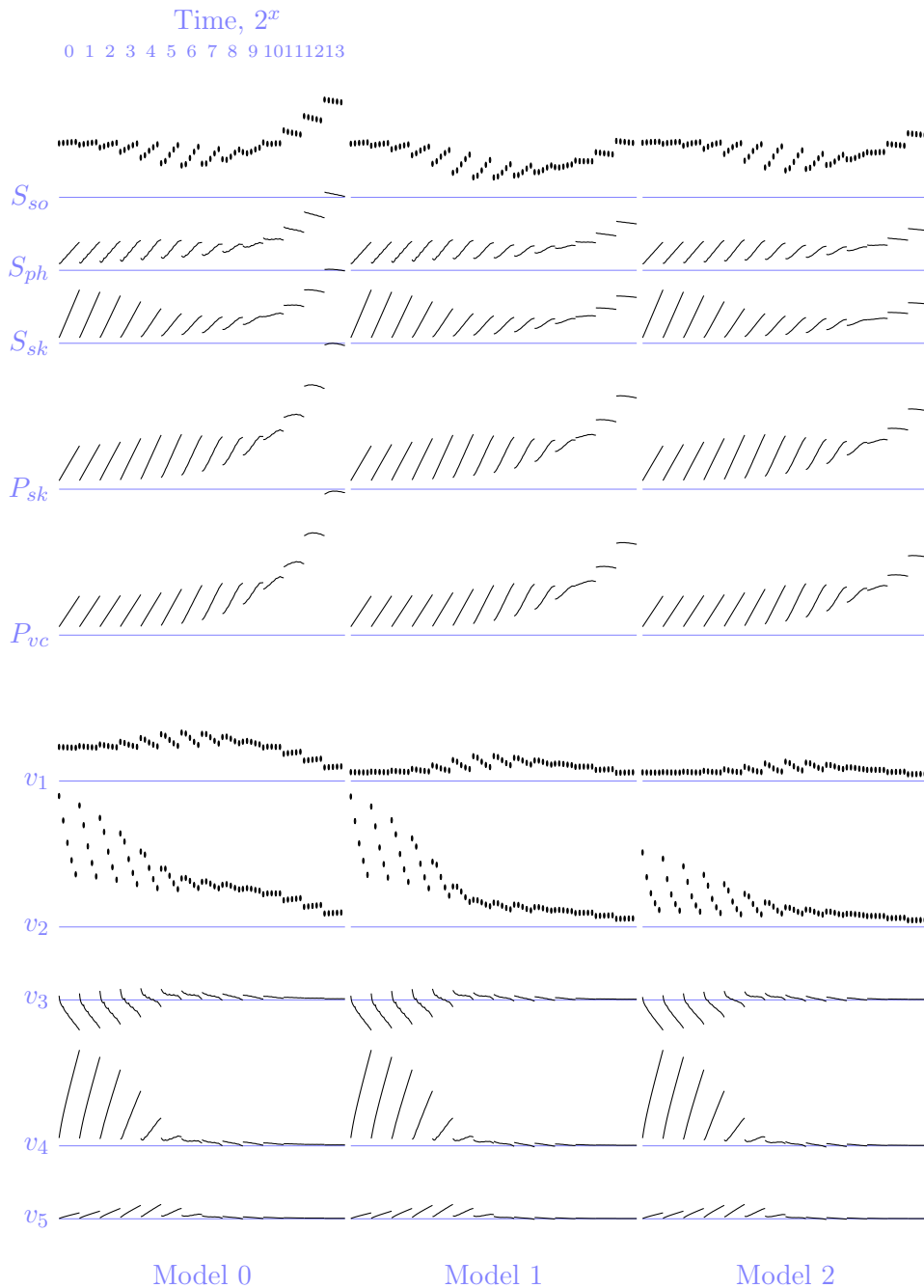
Figure 2.5: Metabolite concentrations and reaction rates for the reference model (Models 0) compared to a model of allosteric feedback of S_{so} on reaction 1 (Model 1) and allosteric feedback of S_{ph} on reaction 2 (Model 2). The results are discussed in the text (see §2.6)
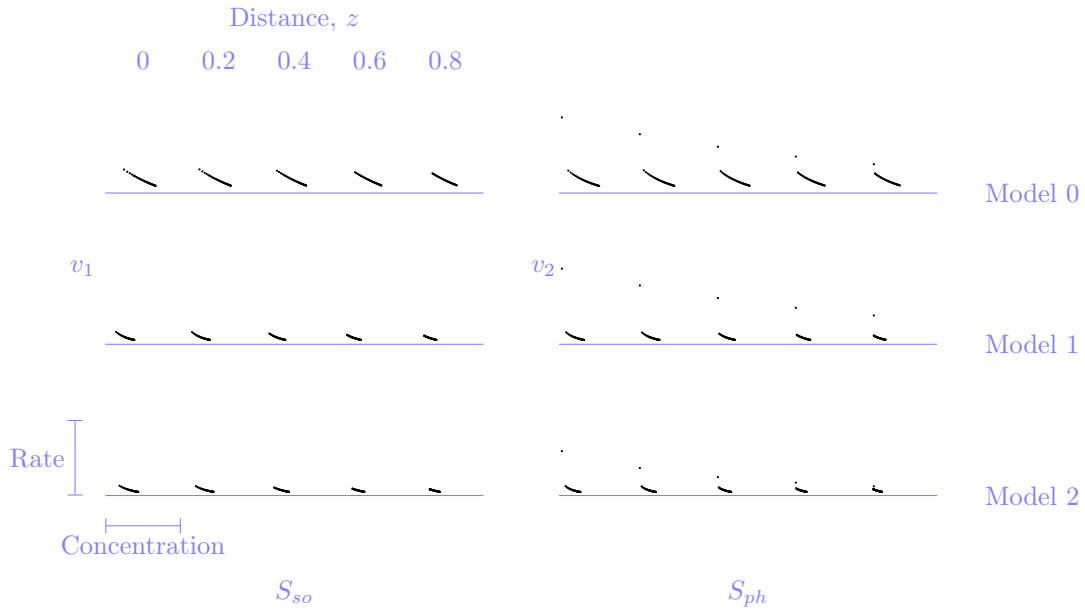
Figure 2.6: Reaction rates of reaction 1 and 2 against concentrations of S_{so} and S_{ph} respectively. The reference model is in the top row, S_{so} feedback on reaction 1 in the middle row and S_{ph} feedback on phloem loading is on the bottom row. A single plot shows the rate against concentration over 2^{13} time steps.

is for the synthesis and phloem loading steps at the nodes to saturate faster than the reference model. Phloem loading rates are lower and the range in which v_1 and v_2 vary is smaller. Allostery results in a narrower range of rates across a narrower range of concentrations Figure 2.6—homoeostasis is better maintained.

The "sock experiment"

Increased photosynthetic rates in response to shading have been experimentally demonstrated in sugarcane [60, 61]. All but one leaf of a sugarcane stalk was shaded and the effect on various sugars and rates measured. Shading of the leaves was argued to correspond to an increase in sink demand. In other words reducing the supply and keeping the demand constant is equivalent to keeping the supply constant and increasing the demand. The latter, is unfortunately not easily accomplished in an experimental setting. Sucrose concentrations decreased in young internodal tissue, while the carboxylation efficiency and rate of electron transport increased [60]. Expression of a number of genes associated with photosynthesis, mitochondrial metabolism and sugar transport were also upregulated [61].

The following event was triggered at $t = 32$ during a simulation of the reference model:

$$V_{\mathrm{f}}^{(1)} = \begin{cases} 1 & n \ (\mathrm{mod}\ 10) \equiv 0 \\ 0 & \text{otherwise} \end{cases} \mapsto V_{\mathrm{f}}^{(1)} = \begin{cases} 1 & n = 10 \\ 0 & \text{otherwise} \end{cases}, \tag{2.30}$$

where n is defined with Equation 2.28, and allowed to persist until the end of the simulation. In other words, all but the second leaf had the maximal velocity for reaction 1 set to 0—one leaf now had to supply the entire stalk. The results of the simulation can be seen in Figure 2.7. The following effects can be noted after the "shading" event, compared to the reference model;

- v_1 and v_2 in the second leaf *increase* above levels of the reference model. They remain higher for the rest of the simulation.

- P_{vc} accumulates more slowly than in the reference model.

- Metabolite concentration profiles decrease more rapidly with z compared to the reference model.

- Assimilate flows up and down the stalk away from the only remaining source.

2.7   Discussion

This section is divided between a discussion of the problem formulation and the solution to the toy model.

Formulation

Equation 2.3 is a general framework that allows the modelling of metabolites that are involved in chemical reactions, advected or diffused. It is a broad framework, which requires that an expression for fluid velocity be provided, compartmentation be defined, rate equations and stoichiometry be specified and, a suitable geometry with boundary conditions be provided. This was shown to work successfully with a "linear" reaction kinetic model. By allowing a linear pathway to vary spatially, more complicated behaviour can be modelled compared to a well-mixed case. Furthermore, the model provides a good first approximation of the modelling of sugarcane geometry. There are of course a number of limitations in the approach followed here.

The use of Darcy's Law to model fluid flow could be interpreted as an oversimplification. Darcy's Law is a phenomenological equation that describes fluid flow in porous media. It requires flow parameters to be measured. The use of Darcy's Law is justified where macroscopic
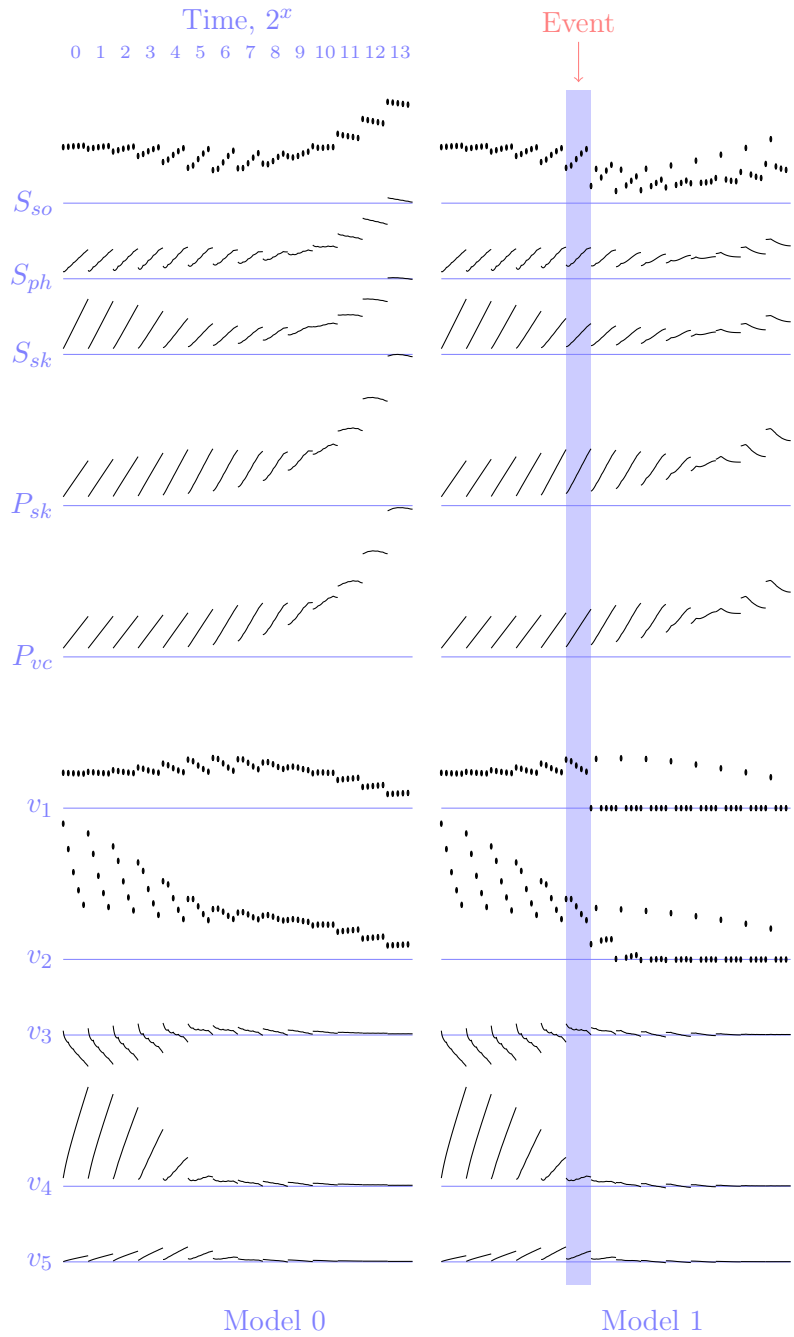
Figure 2.7: Metabolite concentrations and rates, showing an event (Equation 2.30) triggered at $t = 32$ ($x = 5$). The event corresponds to the shading of all the leaves except for the second one from the left. The axis are defined as for Figure 2.4.

flow is modelled. In other words, it is entirely inappropriate for modelling fluid flow in a single
sieve element, but adequate for modelling flow through many sieve elements strung together. A
statistical averaging effect is at work over sufficiently large scales. Phloem flow and translocation
over a whole plant qualifies as such. Despite this, the use of Darcy's Law has advantages. It is
possible to simplify Equation 2.3 by taking into account the mechanism of phloem translocation
[34]. This simplification is both easier to solve, because, a) the convective term is removed and
b) no pressure gradient has to be calculated. The simplification also describes the macroscopic
(or phenomenological) aspects of phloem translocation, i.e. that flow is due to a pressure
gradient *induced* by a solute.

The use of the van't Hoff equation is also a simplifying assumption. This equation is
usually a first approximation for the calculation of osmotic pressure, since it only applies to
dilute solutions. The only viable alternative is to use an interpolative function for a specific
solute using known experimental measurements. The usual way of increasing the accuracy is
by using a virial-like expansion for non-ideal cases. The virial coefficients need to be measured
by experiment [52]. A phenomenological equation has been proposed by [62] and is used by
Thompson & Holbrook [46] and Lacointe & Minchin [56]. Lacointe & Minchin [56] calculated
that the error between a first and higher order approach is in the order of 8%. These alternatives
are meaningless for a toy model with arbitrary parameter values.

Solution

Description   The model is meant to illustrate the formulation and method of solving Equa-
tion 2.3. It is a simplification of what happens in a plant and no substantial conclusions
should be made about the workings of plants and sugarcane in particular. However, the model
does succeed in illustrating a few properties of sink/source relationships in plants. These are
discussed in the following paragraphs.

The "constriction" of symplastic linkage, and thereby slower diffusion across nodes, is a
strong assumption. In the absence of precise knowledge of phloem loading in sugarcane, an
assumption was made based on the work of Botha and Van Bel [63]. They noted that there are
fewer plasmodesmata between adjacent cells at the nodes than in the internodal regions. This
was modelled by choosing diffusion coefficients to be lower at the source elements as opposed
to sink tissue.

Time simulation   Plants do not accumulate assimilate indefinitely. The model will do so
until chemical equilibrium is reached. If plants did that they would die. The model fails
to saturate and reach a true steady-state, but rather tends to equilibrium. This does not
necessarily disqualify the model, since we are interested in the behaviour of the system as it

moves towards a stable state. It is the early dynamic behaviour, rather than the later behaviour
that is of interest. Invariably other processes come into play when the plant is no longer in an
accumulating mode. For example, accumulated carbohydrate is used to fuel new growth.

Allosteric feedback   The only regulation considered on top of saturation binding effects is
allosteric feedback. The model, as it is defined, can only have feedback on the source through
reaction 1 or 2. The aggressive choice of α and γ exaggerated the effect that feedback would
have. Nevertheless, the narrowing of the range of reaction rates and responsible concentrations
is exactly what one would expect. Wild fluctuations in concentrations are seldom seen in
organisms. The introduction of allosteric feedback leads to tighter homoeostatic control of
concentrations [64].

Sock experiment   The model response of v_1 in leaf 2, due to attenuation of v_1 in the other
leaves, is in keeping with the main findings of [60, 61]. Their experimental findings showed an
increase in photosynthetic enzymes in response to a sink perturbation and an accompanying
increase in rate. This can be directly explained by the pseudo-linearity of the pathway. P_{vc}
is accumulated at all sites along the domain. This leads to a local depletion of intermediates
along the chain, specifically S_{ph}. This causes a decrease in Γ_2 which increase the rate at which
S_{so} is depleted and which then decreases Γ_1. The only place where this will have an effect is
in leaf 2.

The model shows how "photosynthetic" rates may respond in the absence of genetic regu-
lation. Further model adaptations could look at the combined effect of mass action responses
and genetic upregulation of an enzyme. The accumulation of P_{vc} is slower in the attenuated
model compared to the reference model. An increase in the maximal velocity of r_1 (genetic
upregulation) would allow the attenuated model to compete with the reference model

The metabolite and rate gradients as seen in Figure 2.7 are probably inaccurate compared
to a real plant. The *local* accumulation of a metabolite reflects the choice of a very low diffusion
coefficient. A higher diffusion coefficient would allow faster movement away from the source.

Conclusion

The modelling approach was successfully applied to a toy model. Despite the simplicity of
the model, a few features of plant behaviour could be investigated. In Chapter 3 the same
framework is used, but with a more elaborate reaction network. In Chapter 4 an existing model
of sucrose accumulation in sugarcane is used. The latter includes more realistic parameters,
length scales and behaviour.

Chapter 3

Vascular transport in plants: Sensitivity analysis of a reaction kinetic model coupled with advection-diffusion equations

3.1 Introduction

The flow of mass between the source and sink tissues of plants is governed by a complex relationship which exists between transport and reaction steps. Chapter 2 emphasised the modelling of phloem translocation. In this chapter we look at what happens if the reaction network becomes more complicated. Only the sink reaction network is elaborated. This is because McCormick *et al.* [60] showed that the rate of photosynthesis is regulated by sink demand.

The phloem and xylem are the main conduits through which mass flow is transacted. The synthesis of sucrose in the leaves, translocation to the storage tissue via the phloem and storage in the parenchyma is a particular example from sugarcane. A toy model is proposed to study the source/sink relationship and the behaviour that relevant reactions may exhibit. A sensitivity analysis method is also introduced to quantify the effect of various parameters on model variables.

3.2 Model outline

It is the intention in this chapter to:

1. build a minimal reaction network with specific similarities to the sucrose accumulation pathway in sugarcane,

2. make this pathway and the reactions in the pathway as feature rich as possible,

3. cast the reaction network as a multi-compartment, advection-diffusion-reaction model,

4. numerically solve this model on a domain, which is itself an idealised model of the geometry (anatomy) of a single sugarcane stalk,

5. calculate the sensitivity of the model output to its parameters,

6. analyse the source response to perturbations in the sink and the other way around, and

7. specifically focus on how sensitivities and responses change along the length of the domain.

The sink component of the reaction network in the toy model has the following features:

- reactions occur in more than one compartment [65–68],

- some metabolite intermediates enter futile cycles [23, 25],

- moiety-conserved cycles (e.g. ATP/ADP) are explicitly considered [69, 70],

- assimilate can be partitioned between respiration or storage [24, 71],

- stored assimilate can be remobilised from the vacuole and [72],

- energy driven anti-porter proton gradients drive accumulation [29, 73],

- energy is captured from metabolite breakdown and consumed by synthesis and transport steps,

- reactions in the respiration branch are subject to negative allosteric feedback (i.e. synonymous with PFK and PK), and

- these reactions are positively cooperative.

The model is cast in the framework presented in Chapter 2. To analyse the model, the Fourier Amplitude Sensitivity Testing (FAST) algorithm is used.

3.3 Fourier Amplitude Sensitivity Test

The Fourier amplitude sensitivity test is a global sensitivity analysis method. Cukier *et al.* [74, 75, 76] and Schaibly *&* Shuler [77] pioneered the technique, with improvements proposed, amongst others, in [78–81]. FAST has long been used in analysing chemical systems [74, 75, 77, 82–87]. The method is described in more detail in Appendix A, but the main idea behind FAST is this: parameters are allowed to oscillate around a point at an assigned frequency; the frequency can be isolated from the model output and allows the contribution of a parameter to the total model variation to be calculated.

The rest of the chapter is organised as follows: Section 3.4 shows how the model is constructed. Section 3.5 presents the results obtained from time simulations, sensitivity analyses and parameter changes. Methods and results are discussed in Section 3.6. Mathematical detail is presented in Appendix A.

3.4 Model

We follow the same procedure as in Chapter 2. We define the problem domain and reaction network. The PDEs and rate equations are formulated, parameters chosen and software considerations are made.

Geometry, domain and compartments

The model is defined on the same domain as introduced in §2.5 (p. 21). Table 3.1 summarises the processes allowed in each compartment.

Pathway

The model is constructed to emulate a single sugarcane stalk. A segment of the whole pathway, a single node/internode pair, is shown in Figure 3.1. The primary storage organ is the stalk (in particular the vacuoles) and sources of assimilate are distributed along the stalk. There are five nodes and internodes, which represent immature to mature tissue. The primary storage organelle is the vacuole, with possible assimilate remobilisation. A futile cycle known to exist in sugarcane is present [23]; sucrose can be broken down into fructose and glucose. The hexoses can then enter the hexose phosphate pool and sucrose can be synthesised again. The model allows a simplified version of this to occur. However, the cycle can either take place in the symplast alone or across the symplast and vacuole. Intermediate metabolites can also be used to regenerate moieties (see reaction 11 in Figure 3.1). A feedback mechanism is also present, reminiscent of the allosteric inhibition of phosphofructokinase by ATP. The following assumptions were
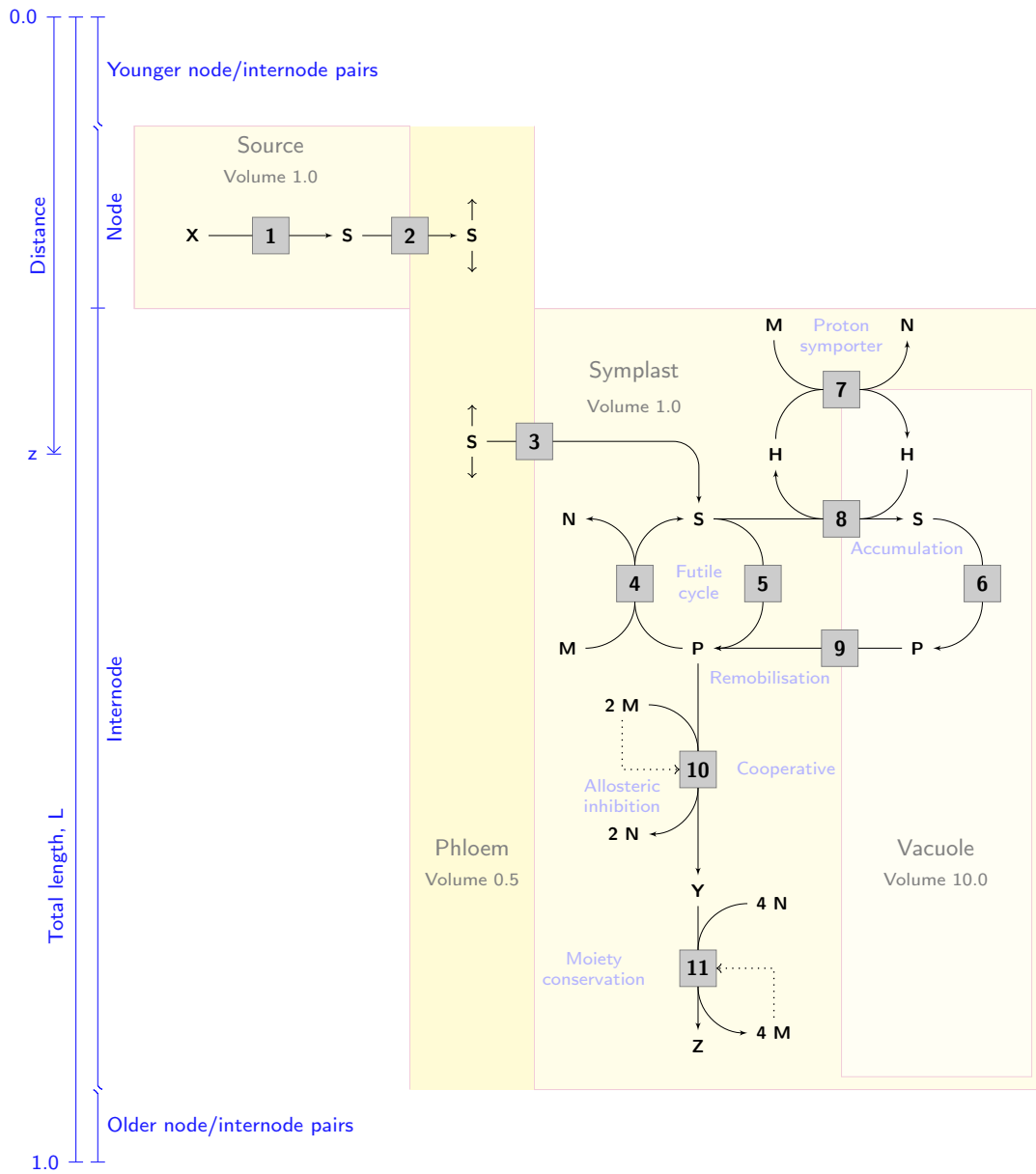
Figure 3.1: A slice through the toy model pathway showing a node/internode pair. Metabolites X and Z are clamped, in other words their concentrations are treated as constant. All other metabolite concentrations are free to vary. M and N behave like a moiety conserved pair, rather like ATP/ADP. Reaction 8 is a proton (H) anti-porter. Futile cycling refers to the energy-consuming breakdown and synthesis of a metabolite, in this case S. Reaction 10 and 11 are reminiscent of phosphofructokinase and pyruvate kinase, both of these are allosterically inhibited by ATP (or M in the case of the model).

Table 3.1: Processes allowed for each compartment

	Advection	Diffusion	Facilitated transport	Reaction
Source			•	•
Phloem	•	•	•	
Symplast		•	•	•
Vacuole			•	•

made about the assimilate uptake mechanism of the vacuole: proton symporters are involved in cellular uptake of metabolites, and similarly, that vacuolar uptake is via a proton antiporter [29].

The inclusion of moiety-conserved cycles in a model can sometimes lead to the introduction of constraints on the steady-state fluxes. These constraints may be unintentional or artefactual. One way of counteracting such a possible side-effect is to introduce a reversible ATP consuming/producing reaction. In the case of this model, however, flux partitioning between reactions 5 and 8 is not constrained by the M/N moiety. Since a futile cycle of sucrose synthesis and breakdown does exist in sugarcane it was decided to add it into the toy model. The model was constructed such that the energy that drives accumulation and resynthesis is also captured. In the present model at steady state the flux partitioning at S will determine the degree of futile cycling because of the constraints imposed by the M/N moiety couple. Such a constraint would indeed be removed by introducing an ATP consuming reaction. However, with this toy model the main aim was not to investigate the response of the system to changing energy demands; we therefore did not include an ATP consuming reaction.

The species H is not meant to refer to protons in a mechanistic way, but is included to generically couple the uptake of S into the vacuole to a secondary concentration gradient. Of course, equating H to protons in a detailed mechanistic model would be inappropriate, but we feel that this level of abstraction is justified in the toy model presented here, the purpose of which is primarily to demonstrate the feasibility of the modelling approach.

Partial differential equations

Table 3.1 gives the terms that will appear in the PDE for a species, depending on the compartment it is found in. The following shorthand will be used,

$$\partial_t = \frac{\partial}{\partial t}, \tag{3.1}$$

$$\Delta x = \frac{\partial}{\partial t} x + D_x \frac{\partial^2}{\partial z^2} x. \tag{3.2}$$

The equations governing the system are divided into four groups. The first group describes those species that are only involved in reactions, in other words species found in the leaf and vacuole,

$$\partial_t S_{so} = v_1 - v_2, \tag{3.3}$$

$$\partial_t S_{vc} = v_8 - v_6, \tag{3.4}$$

$$\partial_t P_{vc} = v_6 - v_9. \tag{3.5}$$

The PDEs governing species behaviour in the symplast are,

$$\Delta S_{sk} = v_3 + v_4 - (v_5 + v_8), \tag{3.6}$$

$$\Delta P_{sk} = v_5 + v_9 - (v_4 + v_{10}), \tag{3.7}$$

$$\Delta Y_{sk} = v_{10} - v_{11}, \tag{3.8}$$

$$\Delta M_{sk} = 4 \cdot v_{11} - (2 \cdot v_{10} + v_4 + v_7), \tag{3.9}$$

$$\Delta H_{sk} = v_8 - v_7. \tag{3.10}$$

Note that the stoichiometry for reaction 10 is $1P + 2M \rightarrow 1Y + 2N$ and for reaction 11 it is $1Y + 4N \rightarrow 1Z + 4M$. Reaction 10 is representative of upper glycolysis, where 2 ATP are used, and reaction 11 of lower glycolysis where 4 ATP are made. All other reactions have unitary stoichiometry. The specific case of assimilate translocation in the phloem is modelled by,

$$\partial_t S_{ph} + \kappa \mu^{-1} \cdot RT\Phi \cdot \partial_z^2 S_{ph} = v_2 - v_3. \tag{3.11}$$

Let C_1 and C_2 be constants, conservation relations are maintained with the algebraic expressions,

$$N_{sk} = C_1 - M_{sk}, \tag{3.12}$$

$$H_{vc} = C_2 - H_{sk}. \tag{3.13}$$

The v_i appearing on the right hand side of the PDEs are themselves functions, specifically $\mathbf{v} = \mathbf{v}(\mathbf{s}, \mathbf{p})$. The vector of reaction rates is a function of a species vector, $\mathbf{s}$ and parameter vector, $\mathbf{p}$.

Rate equations

The most general rate equation (RE) used is the bi-bi generic, reversible Hill equation [55, 88, 89],

$$\frac{v}{V_{\mathrm{f}}} = \left(1 - \frac{\Gamma}{K_{\mathrm{eq}}}\right) \cdot \frac{\left(1 + \gamma\alpha^2 m^h\right) \prod_{i=1,2} s_i \left(s_i + p_i\right)^{(h-1)}}{\mathbf{m} \cdot \mathbf{r}}, \tag{3.14}$$

$$\mathbf{m} = \left[1 + \alpha^0 m^h, 1 + \alpha^1 m^h, 1 + \alpha^2 m^h\right],$$

$$\mathbf{r} = \left[1, (s_1 + p_1)^h + (s_2 + p_2)^h, ((s_1 + p_1)(s_2 + p_2))^h\right]^T,$$

where s, p and m are respectively substrate, product and modifier concentrations scaled by their specific half saturation constants. V_{f} is the maximal forward activity, Γ is the mass action ratio and K_{eq} is the equilibrium constant for the reaction. h is the Hill coefficient [53, 54]. α and γ are the scaling coefficients, either activating or inhibiting the enzyme through, respectively, a K-effect or V-effect [6]. The dot product, $\mathbf{m} \cdot \mathbf{r}$, is used for convenience.

Two enzymes have allosteric and cooperative behaviour (reaction 10 and 11) and are therefore modelled with Equation 3.14. For the rest, $\alpha = \gamma = h = 1$, so in the bi-bi case Equation 3.14 simplifies to,

$$\frac{v}{V_{\mathrm{f}}} = \left(1 - \frac{\Gamma}{K_{\mathrm{eq}}}\right) \cdot \frac{s_1 s_2}{(1 + s_1 + p_1)(1 + s_2 + p_2)}, \tag{3.15}$$

and uni-uni reactions are still simpler,

$$\frac{v}{V_{\mathrm{f}}} = \left(1 - \frac{\Gamma}{K_{\mathrm{eq}}}\right) \cdot \frac{s}{1 + s + p}. \tag{3.16}$$

The solution(s) to the set of governing equations, the PDEs and REs, are determined by the choice of parameters.

Parameters

Because this is a toy model, assigning units to parameters and variables would be arbitrary. However, variables are in amounts, so concentrations are in amount per volume and therefore so are half saturation constants. Rates take their units from the maximal activities and these are in amounts per unit time, *not* concentrations per unit time.

The "ground state" for the model has all parameters set to a value of 1 — so-called vanilla kinetics. Any changes made to the ground state were only done to induce a certain behaviour. Furthermore, parameters were chosen to exaggerate the desired behaviour. This is discussed below.

Thermodynamic parameters Equilibrium constants were chosen with the following points in mind:

1. the preferred direction in which a reaction is to occur,

2. adherence to the Haldane relationship,

3. adherence to the Kirchoff loop rule, and

4. dependencies between equilibrium constants for coupled reactions.

Point 1 was addressed by not assuming any preference for substrates or products, except in the case where "energy equivalents" were made or consumed. The use of generic reversible Hill equations implicitly satisfies Point 2.

Kirchoff's loop rule states that the product of the equilibrium constants in a closed cycle be equal to 1. Points 3 and 4 are closely related. Consider the example, starting at the futile cycle in the model. Reaction 5, $S \rightarrow P$, is the opposite of the half reaction, $P \rightarrow S$, of enzyme 4. By definition, $K_{SP} = K_{PS}^{-1}$, therefore, $K_{SP} K_{PS} = 1$. Reaction 4 is able to have an equilibrium constant larger than K_{PS} because it is *coupled* to the half reaction, $M \rightarrow N$. This reaction does have a large equilibrium constant and $K_4 = K_{PS} K_{MN}$ can be large. But, $M \rightarrow N$, in both directions, is involved in other reactions. This places a constraint on the choice of equilibrium constants for those other reactions, because this equilibrium constant for the half reaction may *not* change.

The easiest way to satisfy all these criteria is to choose all equilibrium constants equal to 1. This we did, except for reactions 4, 7 and 10, which were chosen to be 10. This was because they are "energy driven" reactions. Point 3 is not violated for the proton gradient cycle (reactions 7 and 8). Neither do the half reactions, $P \rightarrow Y$ and $Y \rightarrow Z$ from reactions 10 and 11, because they only occur once in the model. Implicitly, $K_{YZ} = 10$, which is the reason why it can act as the driving force for the regeneration of the moieties, $N \rightarrow M$.

Kinetic parameters All substrate and product half saturation constants are set to 1. For reaction 10 and 11, $\alpha = \gamma = 0.8$ and the modifier half saturation constant is 5. The Hill coefficient in both reactions is 4, because both PFK and PK are tetramers. In reality the Hill coefficients are much lower (usually around 2). However, as mentioned the idea behind this model is to exaggerate slightly to study the desired behaviour in a reasonable amount of CPU time.

Amongst the maximal activities that remain constant with increasing z are those of assimilate synthesis in the leaf and of the phloem loading step. They were chosen to be the highest
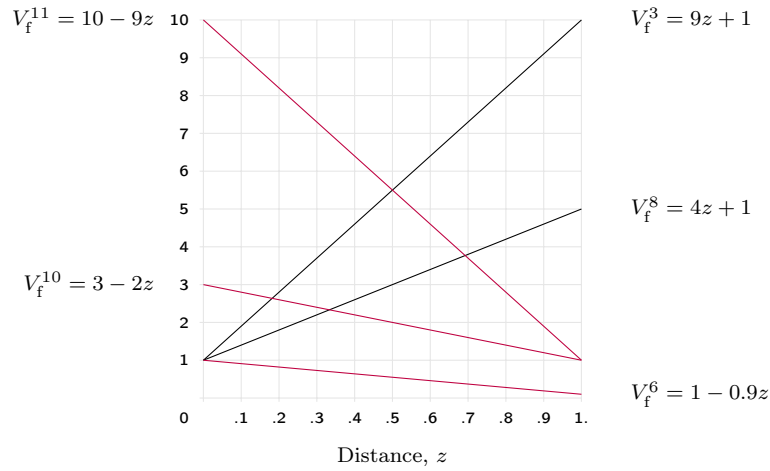
Figure 3.2: The change in maximal activities across stalk length for reactions 3, 6, 8, 10 and 11. The functions to the left and right of the plot are the straight line equations describing the maximal activity profile as a function of z.

activities, because there are only 5 points along the stalk that produce assimilate, but 50 that consume it. They were chosen to be $V_{\text{f}}^{1,2} = 10$.

The second group of activities chosen to remain constant were those of the two reactions involved in the futile cycle, the active proton transport across the vacuole membrane and the remobilisation step from the vacuole—reactions 4, 5, 7 and 9. These were kept in the vanilla state, i.e. equal to 1.

The maximal activities that change with increasing z are shown in Figure 3.2. Recall that z is defined on the interval $z \in [0, L]$ and that $L = 1$ in this geometry. The activities that increase with increasing z are the phloem unloading steps and the vacuolar accumulation steps.

The rough, guiding principle in selecting parameters was to see accumulation of S_{vc} along the stalk and with time. The ground state parameter set, all values equal to unity, unsurprisingly does not do this. The aim was to see if this behaviour could be induced with as few parameter changes as possible.

Flow coefficients Diffusion coefficients at the nodes are set at two orders of magnitude *smaller* (-10^{-7}) than the surrounding internodes (-10^{-5}). This leads to a "constriction" in the flow of metabolites in the symplast. The reason is that plasmodesmatal frequency between parenchymal cells is less at nodes or phloem loading sites [63]. The flow coefficient was given a value of,

$$\kappa/\mu \cdot RT\Phi = -1.0 \times 10^{-3}, \tag{3.17}$$

Table 3.2: Initial values of each species in each compartment

	X	S	P	M	N	H	Y	Z
Source	100	70	0	0	0	0	0	0
Phloem	0	20	0	0	0	0	0	0
Symplast	0	$14z + 1$	2	9	1	1	2	1
Vacuole	0	$140z + 10$	10	0	0	99	0	0

such that the diffusion coefficient in the symplast is at least two orders of magnitude smaller than the flow coefficient in the phloem. Since diffusion and translocation occur in the opposite direction to a concentration gradient, the convention is to choose negative flow parameters, so that fluxes are positive. In other words if the concentration gradient has negative slope, then the direction of flow is positive.

Initial conditions and boundary conditions   Boundary conditions are applied at $z = 0, L$, all concentrations, reaction rates and fluxes are 0. Constant boundary conditions are known as Dirichlet boundary conditions (see Section 3.6 for why one would possibly want to change this to non-constant (Neumann) boundary conditions).

The initial values of each species variable, with units in amounts, are given in Table 3.2. The amounts of the moiety conserved species sum to a constant as follows,

$$M_{sk} + N_{sk} = C_1 = 10 = 9 + 1,$$
$$H_{sk} + H_{vc} = C_2 = 100 = 1 + 99.$$

Software and programming

The model in this chapter was solved using the same software as in Chapter 2. FAST was implemented as shown in Appendix A. The Fast Fourier Transform (FFT) routines from the SciPy module, `scipy.fft`, and probability distributions from the SciPy statistics module, `scipy.stats`, were used.

3.5   Analysis

First of all a time course simulation was calculated. A sensitivity analysis was then performed to determine which parameters had the greatest influence on the variation in model output. Lastly, the reference model as defined in §3.4 was compared to two variants. The reference

model had constant source and phloem loading maximal activities. The first variant had a steep increase in activity, in other words synthesis in the leaf and phloem loading became faster with internode maturity. The second variant was just the opposite, activity decreased down the stalk. The next section summarises the development of concentration and reaction rate profiles during the time simulation.

Time simulation

The results of the time simulation are given in Figures 3.3 (concentration profiles) and 3.4 (reactions rates).

Sawtooth profiles S_{ph}, S_{sk}, S_{vc}, P_{sk} and P_{vc} all have "sawtooth" profiles to some degree. These peaks correspond to the node positions, This is where all the assimilate is being loaded and phloem unloading rates are the highest. Species are advected (phloem) or diffuse (symplast) away from the nodes. If the rate of translocation, advection or diffusion, is slower than the reaction rates or rate of facilitated transport, then species form a heap round the nodes.

"Sucrose" The highest concentrations throughout the simulation is that of the "sucrose" analog, as can be seen on the left hand side of Figure 3.3. S_{so} concentrations start evenly distributed along the stalk and end the simulation at a gradient monotonically decreasing with z. Similarly S_{ph} in general decreases down the stalk, except for the local peaks around the nodes. S_{sk} moves from an initial profile that increases linearly and then becomes constant with z—once gain with the exception of the node peaks. Towards the end of the simulation, the concentrations of S decrease from leaf, to phloem, to symplast and then increase in the vacuole. In other words, assimilate flow is down a concentration gradient. S_{vc} *increases* along the stalk, with concentrations at immature end climbing faster than those at the mature end.

Moieties The moiety pair, M_{sk} and N_{sk} have profiles across z and t that form mirror images of each other. The same is true of H_{sk} and H_{vc}. This is because the pairs always have to sum up to a constant. This is not immediately apparent from Figure 3.3 for H_{sk} and H_{vc}; this is because the vacuolar volume is larger than that of the symplast. The molar amounts of each do sum up to a constant.

Reaction rates As with the concentrations, reaction rates settle into stable profiles (at approximately $t > 128$). The rate of synthesis (v_1) in the leaf increases with z and t; this is due to decreasing S_{ph}. Similarly phloem loading (v_2) increases, because of increasing S_{so} and decreasing S_{ph}. Phloem unloading (v_3) falls to a level much lower than the loading rate,
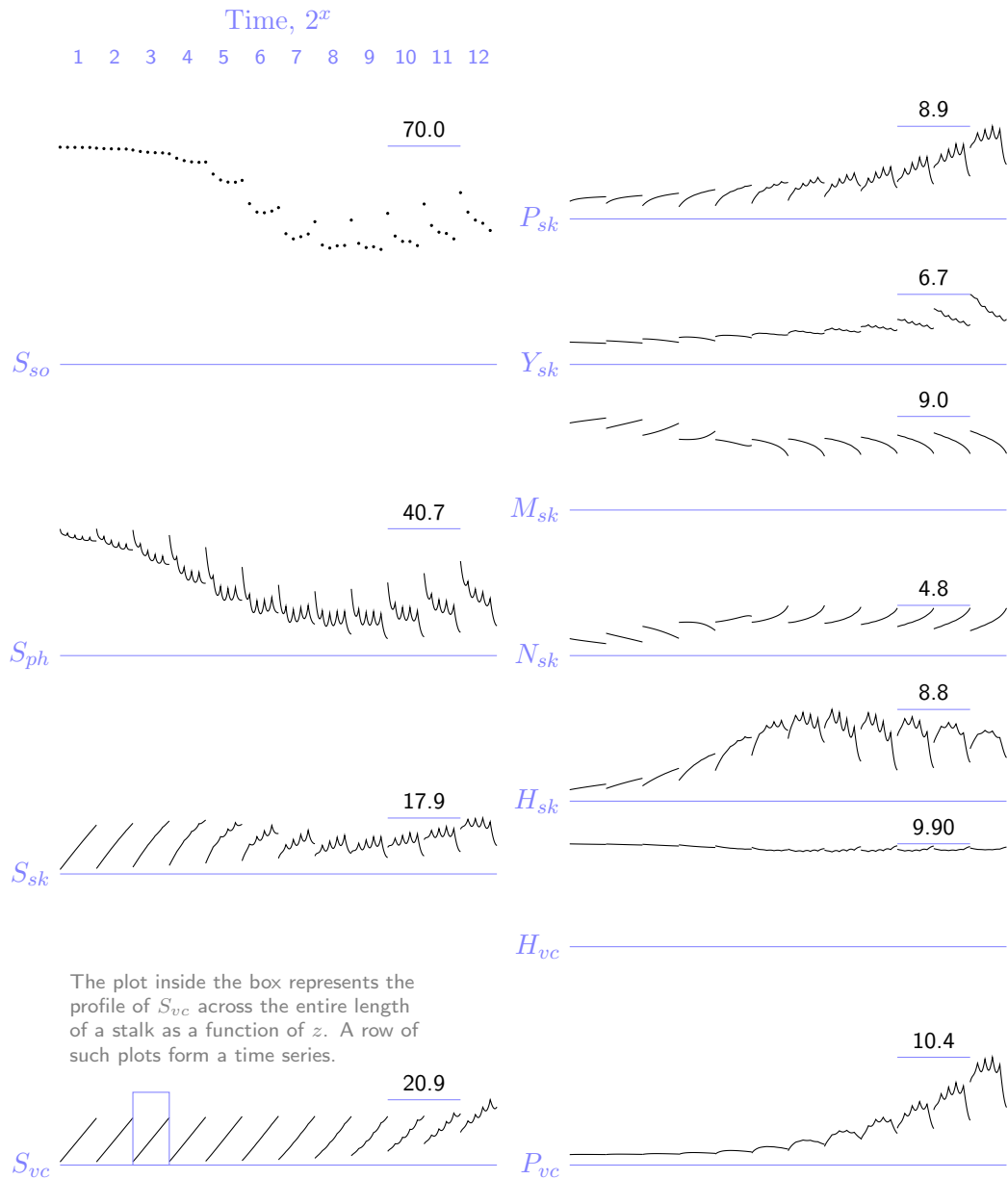
Figure 3.3: High (left) and low (right) concentrations for 2^{12} time steps, from a simulation of the toy model. Concentrations on the right are scaled by a factor of 3.3 compared to those on the left. Horizontal bars show maximum values reached during the simulation and give an indication of scale. S_{so} is only defined at a node and is therefore only plotted as dots. Those concentrations with a "saw-tooth" profile have each small peak corresponding to a node position. Note that the time scale is logarithmic and that all the S species have high concentrations.
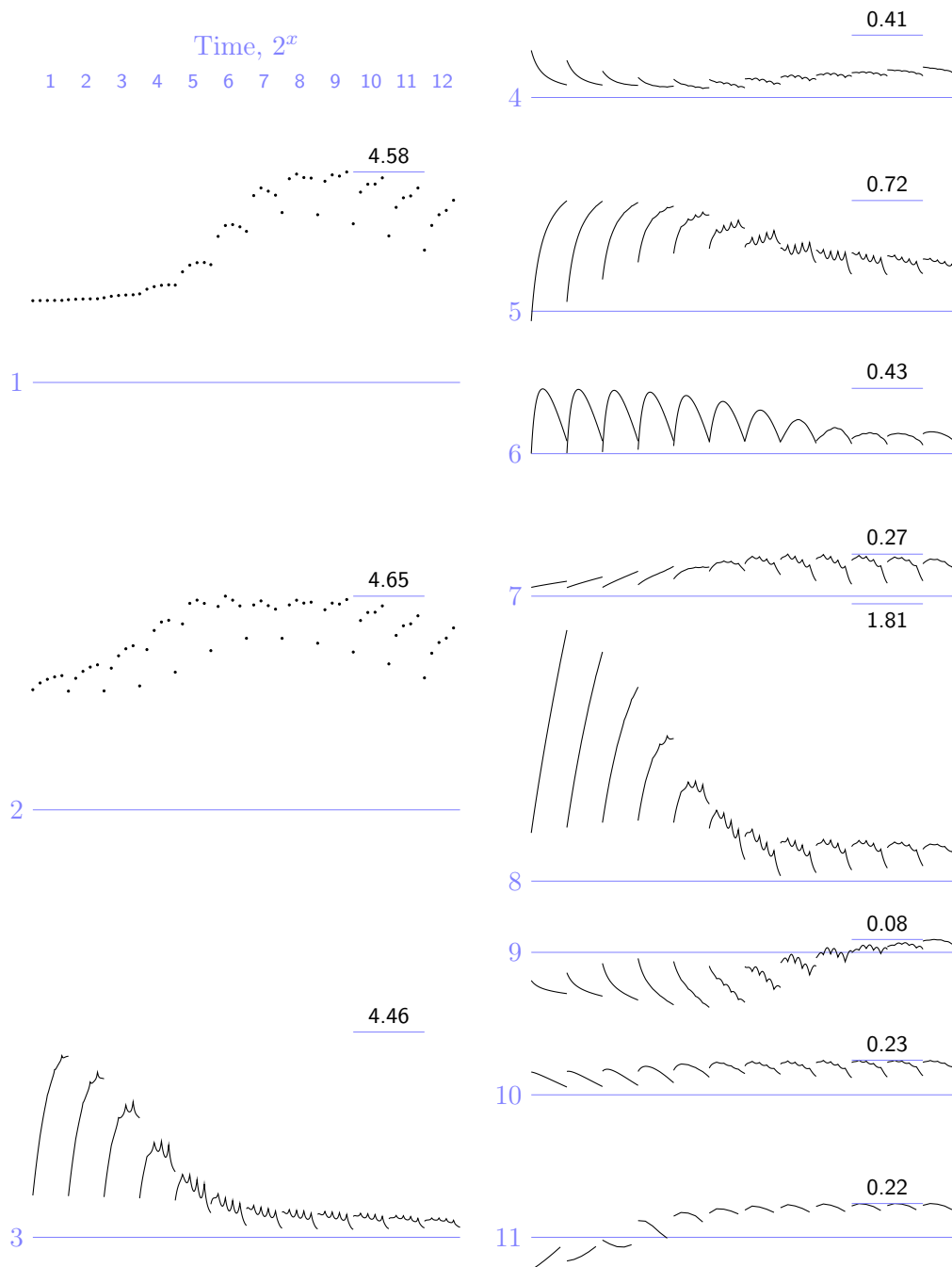
Figure 3.4: High (left) and low (right) reaction rates for 2^{12} time steps, from a simulation of the toy model. Rates on the right are scaled by a factor of 3.3 compared to those on the left. The layout is the same as for Figure 3.3. A single plot from a row represents the rate profile across the entire stalk. The time scale is logarithmic and horizontal bars show the maximum values. The single source reaction, phloem loading and unloading have the highest rates. Note the parabolic profile of reaction 6, this is discussed in Figure 3.9 and the text.
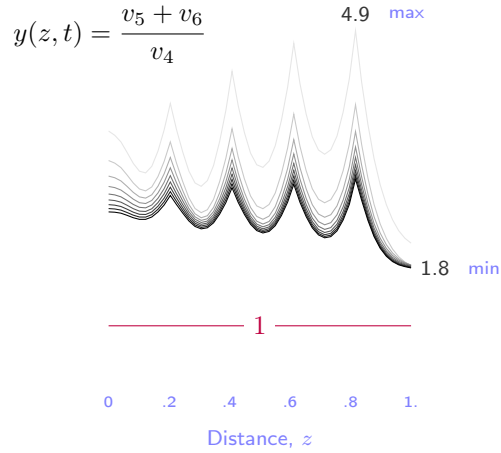
Figure 3.5: The ratio of S breakdown to synthesis as a function of time and distance. The x-axis indicates distance along the stalk. Different shades of grey indicate changes in simulation time, moving from $t = 4 \times 10^2$ (light gray) to $t = 4 \times 10^3$ (black). $y(z,t) > 1$, therefore more S is broken down than resynthesised. The percentage futile cycling is highest around the nodes. As time increases the overall degree of futile cycling decreases.

because 5 source elements have to supply 50 sink elements. Recall that an element with a node defined on it overlaps a part of the symplast. This is because there is parenchymal tissue at the nodes as well as in the internodal regions.

v_{10} and v_{11}, the cooperative, allosteric reactions, become stable relatively quickly, reflecting the allosteric inhibition by M_{sk}—homoeostasis is almost immediate. Since v_{11} is responsible for regenerating the energy equivalents, homoeostasis will impact the vacuolar uptake step. Furthermore, the moiety regeneration and consuming reactions are very close to being in a steady-state. In other words, $4 \cdot v_{11} - (2 \cdot v_4 + v_7 + v_{10}) \cong 0$ for the entire length of the stalk at $t = 2^{12}$ time steps.

v_6 has a very pronounced negative parabolic profile, that gradually disappears with time. This is discussed in detail in Section 3.6 and Figure 3.9.

Futile cycling v_4 and v_5 form a futile cycle in the symplast. v_5 is higher than v_4, therefore more S_{sk} is being broken down than is being regenerated by v_4. Likewise, breakdown in the vacuole by v_6 is also higher than v_4. This is illustrated in Figure 3.5.

Sensitivity of model output to parameters

Methods such as Metabolic Control Analysis [9, 10] exist for analysing steady-state, ODE based reaction kinetic models. The model presented here is neither at steady-state nor ODE based, and therefore a variational sensitivity analysis method, like FAST, was employed.

A sensitivity analysis of the model output, in the stable range, was performed. Specifically, the model was not analysed over the entire time range, but only at $t = 2^{12}$, the right most time point in Figures 3.3 and 3.4. The sensitivity analysis was done using the FAST algorithm as described in Appendix A. Briefly, the parameters are assigned a unique frequency. The parameters are allowed to oscillate at that frequency for a short run of the model, which results in oscillating model output. Because the frequencies of the parameters are known, the fraction of the variance in the model output due to each parameter can be calculated from a Fourier transform of the output.

Any model is only an abstraction or approximation of a real system. This is partly due to uncertainty in model parameters. The aim of the analysis was to find out which parameters had the greatest influence on possible variation in the model output. These would be parameters which cannot afford to have huge uncertainty attached to them. If this were a real experiment, these would need to be measured with greater accuracy than the others, since they would influence the accuracy of the model the most.

Model parameters were allowed to vary within a range of $\pm 10\%$ of their initial values. Not all the parameters were varied at the same time, since the number of model runs required for the analysis increases exponentially with the number of parameters. For N parameters, the number of model runs would be $\sim 2.6\ N^{2.5}$ [74]. The parameters were divided into 4 classes— maximal activities, equilibrium constants, Hill coefficients and half saturation constants. Each class was analysed separately.

The sensitivity of the model output to the maximal activities, equilibrium constants and Hill coefficients are shown in Figure 3.6 and half saturation constants in Figure 3.7. In all cases a characteristic diagonal band can be seen for the sensitivity of a reaction rate to one of the four parameter classes. This reflects the intuitive fact that all rate equations are naturally sensitive to their own parameters.

Sensitivities take values on the interval 0 to 1, in some cases they also sum to 1. As an example consider the S_{ph} columns in Figure 3.6 for each of the three different parameters. All the sensitivities sum to 1 across a particular position along the stalk. This need not be the case, such as when the oscillation of two or more parameters cancels any variation in the model output, in other words when there is confounding or aliasing between parameters. This is quite possible with the models considered here, given the fact that they are highly non-linear. The implementation of FAST used here cannot analyse interactions between parameters and could be the subject of future work. This is discussed further in Appendix A.

Maximal activities, equilibrium constants and Hill coefficients S_{ph} illustrates the fact that sensitivity can vary quite dramatically across the stalk. S_{ph} is most sensitive to parameters
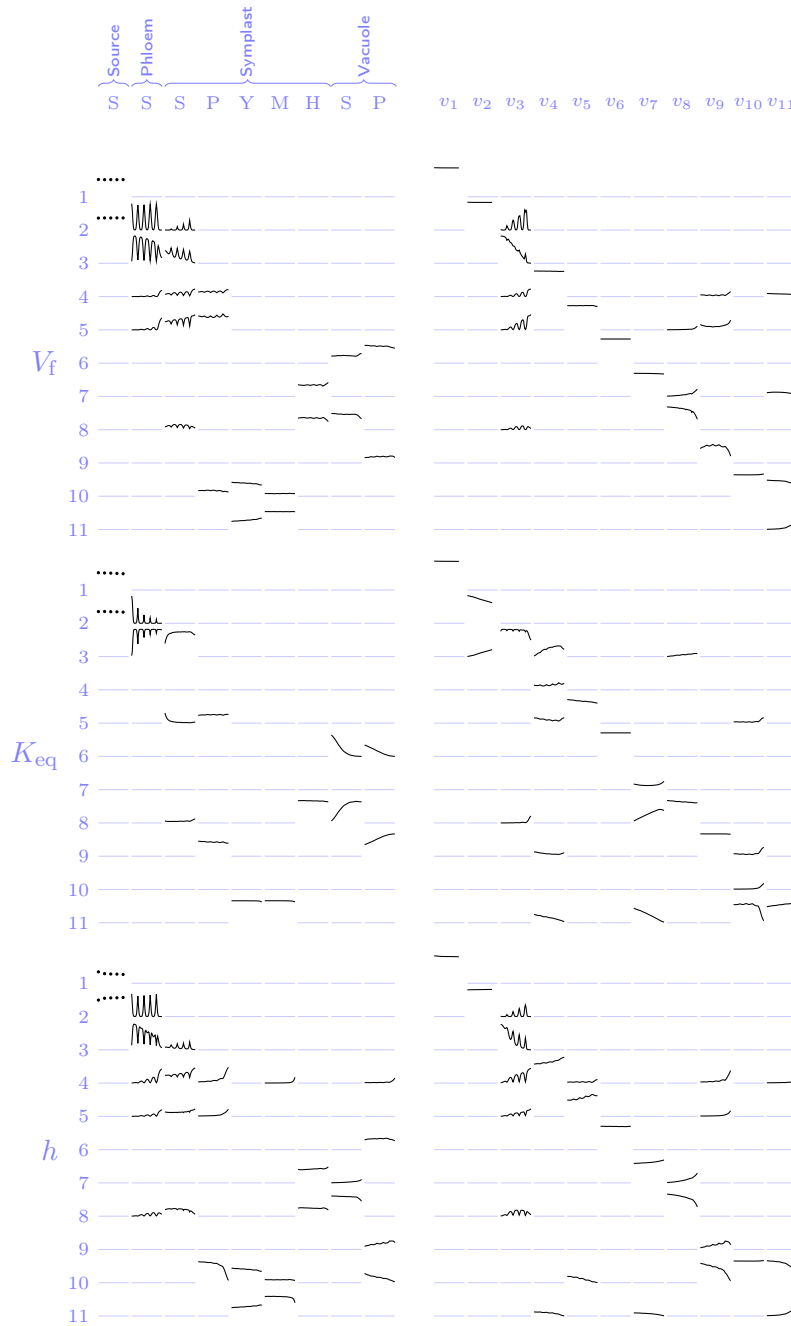
Figure 3.6: Sensitivity of concentrations and reaction rates (columns) to three sets of parameters. The parameters that were varied are arrayed down the left hand side and the state variables (model output) are shown along the top. Not all the parameters were analysed together, maximal activities, equilibrium constants and Hill coefficients were analysed separately. Sensitivities vary between 0 and 1. In most cases they should add up to 1 as well. If they do not then other sources of variation possibly exist. A single, small, plot represents 50 data points, in other words it is the sensitivities across the entire stalk. Sensitivities are only shown if at least one value across the length is higher than 1/11.

Figure 3.7: Sensitivity of concentrations and reaction rates (columns) to 10% variation in the half saturation constants. An upper case S or P denotes substrate or product, subscripts indicate the specific reactant and superscripts associate the reactant to a reaction. The layout is the same as for Figure 3.6.

belonging to reaction 2 *at the nodes* and least in the middle of an internode, inversely so for parameters of reaction 3. The sensitivity profiles for S_{ph} with respect to reactions 2 and 3 are in fact mirror images of each other. At the nodes, S_{sk} is most sensitive to the maximal activities of phloem loading but between the nodes it is more sensitive to unloading than loading. In the middle of an internode, S_{sk} is the most sensitive to the breakdown (reaction 5) maximal activity. This sensitivity also increases along the stalk. S_{vc} is consistently sensitive to its own breakdown and vacuolar uptake across the stalk. v_1 and v_2 are completely insensitive to what happens in the symplast. Phloem unloading becomes increasingly sensitive to phloem loading along the stalk, but only at the nodes, likewise for the symplastic breakdown step, but only in the internodes.

Half saturation constants   In general, concentrations and reaction rates show little sensitivity to half saturation constants of reactions that they are not directly involved in. v_{10} is most sensitive to the half-saturation constants for M_{sk} and N_{sk} (for reaction 10) rather than those for P_{sk} and Y_{sk}. v_{11} is also more sensitive to these two constants rather than its own. A possible reason for this could be that M_{sk} and N_{sk} enter the PDEs with stoichiometries of 2 and 4 for reactions 10 and 11 respectively, thereby amplifying the sensitivity.

Changes in source activity

A comparison of three models each with a different source activity profile is shown in Figure 3.8. Model 0 has the same maximal activities for each leaf. Model 1 has activites that increase across the length of the stalk, consistent with the idea that sugar transporter RNA might increase similarly [90]. Alternatively, Model 2 has an activity profile that decreases along the stalk. This could be explained by the shading of the lower leaves by those higher up on the plant. The comparatively large differences in concentrations are due to very small differences in reaction rates. The reference model has an overall negative S_{ph} gradient and a positive S_{vc} gradient, as opposed to the model with increasing maximal activities, which shows a predominantly positive gradient in the phloem and a steep positive gradient in the vacuole. The third model shows the beginning of a saturation effect. v_1 and v_2 in the third model show a characteristic parabolic profile. The same rates in the second model have a very steep profile, more so than the reference model. Model 2, with decreasing source maximal activities, most closely follows the sucrose gradients found in sugarcane (see for example Komor [14]). This is no doubt the consequence of the choice of decreasing maximal activities.
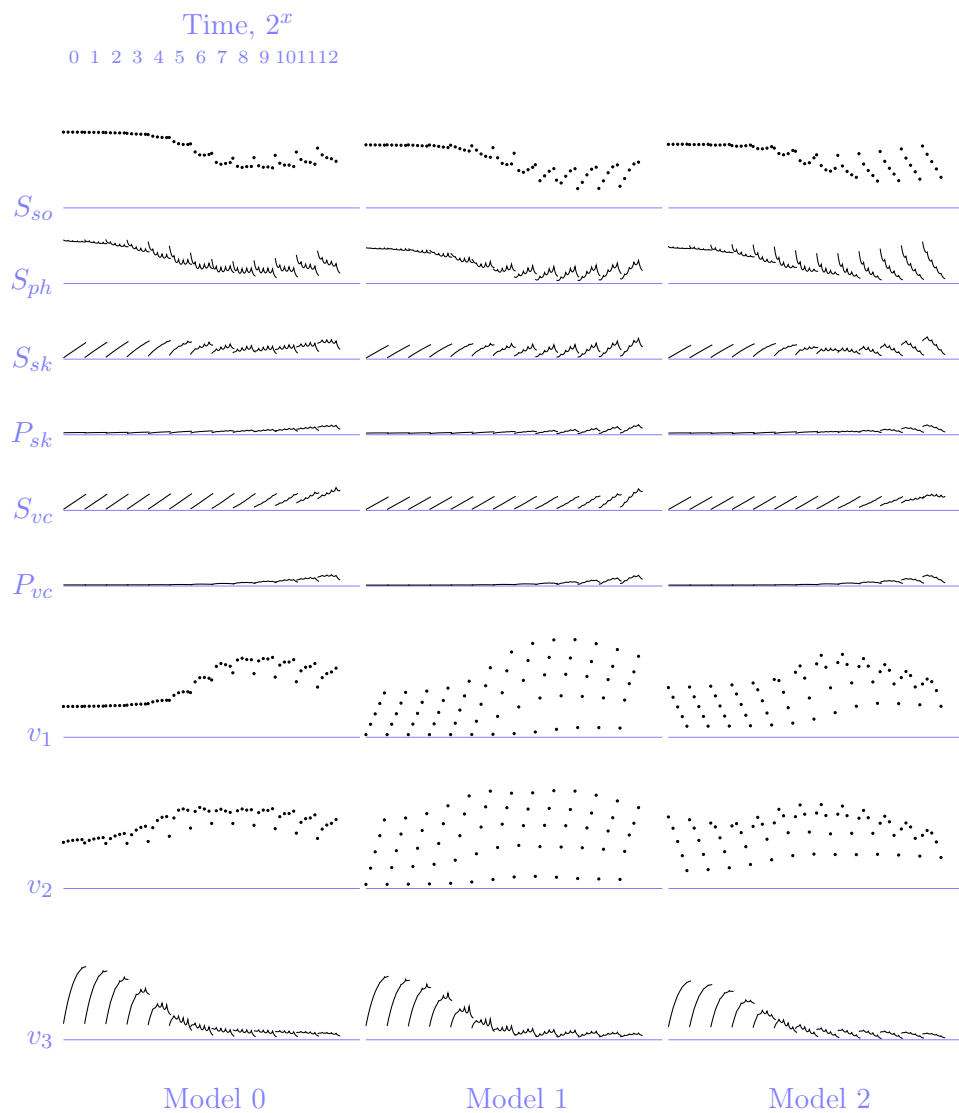
Figure 3.8: Comparison of selected concentrations and rates for three model variants, only those concentrations and rates are shown that differ from the reference model (Model 0). Differences are due to a linear increase (Model 1) and decrease (Model 2) in maximal activities for reaction 1 and 2 over the stalk length z. The reference model has these activities constant across z.

3.6 Discussion

The framework developed in Chapter 2 has been successfully applied to a model with a more intricate reaction network. Furthermore, it was also shown that a generic, global sensitivity analysis method, such as FAST, can be implemented with ease and applied to the model. The greater detail in this model also makes it more applicable to sugarcane and is a step closer to implementing a full scale realistic model of sucrose accumulation.

Modelling and methodology Criticism of the model formulation yields the following points:

1. The intricate network of reactions in the leaf is abbreviated to one reaction in the model. This assumption is partly based on the finding that photosynthetic rates respond to changes in demand rather than the other way around [61, 91].

2. The model does not account for growth or volume changes with time. Large time scales therefore do not give an accurate picture of what happens in the plant. To model growth a method such as "adaptive meshing" would be required to literally adapt the domain to the change in geometry [92]. PDEs that account for volume changes and partitioning of carbohydrates to structural components would be needed as well.

3. There is an achievable method of modelling growth with the current formulation, namely to change the Dirichlet boundary conditions to Neumann boundary conditions. Suppose $y = f(x, \partial x)$ is some function of interest on the interval $[a, b]$, then the Dirichlet boundary condition would be $y(a) = c_1$ and $y(b) = c_2$. The Neumann boundary condition is slightly more complicated, $\partial_x y(a) = c_3$ and $\partial_x y(b) = c_4$. The modelling approach thus far has set all state variables to zero at the boundaries. Although changing these to Neumann boundary conditions would not explicitly model growth, the supply or demand for reactants can take place across the boundaries. Furthermore, this exchange can change with growth.

4. For a particular position z on L, $H_{sk} + H_{vc}$ is equal to the same constant as the same sum at an immediate, neighbouring position. H_{sk} is able to diffuse, but H_{vc} is not. This means they do not have to sum to the same constant as one moves from element to element along the stalk. This is not actually a problem since the total amount of H in the *entire* stalk does not change. Thus, there can be a local violation of the moiety conservation but not across the length of the stalk.

5. To a lesser extent the same applies to M_{sk} and N_{sk}. It is not as big a problem because both these species exist in the same compartment. Diffusive effects even out the concentrations to a uniform distribution if a local rate were to temporarily violate the moiety sum.
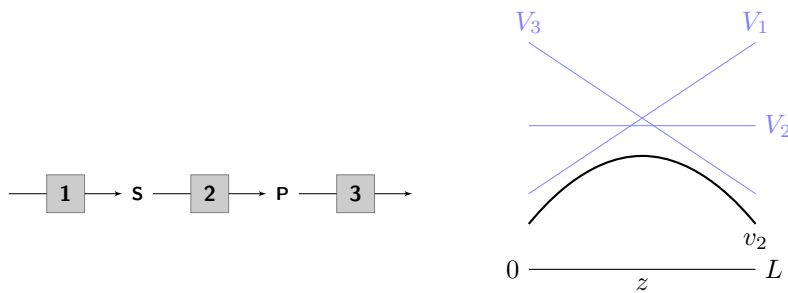
Figure 3.9: A possible explanation for the prevalence of higher rates in the center of the stalk—the origin of parabolic rate profiles. v_6 in the reference model (Figure 3.4) is an example of this.

Time simulation Figure 3.9 attempts to explain the cause of the observed parabolic reaction rate profiles. Suppose a reaction is sandwiched between two others, such as reaction 2 in the scheme on the left. If the maximal activity for the first reaction increases with length and that of the third reaction decreases, such as V_1 and V_3 in the plot on the right, then the highest rate that v_2 can attain will be where V_1 and V_2 crosses. Furthermore assume that its own maximal activity remains constant along z (V_2). Close to the left hand side the rate, v_2, cannot, run faster than v_1 without starting to deplete the linking metabolite/s which will of course slow down v_2. By symmetry the same applies to v_2 and v_3. v_2 is fastest somewhere in the middle of L where it has a steady supply of substrate and its products are being removed fast enough not to become inhibiting. This could account for the observation that rates of growth and accumulation in medium mature tissue in sugarcane is the fastest. It could be a consequence of reciprocal profiles of up and down regulation of enzymes along the stalk. An example of experimentally determined, steady-state fluxes that are higher in the medium mature internodes, rather than the surrounding internodes, is found in [71]. They found that the flux to sucrose from the hexose phosphate pool is 2.85 ± 0.40, 7.63 ± 2.17 and 4.73 ± 1.12 nmol hexose equivalents per mg protein per min, for internodes 3, 6 and 9, representing immature, medium mature and mature tissue.

Sawtooth profiles are a result of phloem loading being faster than translocation away from the source. Since assimilate flow is down a concentration gradient, this means that flow can be up or down the stalk.

Sensitivity analysis The uncertainty in parameters translate into uncertainty or variation in model output. It could also be the case that parameters may vary legitimately within a range and there is nothing uncertain about them. The fact remains that it is desirable to know what the contribution from a particular parameter is to model output variation. To this end the FAST method was used to perform a sensitivity analysis.

Sensitivities were not calculated for the entire model run of 4096 time steps. Although desirable, it would take an inordinate amount of time to do so. The model was only analysed from the stable region onwards for approximately 10 time steps. The sensitivities can possibly increase or decrease with time. The conclusions drawn from a such a time dependent sensitivity analysis may well alter if a different region in the model run was to be analysed.

In almost all cases, reaction rates are the most sensitive to their own parameters. One exception to this is reaction 8 (the vacuolar uptake step) which is sensitive to the parameters of reaction 7 (the proton gradient regeneration step). This is to be expected, since reaction 8 can not accumulate S_{vc} against a gradient without being coupled to an energy releasing reaction. In other words, $S_{vc}/S_{sk} \not> K_8$, if not for the expenditure of energy.

3.7 Conclusion

A model was built according to the guidelines in Section 3.2 and analysed using FAST. Three variants of the model, representing negative, positive and zero slope profiles of source maximal activities, were compared. The main findings were:

1. There is a net flow of assimilate down a concentration gradient in the phloem and a net accumulation of assimilate against a concentration gradient in the vacuole.

2. The rate of uptake by the vacuole is most sensitive to its own parameters and that of the proton gradient regeneration reaction.

3. The parabolic rate profiles across the length of the stalk is a possible explanation for the observation that medium mature tissue grows the fastest.

4. A decrease in the maximal activities of source reactions and phloem loading along the length of the stalk offers the best explanation for the observed saturation effect seen in sugarcane.

This work preempts a more complete and realistic model of sucrose accumulation in sugarcane. It is the aim in Chapter 4 to build such a model.

Chapter 4

Kinetic model of sucrose accumulation coupled to a phenomenological model of vascular transport

4.1 Introduction

Wu & Birch [91] showed that the total sugar content in sugarcane can be doubled by introducing a sucrose isomerase into the storage parenchyma that localises to the vacuole. Sucrose was converted to isomaltulose, a sugar that is metabolised by humans but not plants. This effective increase in sink strength is also accompanied by an increase in photosynthesis and sucrose transport. The regulation of photosynthesis by sink demand was also shown by McCormick *et al.* [60]. Sugarcane evidently has the ability to produce more sucrose and has the space to store it.

This chapter expands on an existing kinetic model of sucrose accumulation in sugarcane and casts it in the advection-diffusion-reaction framework of Chapter 2. The model is also analysed with the FAST algorithm from Chapter 3.

The physical properties of a sugarcane stalk that change with time include, for example, the number, mass and volumes of nodes and internodes. Biochemical properties, such as the amount and type of various proteins, also change. The point is that sugarcane, or any organism for that matter, is a dynamic system comprising many thousands of components. Needless to say, not every change is made explicit in the model. For example, protein and cofactor concentrations, as well as the lengths or volumes of all the internodes and physico-chemical properties, such as viscosity, are treated as constants. The model in this chapter is more realistic than those in the previous chapters in the sense that the physical dimensions of the stalk, maximal activities and

initial concentrations, amongst other factors, are close to experimentally determined values. The assumptions that are made are abstractions, they aid in simplifying the model without necessarily detracting from the validity of the results.

Differences between this model and previous models   The model includes compartments, specifically the phloem, symplast (or the cytoplasmic continuum), apoplast (free space) and the vacuoles. Phloem loading, unloading and assimilate translocation is included. The introduction of the phloem means that all internodes are supplied with sucrose from one "continuous" compartment. This differs from the approach used by Uys *et al.* [33], where each internode was modelled independently.

There are a few changes in the pathway definition between this model and previous versions [26, 33]. There is one explicit source of sucrose, as opposed to two sources of hexoses. This model also spans eight internodes, but internodes are linked by the phloem. This of course means that the internodes are also modelled as being spatially separated. Phloem unloading of sucrose can occur apoplastically or symplastically. The apoplast is now an explicit compartment and an apoplastic invertase has been added. Likewise, the vacuole is also explicit with its own invertase. The vacuole, as before, acts as the primary assimilate sink, but the remobilisation of hexoses is now possible. The phosphorylation of fructose is now solely carried out by fructokinase A. Previous modelling has shown that fructose phosphorylation by hexokinase and fructokinase B is negligible [33]. None of the known isoforms of sucrose synthase are modelled explicitly; all reactions are now modelled using generic reversible Hill equations and most of the reactions are now reversible.

We start, as before, by defining the geometry of the problem.

4.2   Geometry, mesh and domain

Eight nodes and internodes were modelled. These internodes are numbered 3 to 10 and are representative of immature to mature tissue. The labelling follows the convention of numbering from directly below the first visible dewlap at the top of the stalk. In general, internodes 1 and 2 are too small to study and enzyme assays are only performed on tissue from internodes 3 to 10. The sugarcane stalk is approximated by a line segment and divided ("meshed") into 276 finite volumes. The relative and reaction volumes for each internode are given in Tables 4.1 and 4.2. The conversion of the volumes into internodal lengths and the steps to creating a mesh are illustrated in Figure 4.1. Each finite volume corresponds to 1 mL (or cm^3), hence the division into 276 finite volumes to correspond to a length of 52.0 cm. The length of a finite volume is ≈ 0.188 cm. The phloem loading region is defined for two cells at a node.

Table 4.1: Various ratios of compartmental volumes with respect to each other. On the diagonal is the reference volume. Values to the left and right are multipliers to find a compartment volume relative to the reference. Variations between internodes are ignored. Relative phloem volume is estimated from [93], all other data are from [30, 33]. The actual volumes are given in Table 4.2.

	Stalk	Phloem	Apoplast	Symplast	Vacuole
Stalk	1	0.2	0.08	0.072	0.648
Phloem		1	0.4	0.36	3.24
Apoplast		2.50	1	0.9	8.1
Symplast		2.78	1.11	1	9
Vacuole		0.31	0.12	0.11	1

Table 4.2: The specific and total water volumes. By using the conversion factors from Table 4.1 the volume of water per gram fresh weight $(L (g FW)^{-1})$ per compartment per internode can be calculated. These values can then be used to calculate the total water volume per compartment per internode. Internode mass is estimated from data in [38].

	Internode								
	3	4	5	6	7	8	9	10	
Mass (g FW)	15	22	29	35	42	50	59	70	
	Volume of water per gram FW $(L (g FW)^{-1})$								
Stalk	9.20	9.12	8.97	8.76	8.52	8.36	8.27	8.24	$\times 10^{-4}$
Phloem	1.84	1.82	1.79	1.75	1.70	1.67	1.65	1.65	$\times 10^{-4}$
Apoplast	7.36	7.29	7.17	7.01	6.82	6.69	6.62	6.59	$\times 10^{-5}$
Symplast	6.63	6.56	6.46	6.31	6.13	6.02	5.95	5.93	$\times 10^{-5}$
Vacuole	5.96	5.91	5.81	5.68	5.52	5.41	5.36	5.34	$\times 10^{-4}$
	Total water volume per compartment (L)								
Stalk	1.38	2.01	2.55	3.07	3.58	4.18	4.90	5.76	$\times 10^{-2}$
Phloem	2.76	4.01	5.11	6.13	7.17	8.36	9.79	11.5	$\times 10^{-3}$
Apoplast	1.10	1.60	2.04	2.45	2.87	3.34	3.92	4.61	$\times 10^{-3}$
Symplast	0.994	1.44	1.84	2.21	2.58	3.01	3.53	4.15	$\times 10^{-3}$
Vacuole	0.895	1.30	1.66	1.99	2.32	2.71	3.17	3.74	$\times 10^{-2}$
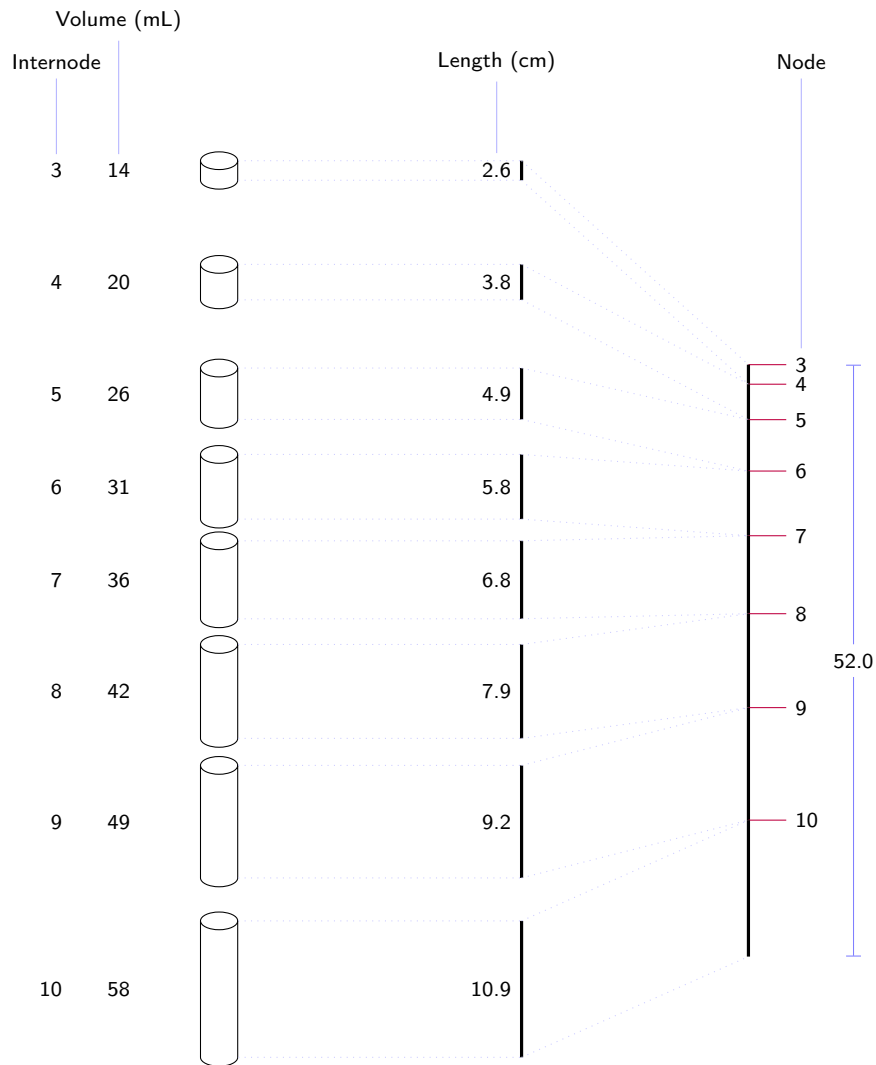
Figure 4.1: The steps taken to calculate internode lengths and finding the number of elements to an internode. The volume of water per gram fresh weight per internode remains fairly constant across the length of the eight internodes (See Table 4.2). Assuming the cross sectional surface area remains constant for internodes 3–10 and using estimates of internode mass [38], the length of an internode can be calculated (in cm). Element size is chosen to correspond to 1 cm^3, i.e. there are as many elements to an internode as there are milliliters. Conversion of moles of reactants to mM takes place before substitution into rate equations. The face where two internodes meet is the site of a point source, i.e. a leaf or a node as indicated on the right.

Table 4.3: Abbreviations and allocation of reactants to compartments. Also indicated is whether a reactant concentration is constant or variable.

● Variable
○ Constant

	Source	Phloem	Apoplast	Symplast	Vacuole	
S	○	●	●	●	●	Sucrose
S^P				●		Sucrose-6-P
F			●	●	●	Fructose
G			●	●	●	Glucose
F^{6P}				●		Fructose-6-P
G^{6P}				●		Glucose-6-P
G^{1P}				●		Glucose-1-P
G^U				●		UDP-Glucose
F_P^P				●		Fructose-1,6-P
GAP				○		Glyceraldehyde-3-P
DHAP				○		Dihydroxyacetone-P
UDPGA				○		UDP-Glucuronic acid
PP_i				○		Pyrophosphate
P_i						Inorganic phosphate
ATP				○		
ADP						
NAD				○		
NADH						

4.3 Pathway and partial differential equations

The pathway for a single node and internode pair is shown in Figure 4.2 and all the reactants, compartments and their abbreviations are listed in Table 4.3. Variables in the model are reactant µmol amounts, although not all reactants are variables. Reactant amounts that are treated as constants are also indicated in Table 4.3. For the purposes of this model it is assumed that a "leaf" overlaps a segment of the stalk by two cells in the mesh.

F^{6P}, G^{6P}, G^{1P} and G^U are grouped into a single hexose phosphate equilibrium block. This is identical to the approach used in [26] and [33]. Figure 4.3 and §4.5 provides more detail.

Terms in the PDEs have units of amount per time, specifically $\mu\text{mol min}^{-1}$. Each reactant in a compartment appears as a separate variable in the model. The rate equations appearing on the right hand side of the PDEs are defined in §4.4. By defining the following abbreviations, the PDE for each variable can be formulated, depending on the type of compartment it is found
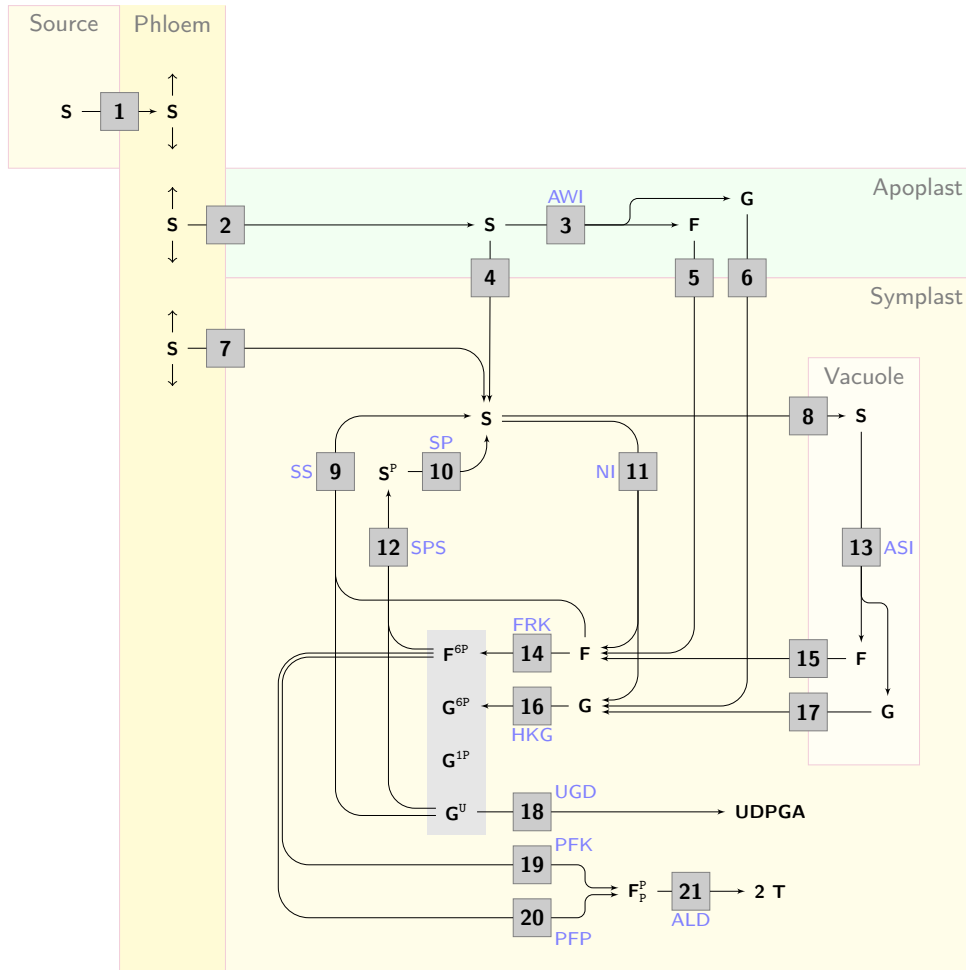
Figure 4.2: The pathway across four model compartments of a node/internode pair. Reactant abbreviations are defined in Table 4.3

in:

$$\partial_t x_k = \frac{\partial}{\partial t} x_k, \tag{4.1}$$

$$\partial_z^2 x_k = \frac{\partial^2}{\partial z^2} x_k, \tag{4.2}$$

$$\Delta x_k = \partial_t x_k + D_x \partial_z^2 x_k, \tag{4.3}$$

where t is time, x is a variable (reactant amount), z is the distance along the stalk and D_x is the diffusion coefficient for a reactant. k refers to a compartment and can be the phloem (ph), apoplast (ap), symplast (sk) or vacuole (vc).

The PDE modelling phloem translocation of S is given below. The only terms that appear are for osmotically driven advection [34] and un/loading of sucrose. Diffusion is neglected, since

its effect is approximately two orders of magnitude smaller than the pressure driven flow,

$$\partial_t S_{ph} + \left(k\mu^{-1} RT\Phi\right) \partial_z^2 S_{ph} = v_1 - (v_2 + v_7). \tag{4.4}$$

Molecular diffusion is modelled in the apoplast, invertase activity and cross-membrane transport. Reactants in the apoplast are modelled with,

$$\Delta S_{ap} = v_2 - (v_3 + v_4), \tag{4.5}$$

$$\Delta F_{ap} = v_3 - v_5, \tag{4.6}$$

$$\Delta G_{ap} = v_3 - v_6. \tag{4.7}$$

The hexose phosphate equilibrium block in the symplast is modelled with the following PDE, the calculation of individual members of the block is given in Equation 4.21,

$$\Delta H = v_{14} + v_{16} - (v_9 + 2 \cdot v_{12} + v_{18} + v_{19} + v_{20}), \tag{4.8}$$

where H is the number of moles of total hexose phosphates. The rest of the reactants in the symplast are governed by,

$$\Delta S_{sk} = v_4 + v_7 + v_9 + v_{10} - (v_8 + v_{11}), \tag{4.9}$$

$$\Delta S_{sk}^{\mathrm{P}} = v_{12} - v_{10}, \tag{4.10}$$

$$\Delta F_{sk} = v_5 + v_{11} + v_{15} - (v_9 + v_{14}), \tag{4.11}$$

$$\Delta G_{sk} = v_6 + v_{11} + v_{17} - v_{16}, \tag{4.12}$$

$$\Delta F_{\mathrm{P}}^{\mathrm{P}} = v_{19} + v_{20} - v_{21}. \tag{4.13}$$

And finally the reactants in the vacuole are only transported across the tonoplast or involved with ASI. They are modelled with,

$$\Delta S_{vc} = v_8 - v_{13}, \tag{4.14}$$

$$\Delta F_{vc} = v_{13} - v_{15}, \tag{4.15}$$

$$\Delta G_{vc} = v_{13} - v_{17}. \tag{4.16}$$

The indexing (i) used for the various reactions rates (v_{i}) is given in Figure 4.2 and Tables 4.4 & 4.5. The particular shape and form of the various rate equations are described next.

4.4   Rate equations

Depending on the enzyme cooperativity, allostery and reaction stoichiometry, various flavours of a generic reversible Hill (GRH) equation are used [53, 55, 89]. The following non-cooperative

GRH (i.e. reversible Michaelis-Menten) is used for modelling reactions with equal numbers of reactants and products,

$$\frac{v}{V_\text{f}} = \left(1 - \frac{\Gamma}{K_\text{eq}}\right) \cdot \prod_i \frac{s_i}{(1 + s_i + p_i)}, \tag{4.17}$$

where,

- v is the rate,

- V_f is the maximal forward activity, with units $\mu\text{mol}\,\text{min}^{-1}$,

- Γ is the mass action ratio (in some literature denoted by Q),

- K_eq is the equilibrium constant,

- $(1 - \Gamma/K_\text{eq})$ therefore determines the direction of the reaction,

- s and p are concentrations scaled by their half-saturation constants,

- i is an index ranging over the set of substrate/ product pairs.

Specifically, reactant terms appear as,

$$s = \frac{S}{S_H \cdot V} = \frac{\text{moles substance}}{\text{half saturation constant} \times \text{volume}}. \tag{4.18}$$

Uni-bi reactions reactions are modelled as,

$$\frac{v}{V_\text{f}} = \left(1 - \frac{\Gamma}{K_\text{eq}}\right) \cdot \frac{s}{1 + p_1 + p_2 + s + p_1 p_2}. \tag{4.19}$$

Setting m to be the scaled modifier (ATP) concentration and h to be the Hill coefficient, PFK is modelled as,

$$\frac{v}{V_\text{f}} = \left(1 - \frac{\Gamma}{K_\text{eq}}\right) \cdot \frac{(1 + \alpha^2 m^h) \prod_i s_i (s_i + p_i)^{(h-1)}}{\mathbf{m} \cdot \mathbf{r}}, \tag{4.20}$$

$$\text{with} \quad \mathbf{m} = \left[1 + m^h, 1 + am^h, 1 + a^2 m^h\right],$$

$$\text{and} \quad \mathbf{r} = \begin{bmatrix} 1 \\ (s_1 + p_1)^h + (s_2 + p_2)^h \\ (s_1 + p_1)^h (s_2 + p_2)^h \end{bmatrix}.$$

The right hand side of Equations 4.17, 4.19 and 4.20 is dimensionless, therefore v takes its units from V_f. The units are $\mu\text{mol}\,\text{min}^{-1}$ for rates and μmol for reactants. Obtaining

concentrations for reactants is easy. The volume for an element in the mesh is chosen to be 1 mL, therefore the number indicating the µmol amount in an element is at the same time the concentration for that reactant in $\mathrm{µmol\,mL^{-1}}$. By implication concentrations are also in $\mathrm{mmol\,L^{-1}}$, or millimolar (mM). *Note that the concentration of a species is thus the concentration in a particular compartment,* and not the concentration across a whole element (refer to Table 4.1).

4.5 Parameters

Where possible, consistency of a data set was the first criterion in the parameter selection process. Therefore equilibrium constants were calculated from transformed standard Gibbs energies of *formation* for reactants and products or from the transformed standard Gibbs energy of a *reaction*. For maximal activity measurements to be compatible with each other, a consistent set of measuring conditions is required. In other words, enzymes should come from the same plant, the same tissue and preferably from the same sample. The same person should analyse the sample, in the same laboratory, with the same reagents, and so forth. This is in most cases intractable, or at least, it has not been done for sugarcane to date. A few enzyme assays come close to fulfilling these requirements and these are discussed below and in Appendix B.

Equilibrium constants Equilibrium constants are shown in Tables 4.4 and 4.5. Equilibrium constants depend on, amongst others, pH (or hydrogen activity), pMg (more generally, ionic strength) and temperature [105, 106]. Where possible, values were taken or calculated from standard tables of transformed thermodynamic properties [94, 95, 105]. Alternatively, experimental data was used [107]. Temperature was taken to be 298 K, pH 7 and ionic strength $250\ \mathrm{mmol\,L^{-1}}$.

The values of the equilibrium constants reported for the SS catalysed reaction, in the **direction of sucrose synthesis** are, 2–8 [96], 1.4 and 1.8 [97]. In the **direction of sucrose breakdown** values of 0.15 [98], 0.39 [99] and 0.15 [108] are reported. The same value as used in [100] and [33] (0.5 in the breakdown direction) is used here.

The concentrations for $\mathrm{G^U}$, $\mathrm{G^{1P}}$, $\mathrm{G^{6P}}$ and $\mathrm{F^{6P}}$ in the hexose phosphate equilibrium block (Figures 4.2 and 4.3), were calculated from the equilibrium constants for UDP-Glucose pyrophosphorylase (UPP, EC 2.7.7.9), phosphoglucomutase (PGM, EC 5.4.2.8) and phosphoglucoisomerase (PGI, EC 5.3.1.9). The solution to the following linear system of equations, with

Table 4.4: Equilibrium and half saturation constants (in mM) for those reactions that are modeled as *non-equilibrium* reactions. The reactions with uni-bi stoichiometry have equilibrium constants with units in mM. Equilibrium constants referenced with [94] were calculated from the transformed standard Gibbs energy of formation for each reactant. Those marked [95] were calculated from the transformed standard Gibbs energy of one or more reactions. Note that the sucrose synthase reaction is defined in the *breakdown* direction. The half-saturation constants appear on the right hand side as sets of triplets, the first is the particular substrate or product, the second is the half-saturation constant and the third is the reference. The Half saturation constants for SS and SPS were obtained from a least squares fit to the equations in [26, 33], see §4.5. Constants for transport steps are given in Table 4.5. *na*–not applicable or irreversible, *est*–estimated or assumed.

				Substrate/product groups					
#	Reaction	E.C.	K	3	2	1	1	2	3
3, 11 & 13	AWI, NI & ASI	3.2.1.26	1.50×10^5 [95]			S 10 [26]	F 15 [26]	G 15 [26]	
9	SS	2.4.1.13	0.5 [96–99]		UDP 0.26 [100]	S 30.7 [100]	F 8.4 [100]	G^U 1.78 [100]	
10	SP	3.1.3.24	na			S^P 0.1 [26]	S	P_i	
12	SPS	2.4.1.14	10 [26, 101]		G^U 0.1 est	F^{6P} 1.5 est	S^P 0.03 est	UDP 0.3 [26]	
14	FRK	2.7.1.1	6.24×10^3 [94]		ATP 0.14 [102]	F 0.028 [102]	F^{6P} 0.1 est	ADP 0.1 est	
16	HKG	2.7.1.4	1.93×10^4 [94]		ATP 0.25 [26]	G 0.07 [26]	G^{6P} 0.1 [26]	ADP 0.1 [26]	
18	UGD	1.1.1.22	na	NAD 0.0722 [103]	NAD 0.0722 [103]	G^U 0.0187 [103]	UDPGA	NADH	NADH
19	PFK	2.7.1.11	1.20×10^4 [95]		ATP 0.155 [33]	F^{6P} 0.758 [33]	F_P^P 0.4 est	ADP 0.5 est	
20	PFP	2.7.1.90	53.8 [95]		PP_i 0.12 [33]	F^{6P} 1 [33]	F_P^P 0.382 [33]	P_i 0.51 [33]	
21	ALD	4.1.2.13	5.6×10^{-4} [104]			F_P^P 0.015 [33]	GAP	DHAP	

Table 4.5: Equilibrium and half saturation constants (in mM) for all the transport steps. An equilibrium constant of 1, with symmetric saturation constants signifies passive transport steps. The half-saturation constants appear on the right hand side as sets of triplets, the first is the particular substrate or product, the second is the half-saturation constant and the third is the reference. The particular compartments involved are shown in the columns. Active transport steps have an equilibrium constant equal to that of ATP hydrolysis to ADP and inorganic phosphate. This is 2.09×10^6 [95] at pH 7 in the symplast. Constants for reactions are given in Table 4.4. *symm*–symmetric, *est*–estimated or assumed.

#	K	Source	Phloem	Apoplast	Symplast	Vacuole
1	1 (est)	S 2 [28] —→	S 2 symm			
2	1 (est)		S 2 [28] —→	S 2 symm		
4	2.09×10^6 (est)			S 2 [28] —→	S 10 est	
5	2.09×10^6 (est)			F 0.2 [26] —→	F 1 [26]	
6	2.09×10^6 (est)			G 0.2 [26] —→	G 1 [26]	
7	1 (est)		S 2 [28] ———→		S 2 symm	
8	2.09×10^6 (est)				S 2 [28] —→	S 10 symm
15	1 (est)				F 0.2 symm ←—	F 0.2 [26]
17	1 (est)				G 0.2 symm ←—	G 0.2 [26]

$p_1 = 0.02\,\text{mM}$ $\qquad$ $p_2 = 0.8\,\text{mM}$

PP$_i$ $\qquad\qquad$ UTP

G^U —— UPP $\longrightarrow$ G^1P —— PGM $\longrightarrow$ G^6P —— PGI $\longrightarrow$ F^6P

$q_1 = 4.55$ $\qquad\qquad$ $q_2 = 17.1$ $\qquad\qquad$ $q_3 = 0.277$

[109] $\qquad\qquad\qquad$ [94] $\qquad\qquad\qquad$ [94]

Figure 4.3: Detail from the hexose phosphate equilibrium block in Figure 4.2. The enzymes UPP, PGM and PGI were not modelled explicitly. Rather, a rapid equilibrium assumption was made and the mole amounts or concentrations for the four species were calculated from the three equilibrium constants, q_i, as well as the fixed concentrations, p_j. See Section 4.5 and Equations 4.21 and 4.22 for detail.

p_i fixed,

$$
\begin{pmatrix}
1 & 1 & 1 & 1 \\
q_1 \frac{p_1}{p_2} & -1 & 0 & 0 \\
0 & q_2 & -1 & 0 \\
0 & 0 & q_3 & -1
\end{pmatrix}
\begin{pmatrix}
G^\text{U} \\
G^\text{1P} \\
G^\text{6P} \\
F^\text{6P}
\end{pmatrix}
=
\begin{pmatrix}
H \\
0 \\
0 \\
0
\end{pmatrix},
\tag{4.21}
$$

where the respective q_i and p_j are defined in Figure 4.3, gives the distribution of the hexose phosphate pool amongst the four species,

$$
\begin{aligned}
G^\text{U} &= 0.278 \cdot H, \\
G^\text{1P} &= 0.032 \cdot H, \\
G^\text{6P} &= 0.541 \cdot H, \\
F^\text{6P} &= 0.150 \cdot H.
\end{aligned}
\tag{4.22}
$$

Maximal activities Reaction maximal activities are given in Table 4.6. Maximal velocities are scaled to be in units of $\mu\text{mol}\,\text{min}^{-1}$. Few consistent sets of maximal activities exist for sugarcane; however Botha *et al.* have determined at least two of these, one of them unpublished (see Appendix B for further details). The same group generated both data sets, with one difference though. The unpublished data set includes maximal activities for SPS, whereas the other does not. The relative changes between activities of different enzymes inside a data set is reasonably consistent. This is not the case between the two data sets, so much so that SPS activity is roughly twice that of SS in the unpublished dataset but SPS from the unpublished dataset is roughly half of the published SS value [111].

Each maximal activity represents a single sample from an internode. However, activities can vary in both a longitudinal or radial direction across an internode (see for example [31]).

Table 4.6: Maximal forward activities for all *non-equilibrium* reactions. Values are shown here in units of nmol min^{-1}. The graphical representation plots the maximal activity against distance (see Figure 4.1). The inflection points correspond to nodes.

#	Reaction	Graphic	3	4	5	6	7	8	9	10
3	AWI		41.0	39.7	38.8	38.9	44.2	28.6	33.9	38.0
9	SS		51.2	51.6	52.9	50.5	53.4	43.4	59.0	24.2
10	SP		36.2	43.7	44.3	44.3	50.9	39.6	40.6	48.3
11	NI		32.4	33.8	29.1	29.0	23.5	26.6	21.8	24.4
12	SPS		24.1	29.1	29.5	29.5	33.9	26.4	27.1	32.2
13	ASI		12.7	14.1	14.8	11.4	11.3	10.4	9.9	11.7
14	FRK		33.2	22.1	12.8	17.5	13.7	14.7	10.0	12.0
16	HKG		20.9	14.8	15.4	15.8	17.1	17.2	22.5	17.4
18	UGD		52.7	20.9	21.6	16.8	14.0	11.3	7.6	4.7
19	PFK		33.6	30.7	24.2	26.7	34.0	41.9	39.9	42.5
20	PFP		52.1	42.9	47.4	60.5	63.4	58.6	60.9	62.3
21	ALD		101.0	45.5	54.6	50.2	51.5	54.2	51.8	56.7
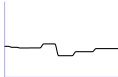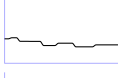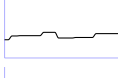
Table 4.7: The active and facilitated transport maximal activities (in $\mathrm{nmol\,min^{-1}}$). Values followed by a dotted arrow apply to all internodes, these values are also rough estimates. The maximal activities for reaction 2 and 7 were estimated from Titus [110].

#	3	4	5	6	7	8	9	10
1	300.0							$\cdots\cdots\rightarrow$
2 & 7	10.7	7.5	5.8	4.8	4.2	3.6	3.1	2.6
4	4.0							$\cdots\cdots\rightarrow$
5 & 6	25.0							$\cdots\cdots\rightarrow$
8	100.0							$\cdots\cdots\rightarrow$
15 & 17	1.0							$\cdots\cdots\rightarrow$

Here, it was assumed that activities are constant across an internode. This means that sharp discontinuities were introduced at the nodes. §4.7 shows how these were dealt with.

Half saturation constants and optimisation   Half saturation constants are shown in Tables 4.4 and 4.5. Some enzymes, such as SS, have well characterised isoforms [31, 100, 112]. Each isozyme has its own unique parameters. In plants, isoform proliferation is very common. For the sake of model simplicity and clarity we modelled each enzyme as a single reaction. Half saturation constants for the predominant isoform (FRKA) of FRK were chosen [102, 113]. This is because FRKB is strongly inhibited by F and contributes virtually nothing to the flux in the direction of F^{6P} [33]. The half-saturation constants for a general, phenomenological SS equation were obtained from a least-squares fit to simulated rates calculated from the sum of SSA, B and C, over a wide range of concentrations.

SPS was originally modelled with a reversible, ordered, bi-reactant mechanism [26]. As with SS a phenomenological equation is preferred and the half saturation constants for F^{6P}, G^{U} and S^{P} were fitted to the old equation. A better fit was obtained if the half saturation constant for UDP was omitted. Since UDP is constant throughout the model, this was deemed not to be a problem.

SPS and SS were the only two reactions for which half saturation constants were changed from [33]. In general half saturation constants, or K_{m} values, from the literature are more reproducible than maximal activities, as they do not depend on enzyme concentration. K_{m} values also tend to remain in the same order of magnitude across related species (see for example the BRENDA database [114, 115]). This is often true, even if the criteria for relation is as broad as "all K_{m}s for an enzyme in plants". For these reasons K_{m}s from different sources may be used, though preferably taken from studies in sugarcane or alternatively, from other plants such as maize (*Zea mays*) or wheat (*Triticum aestivum*). However, many of the constants remain

estimates, especially those for the transport steps.

Hydraulic conductivity and coefficients of diffusion   The estimation of the hydraulic conductivity for phloem flow was obtained from [47]. The value for κ is 0.31 μm^2 [47], μ is 0.156 J min m^{-3} [48] and Φ is 600 mol m^{-3} [47].

4.6   Time steps, sweeps, initial and boundary conditions

The choice of time step for a simulation depends on a number of factors. The following points were taken into consideration.

1. The numerical stability of the solution. As already alluded to in §4.5, and further discussed in §4.7, numerical solutions can become unstable and "blow up". A sufficiently large time step can also lead to such instability. The definition of "sufficiently large" is highly model dependent. Choosing smaller cell sizes or time steps can prevent instability, but is not always feasible because the model still has to complete a run in a reasonable amount of time.

2. Before a time step is incremented, a number of "sweeps" are performed to drive down the residual error of the solution. Finite volume methods iteratively approximate PDEs. Sweeping refers to the process of finding better and better approximations within a time step. Ideally the error should be as small as possible, because this reduces the probability of numerical instability and increases the accuracy of the solution. Often, the greater the time step, the more sweeps have to be performed per time step.

3. For a given model time frame, a certain number of time steps need to be taken. This depends on the time units in which parameters are defined, since the

$$\text{total steps} = \text{total time} \times (\text{time unit/time step}).$$

   The larger the time step, the fewer total steps need to be taken in order to get a time series.

To minimise the residual error and have the model run complete in a reasonable amount of time an adaptive time stepping approach was used (see Figure 4.4 and §4.7). The PID algorithm [116] was used as implemented in FiPy [58]. The time step was continuously increased until the residual error crossed a certain threshold. The model was then reverted to a previous state and a smaller time step increase was tried. If that failed, the next time step was chosen to be less than the previous time step provided the residual error was sufficiently small.
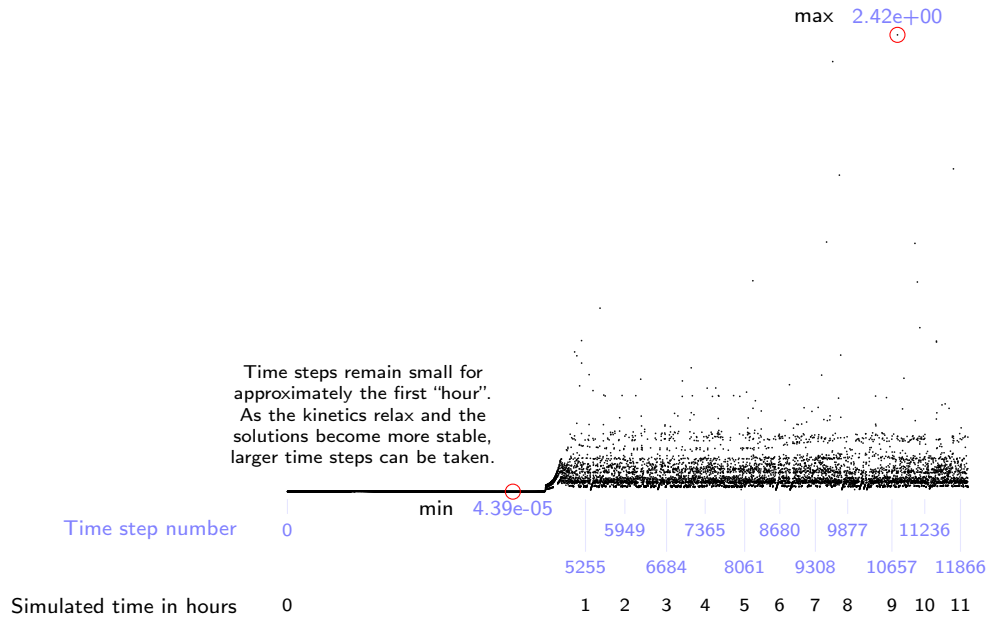
Figure 4.4: Time step sizes for all 12000 steps, illustrating the use of an adaptive time stepper. The y-axis represents Δt. PID controllers use a feedback mechanism to adaptively adjust the time step to its maximal value while keeping the residual error below a certain threshold.

Initialisation values for variables are shown with the time simulation results in §4.8. Two properties separate the choice of initial values from the parameter values: a) initial values are the average from as many different sources as possible, and b) they were initialised as a linear gradient along the entire stalk.

The concentration of a reactant is expressed in $mmol\,L^{-1}$. Since a mesh element is chosen to have a volume of 1 mL the value of the concentration is also the amount of that reactant in µmol.

More often than not, experimentally determined concentrations represent the total concentration for a reactant across all compartments. The partitioning of reactants between compartments had to be estimated. Some reactants, such as the hexose phosphate pool, were assumed to be located in the symplast alone. Others, such as phloem sucrose, were assumed to be more highly concentrated in the immature phloem tissue, moving down a gradient to the more mature tissue. Vacuolar sucrose followed a reversed profile, starting low and ending high.

The eight internodes under consideration should be considered a "moving window" along the stalk. Growth is not explicitly modelled, yet processes on either side of the mesh boundaries cannot be ignored. With the current approach, the easiest way to account for this is to set the boundary conditions at a fixed *concentration* flux (or efflux as the case may be). Since phloem flow is modelled implicitly no special consideration need be given to the *volumetric* flux at the
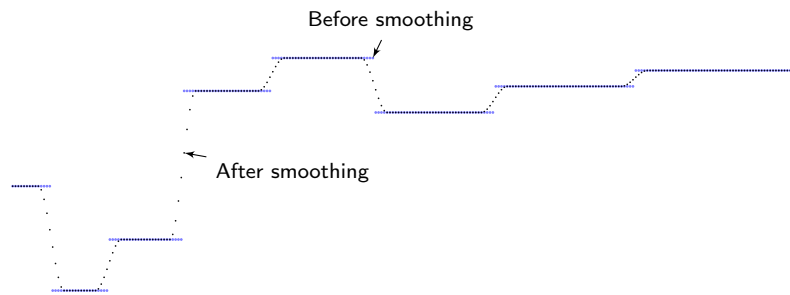
Figure 4.5: As an example, the maximal activity profile for PFP, before and after smoothing. Points -5 from a node to +5 were replaced with points from a third order Chebyshev polynomial of the second kind. The choice of a Chebyshev polynomial is arbitrary, except that it was convenient (available in SciPy), provided a smooth transition (it is S-shaped) and is easily scaled to fill gaps (Chebyshev polynomials are normed on the unit interval).

boundaries. The time scale under consideration also means that the boundary conditions need not change with time as supply or demand of solute at either end should remain relatively constant over a few hours.

4.7 Software and programming

The discontinuity of maximal activities at the nodes were removed by introducing an activity gradient spanning 5 elements either side of the node. Figure 4.5 gives the detail. The smoothing was necessary because numerical solvers, in general, become unstable around discontinuities and solutions tend to "blow up".

The advantages to using a time stepper can be seen in Figure 4.4. After an initial "burning in" period, time steps take on much larger values. The model completes an 11 hour simulation approximately 260 times faster.

Storing the complete model runs when applying FAST would require close to 6 Gigabytes of storage. Methods such as memory mapped arrays from NumPy are limited to file sizes less than 2 Gigabytes. This was sufficient for the toy model in Chapter 3, but not for the detailed model presented here. For the sensitivity analysis in this chapter data was stored in the HDF5 file format. All HDF5 files were created and managed using the PyTables wrapper for the HDF5 libraries [117].

4.8 Time course simulation

The model was solved numerically, giving an 11 hour simulation over time. The results are shown in Figures 4.6–4.8. The model was initialised with concentration values, such that the
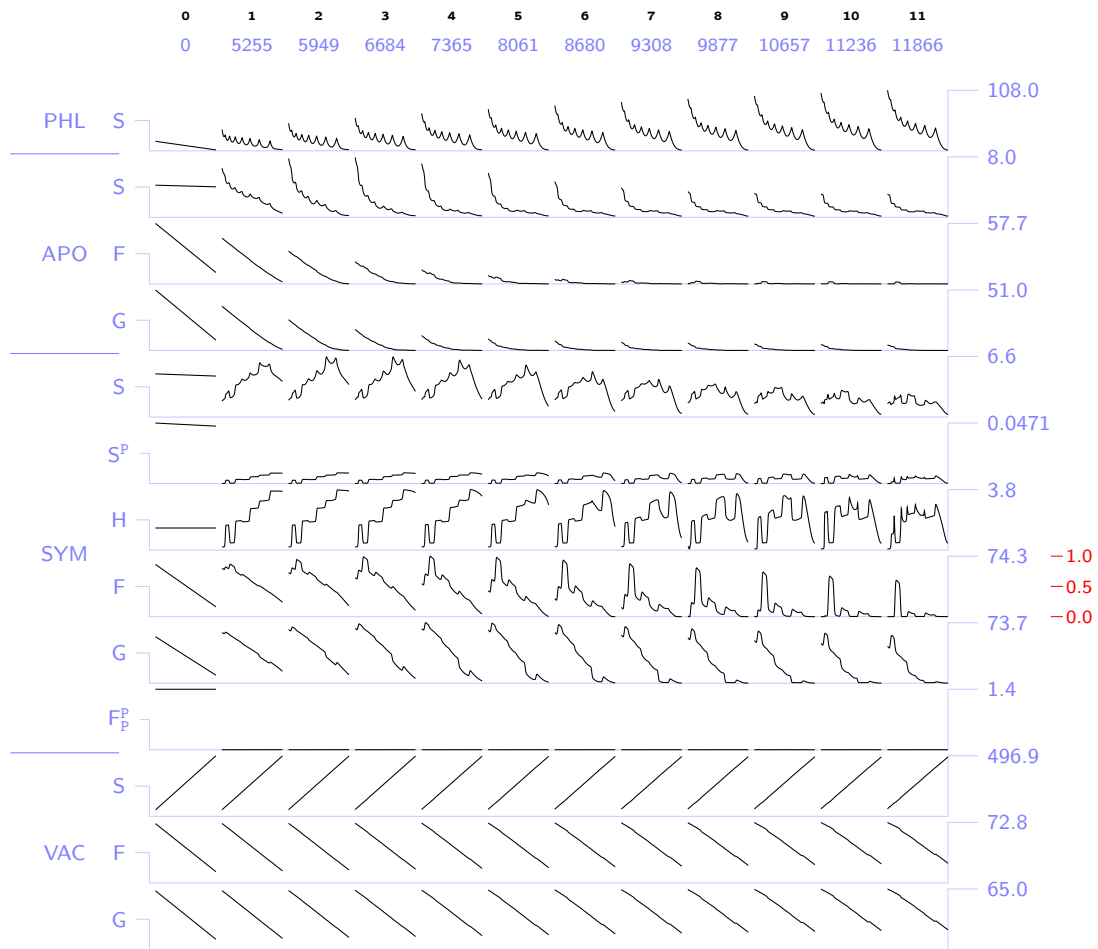
Figure 4.6: Variable concentrations, in other words compartmentalised reactant concentrations, for every hour over 11 hours in total. Each variable was scaled to the unit interval by its maximum value over the whole time course, indicated on the right axis. The units for the concentrations are in $\mathrm{mmol\,L^{-1}}$. Since the finite volumes are all 1 mL, the values are simultaneously in µmol.

total amount of a reactant across all compartments at a point along the stalk, was close to the best available measured values. However, the distribution of a particular reactant amongst the various compartments had to be estimated.

There was a greater change from the initialisation concentration values in the phloem, apoplast and symplast, than in the vacuole. The change from the initial conditions does depend on the actual initial concentrations. If there is a drastic change from those conditions, it probably reflects the fact that the estimated partitioning of known total stalk concentrations did not reflect the actual partitioning in the sugarcane stalk, for which there, however, is inadequate data. For example, it could be that the values used for F_P^P are inconsistent with the other initial values because they were sourced from different experimental data sets. The bulk
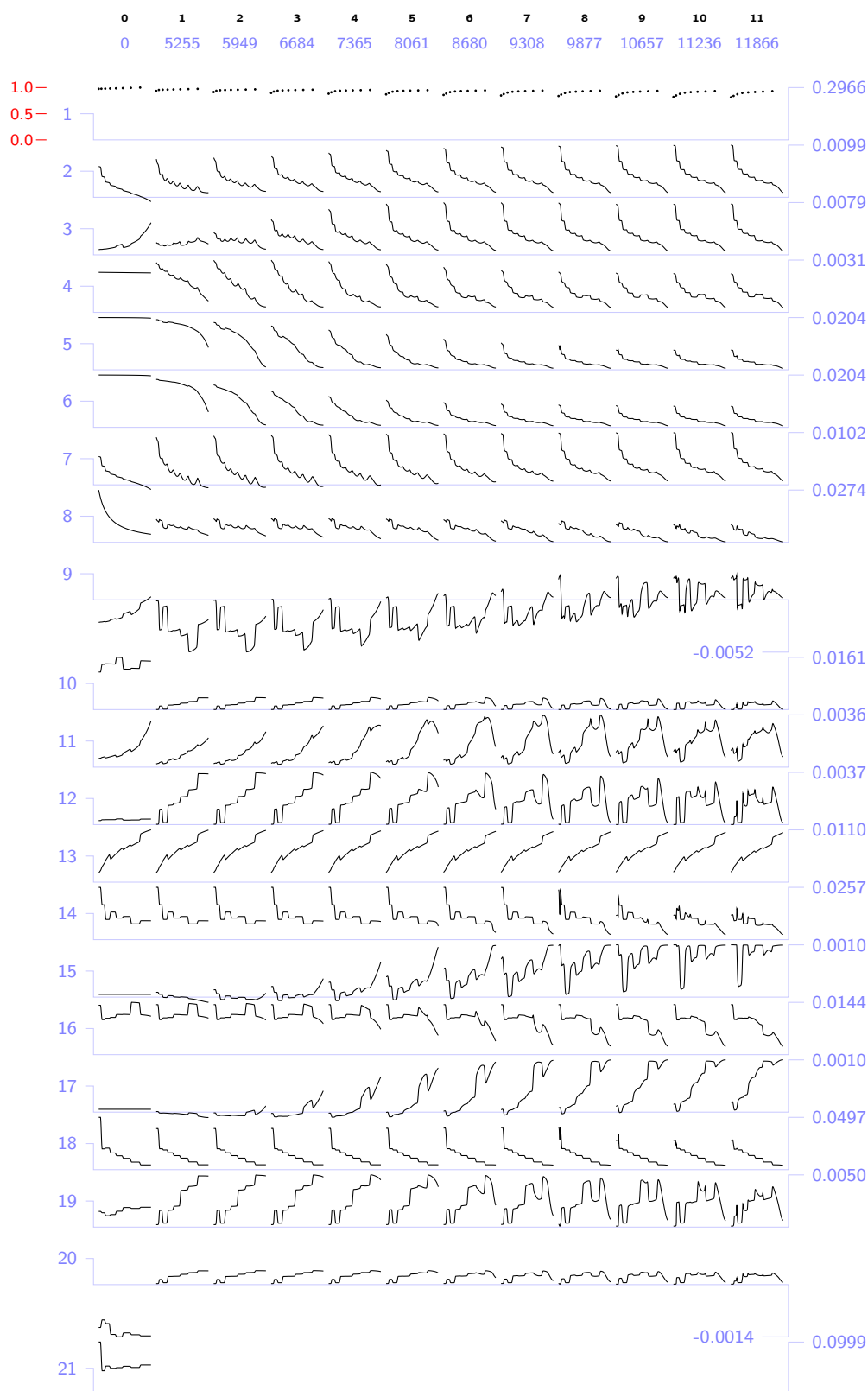
Figure 4.7: Time course reaction rates. Each set of rates was scaled to the unit interval by its maximum value over the whole time course. Reactions 9 and 20 have negative values.

Table 4.8: Sucrose, fructose and glucose concentrations at the immature (i, cell number 1) and mature (m, cell number 276) ends over eleven hours. All three reactants increase in their concentration at the immature end. However, sucrose decreases at the mature end while fructose and sucrose increase. More fructose and glucose were gained, than sucrose was lost, therefore there is a net increase of carbohydrate contained in the vacuole.

| | | Sucrose | | Fructose | | Glucose | |
Time	Step	i	m	i	m	i	m
0	0	52.4	496.9	71.2	13.4	63.0	10.8
1	5255	53.6	496.2	71.4	14.4	63.2	11.8
2	5949	54.5	495.6	71.6	15.4	63.4	12.8
3	6684	55.5	494.8	71.8	16.4	63.5	13.8
4	7365	56.5	494.1	71.9	17.3	63.7	14.8
5	8061	57.4	493.2	72.1	18.3	63.9	15.7
6	8680	58.4	492.3	72.2	19.2	64.1	16.6
7	9308	59.3	491.4	72.3	20.1	64.3	17.5
8	9877	60.1	490.4	72.5	20.9	64.5	18.4
9	10657	60.8	489.5	72.6	21.8	64.7	19.3
10	11236	61.4	488.5	72.7	22.7	64.8	20.1
11	11866	62.1	487.6	72.8	23.6	65.0	21.0

of the initial sucrose, fructose and glucose was placed in the vacuole and that is where it stayed. It is not immediately apparent from Figure 4.6, but the sucrose concentrations increased at the immature end and decreased at the mature end of the stalk. Table 4.8 shows what happens numerically. There was however a net accumulation of carbohydrate in the vacuole. The left hand plot in Figure 4.8 shows that the transport rate into the vacuole was greater than the rate of carbohydrate loss.

The apoplast, on the other hand, is approaching a steady state. That is, the rate of sucrose unloading into the apoplast is approaching the rate of carbohydrate uptake by the symplast. The apoplastic concentrations remained constant after about six hours. A concentration gradient along the stalk also failed to develop. This is probably because the symplastic uptake from out of the apoplast is actively driven where as phloem unloading into the apoplast is passive. The implication from this is that the apoplast is not a centre of assimilate accumulation.

The phloem sucrose concentration increased consistently with time. The sucrose gradient also increased by becoming steeper. Characteristic saw-tooth spikes also appeared at the nodes. The "amplitude" of these spikes after they had formed remained relatively constant with time.

The symplastic sucrose, sucrose phosphate and fructose bisphosphate concentrations dropped to below their initialisation values. The hexoses and hexose phosphate pool increased initially and later dropped.

Loading rates started to fall at the immature end as phloem concentrations increased.

Reactions 2–7 developed upright sigmoidal curves, that is they proceeded at their fastest

at the immature end, becoming constant for the medium mature tissue and finally tapered off at the mature end.

Vacuolar uptake was at it highest in internode 3 and gradually decreased down to internode 10. The hexose remobilisation steps, reaction 15 and 17, both approached their maximal activity. Invertase activity increased with internode maturity. Likewise, the futile cycling of sucrose in the symplast and vacuole combined also increased as is shown in Figure 4.8.

Reaction 9, sucrose synthase, is able to run in the forward or reverse directions depending on the position along the stalk. This is because it has an equilibrium constant close to unity.

There are two non-redeemable carbon sequestration pathways, the formation of UDP-Glucuronic acid (the precursor to hemicellulose and pectin, themselves the precursors of insoluble fibre) and glycolysis. The rate of fibre formation decreased stepwise with internode maturity. A close-up of the reaction rates leading to lower glycolysis is shown in Figure 4.9. Figure 4.8 (left hand plot) shows the difference between the total uptake of sucrose by the parenchyma and the partitioning to fibre and glycolysis. The free carbohydrate pool increased rapidly in the immature tissue. Rapid growth, with concomitant energy requirements, sees the balance dip below zero. In other words, biomass synthesis and respiration is favoured.

The sensitivity analysis of the model concentrations and reaction rates to a perturbation in the maximal activities is shown in Figure 4.10. In general, reactant concentrations are most sensitive to those reactions in which they are directly involved, with one or more reactions dominating. Likewise, reaction rates are most sensitive to the maximal activity of the particular enzyme catalysing that reaction. There are two exceptions, sucrose-6-phosphate phosphatase and aldolase. The former is most sensitive to the maximal activity of SPS and the latter to PFK.

The balances of various rates around compartments or specific reactants are shown in Figure 4.8. A sensitivity analysis of these sums is given in Figure 4.11. The variables $y_{1,2,3,4}$ are defined as follows: y_1 is the difference between parenchymal sucrose uptake and carbohydrate loss through respiration and fibre formation, y_2 is the difference between apoplastic sucrose uptake and symplastic uptake from the apoplast, y_3 is the difference between all the uptake and reaction rates, that introduce sucrose into the combined symplastic and vacuolar space, and the two invertases in this space that break down sucrose and finally, y_4 is the difference between vacuolar uptake of sucrose and the remobilisation from the vacuole as hexoses.

In the case of total parenchymal accumulation (y_1), the output is not only sensitive to the input and output rates, but also to the glucose phosphorylation step. This is most probably because glucose-6-phosphate, in equilibrium with UDP-glucose, is a direct precursor for fibre. Similarly, reaction 3 (AWI) affects y_2 because it is the linking reaction between apoplastic input and output. Notice how the apoplast approaches a steady state. Vacuolar accumulation (y_3) is
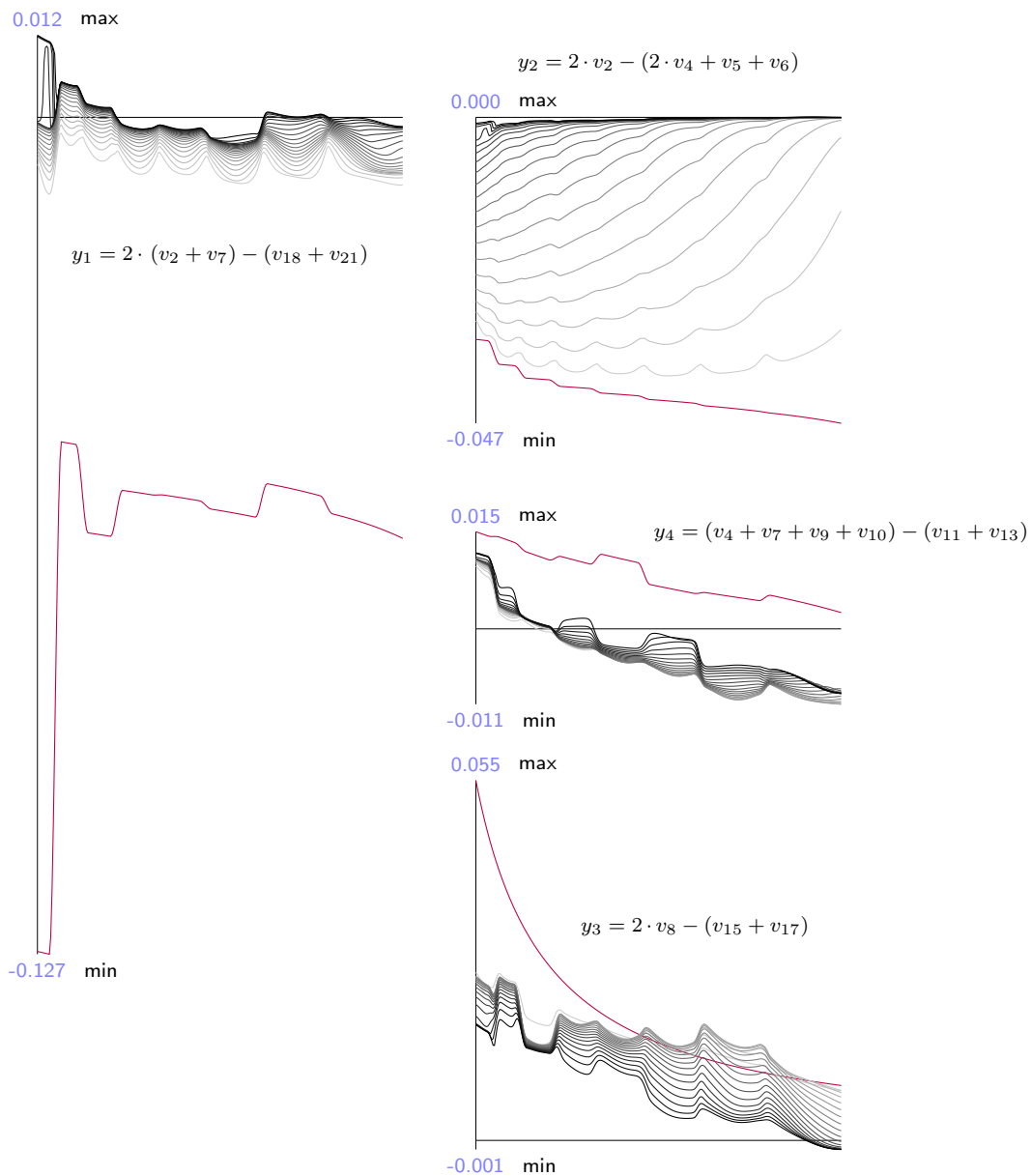
Figure 4.8: The sum of rates in half hour intervals (light grey to black) from initial conditions (red) up to 11 hours later. Four different sums are considered. *Left* The rate of hexoses leaving the parenchyma subtracted from the rate of apoplastic and symplastic sucrose uptake. *Top right* The difference between the rates entering and leaving the apoplast. *Middle right* The rate of sucrose cleavage subtracted from the rates introducing sucrose into the symplast. *Bottom right* The balance between sucrose being taken up into the vacuole and hexose remobilisation. Notice that carbohydrates are being accumulated, since the difference is positive, with a slight dip at the mature end of the stalk.
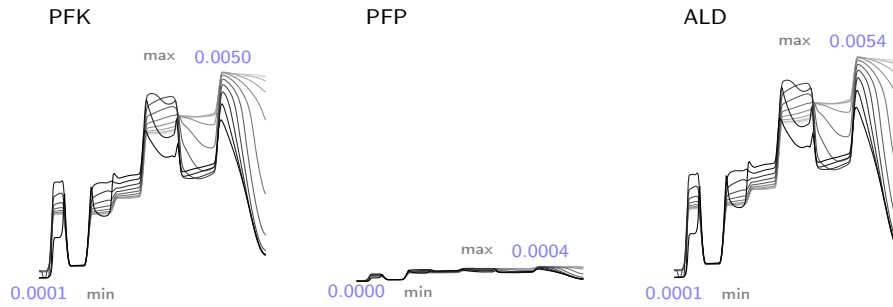
Figure 4.9: Reaction rate gradients over time for reactions 19, 20 and 21. Time is indicated by a change from light grey to black. These reactions represent the partitioning of carbohydrate into glycolysis. F^{6P} phosphorylation via PFK runs about 10—12 times faster than via PFP. After 11 hours the highest rate to glycolysis is in the middle of the stalk.
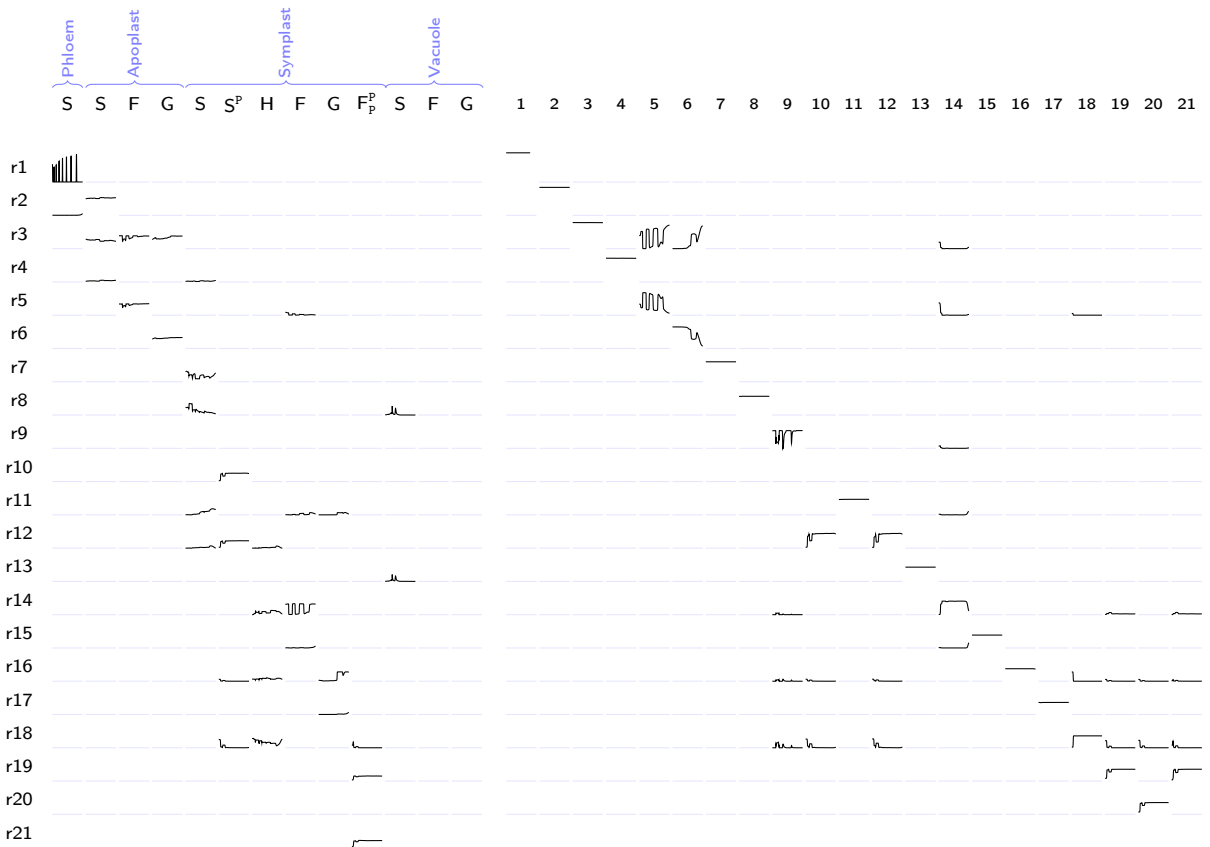

Figure 4.10: Sensitivity analysis of reaction rates and concentrations to a 1% perturbation in maximal activities. y-axis values can range between 0 and 1. At least one value has to be greater than $1/21$ for the entire stalk's sensitivity values to be shown.

$$y_1 = 2 \cdot (v_2 + v_7) - (v_{18} + v_{21})$$
$$y_2 = 2 \cdot v_2 - (2 \cdot v_4 + v_5 + v_6)$$
$$y_3 = 2 \cdot v_8 - (v_{15} + v_{17})$$
$$y_4 = (v_4 + v_7 + v_9 + v_{10}) - (v_{11} + v_{13})$$

Figure 4.11: A sensitivity analysis of the rate sums in Figure 4.8 to a 1% perturbation in maximal activities. y_1, y_2 and y_3 are the net rate through the parenchyma, apoplast and vacuole respectively. y_4 is the fraction of sucrose that enters the futile cycle.
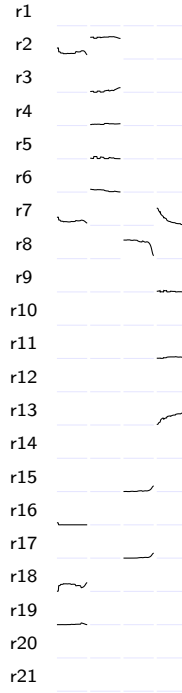
most sensitive to the rate of vacuolar uptake. y_4 clearly shows how the system becomes more sensitive to futile cycling as the internodes mature.

4.9   Discussion

This chapter presented a realistic model of sucrose accumulation in sugarcane. The approach followed here departed from previous efforts by including explicit compartmentation and phloem flow. Furthermore, realistic initial concentration values were used and a global sensitivity analysis of the reaction maximal activities was performed. Though much of the known behaviour of sugarcane could be approximated by the model, it does fall short on a number of points.

Comparisons with previous modelling, experimental values and similar toy models   A comparison of model predicted rates to experimental flux measurements and previous modelling results (Appendix B) is shown in Figure 4.12. The current model overestimates the rate of fibre formation by an order of magnitude. The glycolytic rate is also larger, but falls in the same order of magnitude. This only serves as a rough guideline, as direct comparison
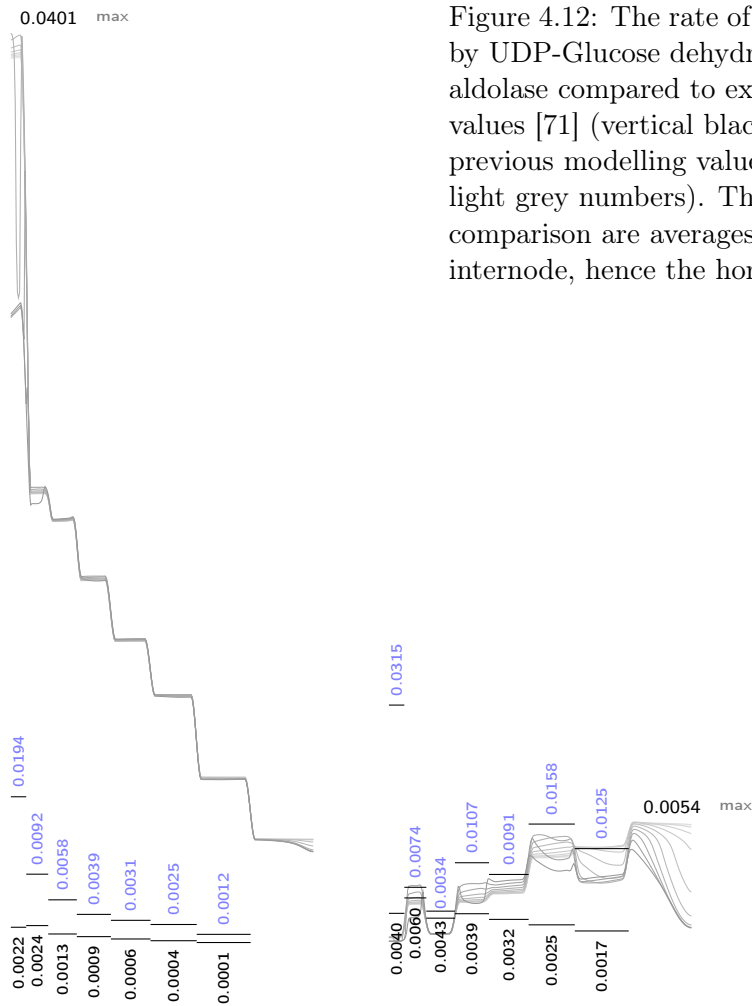
Figure 4.12: The rate of hexose utilisation by UDP-Glucose dehydrogenase and aldolase compared to experimental flux values [71] (vertical black numbers) and previous modelling values [33] (vertical light grey numbers). The values used for comparison are averages across an internode, hence the horizontal lines.

is not really "fair". The experimental values were obtained from Bindon & Botha [71]. They measured radiolabeled carbon distributions after feeding tissue disks labelled glucose and unlabelled fructose. The model stalk parenchyma, on the other hand, was fed by sucrose from the phloem, as well as sucrose, glucose and fructose from the apoplast.

The previous models of Rohwer & Botha [26] and Uys *et al.* [33] kept external carbohydrate concentrations constant (5 mM). In contrast, with the introduction of the phloem and the accompanying sucrose translocation, external carbohydrate concentrations vary and climb higher than the phloem sucrose initialisation values. The higher carbohydrate feed drives all rates and concentrations higher than previous model values. These high concentrations have some unintended consequences.

An apparent idiosyncrasy in this model is the high concentration values relative to the substrate and product saturation constants. Reactant concentrations are much higher leading to a certain amount of "saturation gridlock". The reactions all run at near maximal velocity

meaning very little kinetic regulation is taking place. For example, the rate of hexoses leaving the vacuole is close to the maximal activity for those steps.

The high degree of saturation decreases the overall ability of the system to regulate itself kinetically. Therefore, the only sensitivities presented are those of the output variables to changes in maximal activities. A sensitivity analysis of the half saturation constants was not conclusive (data not shown). The variation in model output generated by perturbations in the half-saturation constants was to small to extract meaningful data from a Fourier transform.

The sensitivity analysis shows, that regardless of compartment, sucrose concentrations are most sensitive to the transport and breakdown steps. The parenchymal sucrose synthesis steps have very little effect on accumulation.

The SS rate can be negative in some parts of the stalk and positive in others. This is because of the equilibrium constant for the reaction (close to 1) combined with the existence of concentration gradients. This might explain contradicting reports that SS both breaks down sucrose and synthesises it [31, 100, 112]. There is no reason why the enzyme cannot run in both directions in the same plant depending on the local mass action ratio.

There are a number of factors that affects the modelling process itself. In this study the most important was the time it took for the model to run. One possible solution to this would be to move the whole software stack to a distributed environment. FiPy has support for the Trilinos suite of solvers [118, 119], which has support for distributing matrix computations over a cluster. Other software could also be tried, such as reprogramming the model in FORTRAN combined with the MPI libraries for distributed computing. Whichever solution is used should minimise the amount of time it takes the model to complete a run. This would especially be useful for sensitivity analyses that require multiple model runs (such as FAST).

Another possibility to speed up execution time would be to improve on the time stepping algorithm. The PID stepper was used to adaptively adjust the integration time step as a function of the residual error. This worked, but can be improved upon. PID controllers take three parameters that determine the contribution of the proportional, integral and derivative terms in the transfer function. It is a well established fact that these have to be "tuned" to suit a specific problem. In this work the parameters as found by [116] were used. This is a reasonable assumption because they found these default values working on an example fluid flow problem to demonstrate the use of PID controllers for adaptive time stepping. It would be worth investigating other values to see if better (i.e. faster) time stepping can be achieved. It is also very likely that other values will avoid the controller getting stuck in a stable oscillation. Further reduction in modelling time can be achieved by cutting out sensitivity analysis of parameters to which model output is known to be insensitive.

FAST is a computationally expensive method. To avoid calculating unnecessary sensitivity

values, the Morris method could be used to rank parameters before FAST is used [120]. The Morris method is a "one at a time" sensitivity analysis that ranks parameters according to their main effects. It is normally employed as an initial screening test to remove inconsequential parameters before a more detailed sensitivity analysis is performed. Parameters with high Morris sensitivities could then be further analysed using FAST.

FAST should only be used for the most important parameters. However, it is also necessary that sensitivity values are obtained for every time step, since sensitivities change with time. It has also become apparent that sensitivities change as a result of the size of the parameter perturbation.

The means to run the model faster would also allow parameter estimation to be performed, by either a brute force approach where all parameters are changed to maximise some effect or by simply changing those parameters identified by Morris or FAST. To perform a global parameter estimation differential evolution could be used [121]. This is a stochastic method that uses vector differences to mutate parameter populations in a genetic algorithm framework. This approach could sketch a portrait of the ideal sugarcane parameter set.

4.10   Conclusion

This chapter presented a model of sucrose accumulation in sugarcane that spans eight internodes and four compartments. Reactions and translocation in these compartments were included. To our knowledge, this is the most comprehensive biochemical model of this nature to date. Given the scale and amount of detail contained in the model, it could nevertheless still be solved in a reasonable time frame. Furthermore, a sensitivity analysis of the maximal activities was successfully carried out. This work has shown that integrating kinetic modelling, as has been done to date, to include physical process, like advection, is tractable.

Modelling is seldom an end in itself. The model presented here illustrates the need for further experimentation and measurements to obtain consistent data on sugarcane sucrose metabolism. This will in turn lead to a better model, thus better understanding of sugarcane and point the way for better experiments.

In Chapter 5 a general overview and discussion of the work presented in the last three chapters will be presented.

Chapter 5

General discussion and perspectives

This chapter takes a broad view of the work presented thus far. In §5.1 the various models and results are summarised. §5.2 discusses the merits of the approach followed and the validity of the results presented. The possible implications and future work are discussed in §5.3 and §5.4. Concluding remarks are made in §5.5.

5.1 Synopsis

Chapter 2 introduced an advection-diffusion-reaction modelling framework that expands the usual formulation of reaction kinetic models. This more general formulation does away with the requirement that the system have homogeneously distributed reactants in the reaction volume—the assumption of a "well-mixed" reaction. This allows long distance transport, as occurs in plant vascular tissue, to be modelled. The metabolic pathway also spanned a number of different compartments. The method was successfully demonstrated with a simple model.

Concentration and rate profiles showed "saw-tooth" profiles, the peaks of which corresponded with node positions (see for example Figures 2.4, 3.3 and 4.6). In other words assimilate flowed up *and* down the stalk. The ability to maintain homoeostasis was improved when allosteric feedback was introduced on the leaf synthesis and phloem loading steps respectively. The model could furthermore mimic the upregulation of the assimilate synthesis in a leaf, if all but one of the leaves stopped assimilate production (Figure 2.7).

Chapter 3 introduced a toy model, also referred to as a core model, which captured many of the kinetic and structural features of sucrose metabolism and accumulation in sugarcane. Furthermore, the Fourier Amplitude Sensitivity Test (FAST) was successfully used to perform a sensitivity analysis. Established methods of model analysis, such as Metabolic Control Analysis would be impossible to apply to transient systems of PDEs. This is because MCA is only applicable to ODE based models, which are furthermore at steady-state. Recently MCA has

been extended to non-steady-state conditions, but none of these treatments has dealt with PDEs.

Amongst other results, the model showed that futile cycling decreases with internode age (Figure 3.5). Furthermore, futile cycling was highest around the nodes, in other words where concentrations were the highest. FAST showed that the concentrations of the assimilate of interest were most sensitive to uptake (membrane transport) and breakdown reactions—the sucrose cleavage reactions such as the various invertases. An explanation is also given as to why parabolic rate profiles are generated, see Figure 3.9. These profiles are sometimes seen in experiment [71].

Chapter 4 introduced the most detailed biochemical and biophysical model of sucrose accumulation in sugarcane to date. The model spans eight internodes, all of them coupled by advective flow in the phloem and diffusive flow in the symplast or apoplast. Furthermore, the model was initialised with realistic metabolite concentration values and exhibited many of the traits associated with sugarcane, such as accumulation of carbohydrates and substantial futile cycling of sucrose.

Realistic initial values were used. In order for the model to exhibit kinetic regulation, as opposed to saturation, most of the sucrose, fructose and glucose had to be placed in the vacuole. This was because the concentrations are, more often than not, much higher than the half saturation constants of the various enzymes. This situation leads to a "saturation gridlock", all reactions run at maximal velocity and no kinetic regulation occurs. The rate of phloem unloading into the apoplast and symplastic uptake reached a steady state. There was also a net accumulation of carbohydrate in the vacuole. All of this would suggest that the vacuole really is the compartment that accounts for almost all the accumulation of sucrose. A sensitivity analysis was only performed on the set of maximal activities. As with the toy model from Chapter 3, sucrose concentrations were the most sensitive to transport and invertase reaction steps.

5.2   Critique

The various models need to be judged on a number of scores:

1. the degree to which the model geometry is a fair representation of sugarcane anatomy,

2. the compartmentation in relation to sugarcane physiology,

3. whether the reaction schemes capture the salient features of sugarcane biochemistry,

4. mathematical formulation and the biophysics of sugarcane,

5. parameterisation, as in what has been measured, what has not and how fair are the estimates made,

6. the methods used to solve and analyse the models, and lastly

7. the validity of the conclusions that were made.

Geometry   The geometry is a sort of scaffold from which the whole modelling edifice hangs, and profoundly affects the solution to a model—it is the context. The domain on which each variable is defined is directly linked to the geometry. It is conceivable that the exact same governing equations, as used here, could fit a huge array of alternative geometries, with many different solutions. The main reason why the models that were presented here are actual models of sugarcane, is because of the geometry and the layout of the variable domains.

In all three models the sugarcane stalk was approximated by a straight line segment. Given the fact that the stalk is much longer than it is wide, this was a reasonable assumption to make. The amount of time taken to solve the models was significantly reduced since a one dimensional mesh could be used. This does not deny the fact that there are well documented cases of radial changes in sugarcane (see for example [31]). However the radial changes are small compared to longitudinal changes.

The choice of geometry also enabled a convenient simplification to be made. All the elements in the mesh were of uniform volume. This volume was chosen to be 1 mL, with reactant amounts in µmol. In other words the solution values to all the variables were both the micromole amounts and millimolar concentrations—no conversion between the two was necessary, which greatly facilitates interpretation.

Compartmentation   The model treated the phloem as one continuous tube, rather than the series of sieve elements that it is. Assimilate is loaded into the phloem and is subject to advection. Likewise, the symplast (and later the apoplast) is treated as a single compartment instead of as a collection of cells. Metabolites could diffuse slowly up or down the stalk. This is because of the prevalence of plasmodesmatal linkages between cells [63]. The choice of a small diffusion coefficient, compared to the flow coefficient used in the phloem, meant that reactions played the largest role in concentration changes. The motivation for assuming that phloem flow and metabolism occurs in these "meta-compartments" is that given a large number of small compartments, single parenchymal cells or sieve elements, average behaviour emerges.

Pathways   The reaction schemes became more complex with each new model. The first model was not particularly concerned with the intricacies of metabolism in the symplast, the focus was

more on how the geometry influenced concentration and rates along the stalk. Although not explicitly stated, it illustrated the large amount of new information that could be gained from casting a linear pathway in a PDE framework as opposed to an ODE setting. The pathway in the second model contained most of the known features of central carbohydrate metabolism in the storage parenchyma. The analysis considered the interaction between the geometry and metabolism. The parameter set was still estimated so as to force behaviour such as increased phloem unloading and consequently assimilate accumulation along the stalk.

The last model had the biochemically most accurate pathway. The combination with the realistic stalk geometry, initial values and parameters also made it the most difficult to construct and solve. This progression in model complexity demonstrated the trade-off that exists between the amount of detail in a model and the amount of time it takes to solve.

As with previous modelling [26, 33], the realistic model presented in Chapter 4 had the cofactor concentrations treated as constants. The model in Chapter 3, on the other hand, had both cofactors and protons as variables and, as was shown, "floating" these concentrations has an effect on the pathway behaviour. If the data is available to model these realistically, attempts should be made to include variable moiety concentrations. Unfortunately, very little information exists on moiety regeneration in sugarcane. Certainly the reactions that regenerate ATP and NADH are known, what is missing are the kinetic parameters of these reactions. In addition, if the moieties are to be explicitly modelled as variables, *all* such relevant consuming and regenerating reactions need to be included.

Mathematical formulation   The formulation as presented in Chapter 2 is very general and a lot of scope remains in the choice of governing equations. All the equations used to solve the various terms—velocity, pressure, reaction rates—in the models were phenomenological equations. The reasons for this are given in §2.1. There are some problems associated with using some of these equations. For example, pressure gradients could be calculated from more accurate expansions of the Van't Hoff equation. Furthermore, viscosity, though treated as a constant in all the models, could be calculated from more accurate, experimentally fitted equations [62]. In other words, viscosity could be made a function of sucrose concentration.

It is debatable whether the added resolution gained from more accurate equations would add to the accuracy of the model output. Given the fact that there are more than a few plausible solutions to the various models, the gain in accuracy would not necessarily outweigh the need for simplicity in representation and ease of implementation. We aimed at achieving a suitably detailed model description at an intermediate level of complexity.

Parameters All the models presented here are highly parameterised, in other words many measured quantities are required to pin the model to one solution. For the first two models this was not really that important, because they were not expected to be anything more than toy models. The selection criteria for parameters in these models, was simply that the model behaviour conform to a rough notion of sugarcane behaviour.

The case is different for the more realistic model in Chapter 4. Parameters could not be chosen according to the model behaviour, but were rather taken from the literature. It would be very optimistic to expect that all the model parameters had been measured experimentally. Therefore it is inevitable that many of the parameters are estimates. As with experimentally measured parameters, estimated parameters have large uncertainty attached to them and this propagates through to the model output.

The guiding principle in the selection of parameters was consistency. For example, almost all the maximal activities as shown in Appendix B were from exactly the same source. Likewise, the equilibrium constants from Chapter 4 were calculated, as far as possible, from tables of transformed standard Gibbs energies of formation/enthalpy [105]. As was shown in Figure 3.6, a model can be quite sensitive to uncertainty in an equilibrium constant. Even though tables of thermodynamic data are comprehensive, they are not yet complete. Therefore, equilibrium constants that were not calculated from a table (see Figure 4.3) break the consistency criterion outlined in §4.5. For example, equilibrium constants could have been measured at a different pH to the one used in the calculation of the others.

The half saturation constants for some enzymes, such as FRK, are a few orders of magnitude smaller than the total concentration of the associated substrate or product. Either these values are wrong or most carbohydrates are sequestered somewhere like the vacuole, so that these enzymes can operate around concentrations close to the half saturation constants. Moreover, the fact that not all of these constants have been measured in sugarcane, and that some estimates had to be made from other plant species, begs further, comprehensive measurement of half saturation constants.

Methods FiPy is convenient but slow because it is implemented in Python, an interpreted language. The benefit to using FiPy is that it is extremely easy to program complicated PDEs in a short amount of time. It is also possible to dynamically generate equations given a pathway definition.

To decrease the modelling time, the tolerance on the residual error of the numerical integration had to be increased. With modelling there are always trade-offs; this is unfortunately one of them. If the model was to complete any run in a reasonable amount of time, this sacrifice had to be made. The results are however accurate to 5 decimal places.

The PID controller introduced in Chapter 4 increased the efficiency of solving the model. However it can still be improved upon. The model kinetics take a while to relax before larger time steps can be taken. Approximately half the modelling time was spent on a tenth of the simulated time. Fine tuning of the PID parameters could hopefully improve on this.

The number of model runs required by FAST grows exponentially with the number of parameters [74]. The usual approach in such a case is to perform screening studies, using for example the Method of Morris [120]. This reduces the number of parameters for which detailed sensitivity analysis needs to be performed. Unfortunately this was realised to late to be of any use in this study, but will certainly be applied in future work.

Solutions The detailed model predicted much higher reaction rates than have been measured (see Figure 4.12). This is closely related to the saturation gridlock effect. It is quite likely that calculated intra-symplastic concentrations are still to high, leading to higher reaction rates. Possibly the relative volumes of the various compartments need to be adjusted. For example, a smaller phloem volume would allow less sucrose to maintain the same concentration in the phloem. A higher vacuolar volume would decrease the sucrose concentration allowing more sucrose to be transported faster into the vacuole. The relative phloem volumes were estimated from stained cross-sections [93] and were possibly overestimated (see Table 4.1).

From this work it can be concluded that the main factors that influence sucrose accumulation are futile cycling and the rates of cross-membrane transport (see Figure 4.11). The less sucrose is broken down and the faster it is transported into the vacuole, the more sucrose is accumulated. These findings are consistent with the modelling results of Rohwer & Botha [26] and Uys *et al.* [33].

5.3 Implications

The framework presented here has applications beyond sugarcane. The most obvious extension of this work would be to include the xylem into the model. Although both Hölttä *et al.* [44] and Lacointe & Minchin [56] have modelled combined phloem and xylem transport, neither have explicitly added detailed reaction pathways. The modelling of coupled phloem-xylem-reaction systems is quite possible with the framework presented here.

The modelling can also be extended to two or three dimensions. A three dimensional mesh would allow changes in all three spatial dimensions to be modelled. However, it should be kept in mind that the computational cost of modelling on higher dimensional meshes increases dramatically with size and dimension.

Methods such as adaptive meshing should allow more complex growth models to be con-

structed [92]. Projects such as Algorithmic Botany have successfully been modelling morphological changes as plants grow ([122–124] and `http://algorithmicbotany.org`). However, there is seldom any detailed reference to the underlying biochemistry. Génard *et al.* [125] gives a review of carbon allocation modelling with an emphasis on peach trees. They follow a whole plant modelling approach, once again with scant reference to the biochemistry.

A further application of the ADR framework could be in the modelling of bacterial biofilms and quorum sensing. Ward *et al.* [126] created an ODE based model of quorum sensing in bacteria. It is possible to extend such a model to include advection and diffusion processes as was shown by [127]. Duddu *et al.* [128] modelled biofilm growth, while Janakiraman *et al.* [129] created a model of both biofilm formation and quorum sensing. All these models fall under the heading of ADR models and could be easily solved and analysed with the software used here.

Slightly more difficult would be solving mechanical systems, such as mammalian vascular systems with their beating hearts. This is an endeavour best left to the Physiome Project (`www.physiome.org.nz` and [130]). Fermentations in stirred bioreactors are also examples of dynamic mechanical systems; these should be slightly easier to solve [131]. The difficulty in solving these two examples stems from the fact that they both require the modelling of a moving boundary. This is not impossible, but the tools and approach presented in this dissertation would make it a very complicated and time consuming computational effort.

5.4 Future work

Any model is only ever an approximation of a real system. A model's fit to reality may be considered its degree of resolution. In that sense, the modelling approach and sugarcane model presented here can certainly be further resolved.

Enzymes such as SPS are subject to regulation by phosphorylation [101], others such as PFP are allosterically regulated by fructose-2,6-bisphosphate [132]. The kinase and phosphatase which produce and degrade fructose-2,6-bisphosphate may also be phosphorylated. Enzyme concentrations depend on enzyme expression, in other words genetic regulation. These forms of regulation are not captured by the model from Chapter 4. Future versions of this model can only benefit from having more known regulatory mechanisms included.

Uys *et al.* [33] studied the effect of isoforms on sucrose metabolism. Since internodes are now able to interact with each other, the effect of isoforms on sucrose metabolism could be investigated again in a more general setting.

Faster and more accurate methods of solving and analysing the model need to be considered. Firstly, one of the strengths of modelling is the possibility to gauge the effect of changing model parameters. Invariably this involves numerous model runs and better methods for solving the

model would make studying various parameter configurations more efficient. Secondly, the easier it is to use, the easier it becomes to have other researchers use and study the model. In this way a model is really tested by its acceptance in the field.

A possible generalisation of MCA to cover models cast as PDEs could be very useful. MCA analyses the distribution of control in a metabolic system, something that methods of sensitivity analysis, such as FAST, cannot do. The problem with generalising MCA lies in the number of the functional relationships between terms, much more than for ODE based models. However, it should be possible to solve the problem. The spatial control—the control of a reaction on a flux in a different part of the plant—could then be quantified. The second-order control coefficient formulation in [3, 133] could possibly be adapted to the task.

Despite all the above proposals for adding finer detail and more extensions to the model, it should always be kept in mind that this is not always desirable. The level of abstraction that is required for a given problem needs to be carefully considered. There should be enough detail that the behaviour being studied is fairly represented, but no so much that the behaviour becomes obfuscated by irrelevant features.

5.5 Conclusion

Mathematical modelling provides a powerful framework in which to summarise, integrate, analyse and reason about experimental observation. This dissertation showed that it is possible to build large models of plant physiology, with detailed aspects of biochemistry and biophysics and solve them. Besides expanding the sugarcane model presented here, there is also scope for adapting the modelling framework to novel systems and pathways.

Appendix A

Fourier amplitude sensitivity test

The following linear pathway and rate equations will be used to illustrate the FAST algorithm.
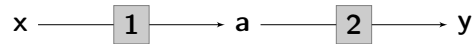
$$v_1 = \frac{V_1 \cdot x}{k_x + x} \qquad v_2 = \frac{V_2 \cdot a}{k_a + a}$$

The two enzymes follow Michaelis-Menten kinetics and the concentrations of x and y are clamped.

Let $f : \mathbf{v} \in \mathbb{R}^n \xrightarrow{\mathbf{N}} \mathbf{0}$ define an ODE based model of this pathway at steady-state such that the following holds,

$$\frac{da}{dt} = \mathbf{Nv} = \begin{pmatrix} 1 & -1 \end{pmatrix} \begin{pmatrix} v_1 & v_2 \end{pmatrix}^T = v_1 - v_2 = 0. \tag{A.1}$$

Since this model is for illustrative purposes only, diffusion and advection are neglected.

Furthermore, let $f(p)$ be the model output and p a parameter vector distributed around some expected value, $E(p)$, with variance, $\mathrm{Var}(p)$. For the example above that could be,

$$p = \begin{pmatrix} V_1 & V_2 & k_x & k_a \end{pmatrix},$$
$$E(p) = \begin{pmatrix} 1 & 1 & 1 & 1 \end{pmatrix},$$
$$\mathrm{Var}(p) = \begin{pmatrix} 0.01 & 0.01 & 0.01 & 0.01 \end{pmatrix},$$

such that $p \sim \mathrm{pdf}(p) = \mathcal{N}\left(E(p), \mathrm{Var}(p)\right)$, in other words p is normally distributed with the marginal probability density functions given by $\mathrm{pdf}(.)$. The following three points need to be noted; (1) The algorithm does not demand that parameters be normally distributed, any distribution will do. Moreover, the variance need not be a 1% perturbation, but was chosen for illustrative purposes. The variance is chosen to reflect the uncertainty in a parameter —

typically the standard error in an experimental measurement. (2) $\text{Var}(p)$ is the diagonal of the covariance matrix and we treat all parameters as independent of each other (off-diagonal entries are zero). In other words we assume that there are no confounding influences amongst parameters and that changing a parameter does not influence another parameter. The original FAST algorithm, as implemented here, cannot deal with parameters that interact with each other. However, there are methods to do so, for example see Xu & Gertner [80, 81]. (3) In this example the model output will be steady-state fluxes and concentrations. Nothing prevents the output from being something else, for example the output could be the ratio of two concentrations, the sum of a subset of the fluxes or even the concentrations and rates when the model is not at steady-state. The last two properties are exploited in Chapter 4 where a non-steady-state model is analysed.

Define a search function to step through the parameter space,

$$p = \text{cdf}^{-1}(p^*), \tag{A.2}$$

such that $\text{cdf}(\cdot)$ is the cumulative distribution function of p and p^* oscillates in the unit interval,

$$p^* = \Omega(\omega_p, s) = \frac{1}{2} + \frac{\arcsin(\sin(\omega_p \cdot s))}{\pi}. \tag{A.3}$$

Ω is defined on the interval $s \in [-\pi, +\pi]$ and ω_p is a characteristic integer frequency *explicitly* defined for each element of p. ω_p ensures that each parameter oscillates at a unique frequency, so that the contribution of that parameter to the model variation can be isolated. In this example the frequencies are 5, 11, 19 and 23. These are chosen according to an algorithm by Cukier *et al.* [74] so as to minimise the amount of interference between frequencies, thereby isolating the effect of a parameter perturbation in the model output. The case for $\{V_1, V_2\}$ is illustrated in Figure A.1.

For p a 4-vector, $\Omega(\omega_1, s) \times \Omega(\omega_2, s) \times \Omega(\omega_3, s) \times \Omega(\omega_4, s)$ defines a function that takes on values from the unit hypercube, parameterised by s. Using an appropriate cdf and iterating over all the points in the hypercube, values for p can be obtained. Given the definition of f, $f(s) = f(p(s))$ can then be calculated. The model output is plotted in Figure A.2. Once the output is obtained, a Discrete Fourier Transform (DFT) is performed. The complex coefficients, $\alpha_{\pm k}$, for $k = 1, 2, ..., (N-1)/2$, of the DFT for the steady-state fluxes are shown in Figure A.3. N is the number of parameter sets generated by the search function and is therefore also the number of times the model needs to evaluated to produce the output.

The Fourier spectrum (Λ) is defined as the set of all Λ_k, where,

$$\Lambda_k = 2(\alpha_{+k} \cdot \alpha_{-k}), \tag{A.4}$$
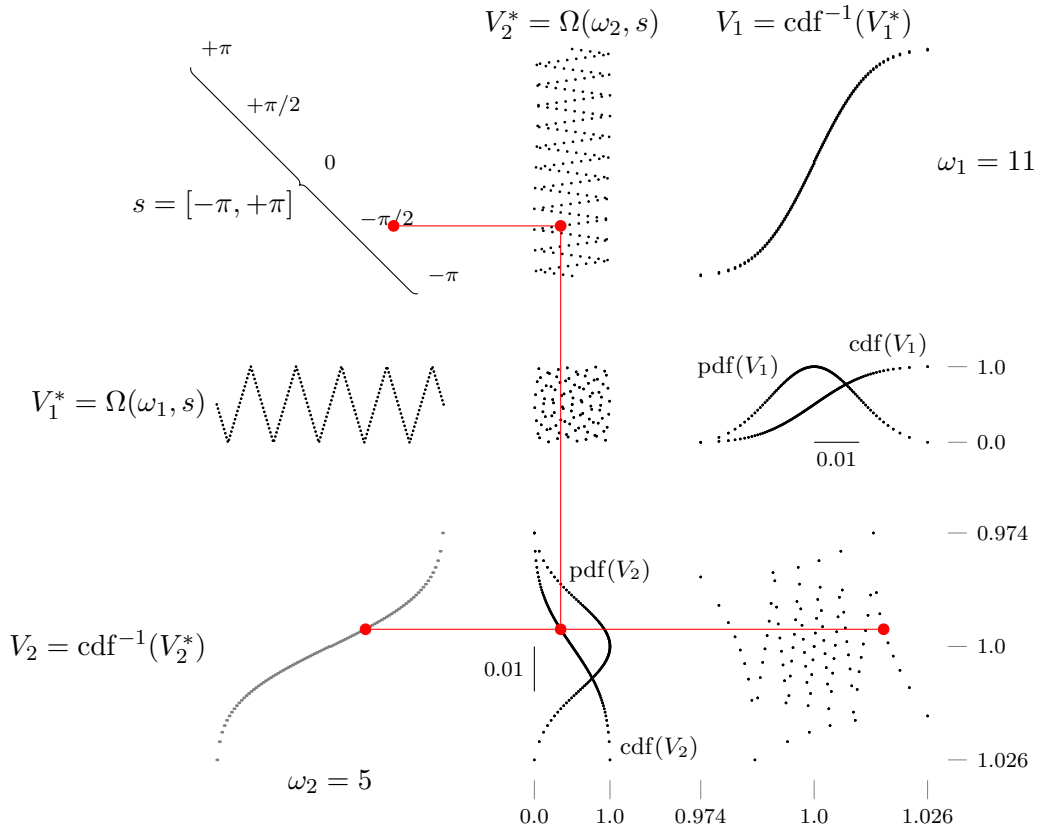
Figure A.1: The workings of the search function used in the FAST algorithm illustrated with two example parameters — the maximal velocities, V_1 and V_2, of the respective rate equations. The diagram shows the relationship between the interval on which s is defined (top left hand corner) and the parameter search space (lower right hand corner). As an example, following the red line from a value of s to the right, a particular value is obtained for V_2^* which is oscillating at a frequency of $\omega_2 = 5$ between 0 and 1. Moving down the red line to the cumulative density function for V_2, a value is obtained for V_2 in the bottom left hand corner as a function of s. If these values are combined with those of V_1 then the parameter space is obtained in the lower right hand corner.

Flux, J
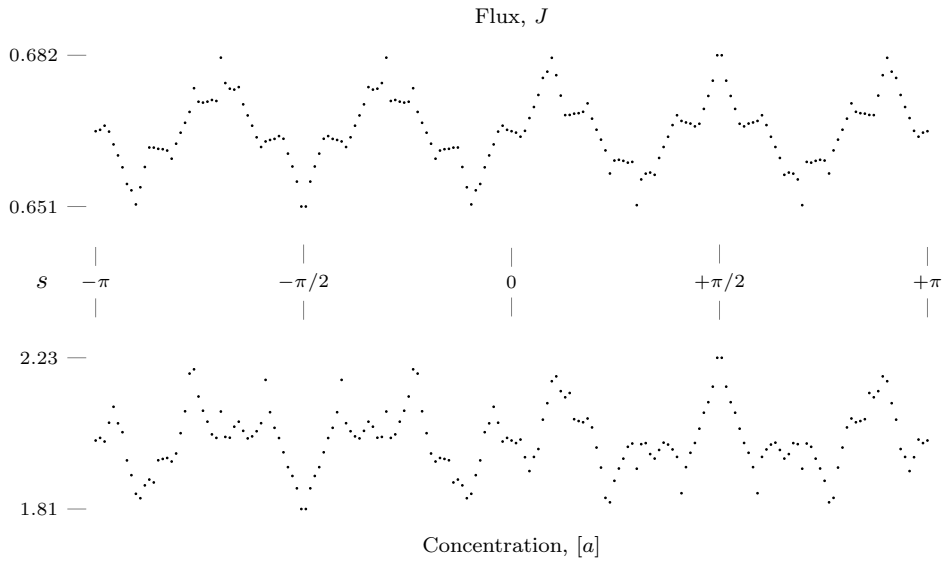
Figure A.2: $f(s)$ plotted against s.
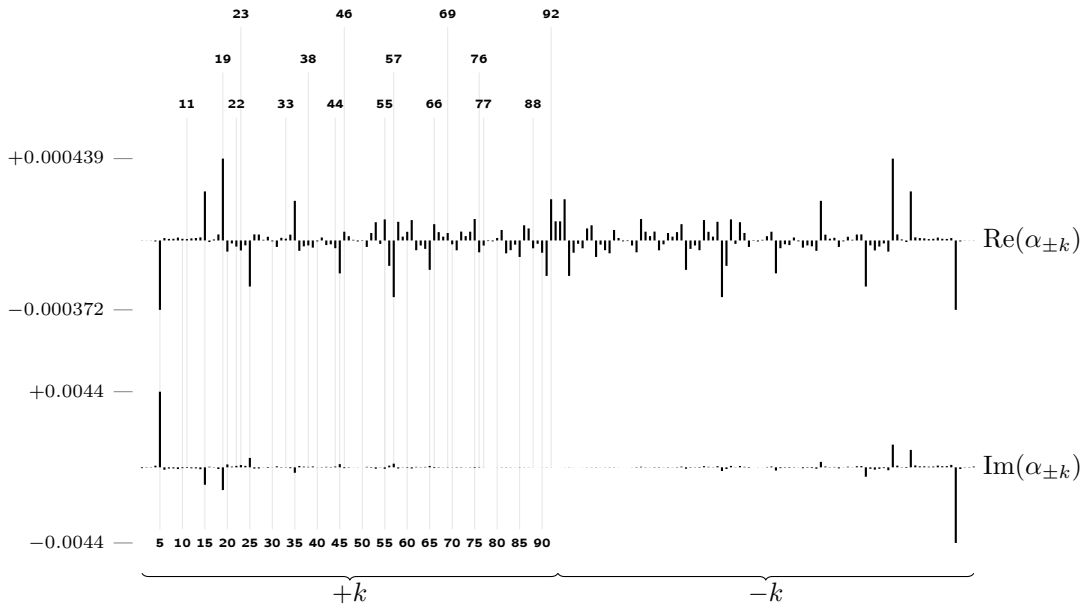
Figure A.3: The Discrete Fourier Transform (DFT) of the steady-state flux. The coefficients have been split into their real and imaginary components. $\pm k$ denotes the positive or negative frequency. The frequencies 5, 11, 19 and 23 and their respective multiples correspond directly to the parameters V_1, V_2, k_x and k_a.
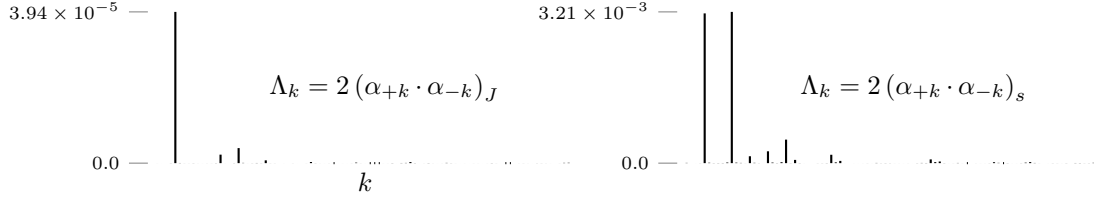
Figure A.4: The Fourier spectrum of $f(s)$.

and $\pm k$ denotes the positive or negative frequency. The Fourier spectrum for the steady-state flux and concentration is shown in Figure A.4. The expected value of the model output is,

$$E(f(s)) = \frac{1}{N} \sum_{i=1}^{N} f(s_i) = \alpha_0, \tag{A.5}$$

in other words the mean value of the output is equal to the zero frequency coefficient and the *total* model variance is,

$$\mathrm{Var}(f(s)) = \frac{1}{N} \sum_{i=1}^{N} (f(s_i) - E(f(s)))^2 = \sum_{k} \Lambda_k. \tag{A.6}$$

The fraction of the total variance of the model that is due to the variance in a particular parameter can then be defined as,

$$D_p = \mathrm{Var}(f(s))(\mathrm{Var}(p)) = \frac{\sum_l \Lambda_{l\omega_p}}{\sum_k \Lambda_k}, \tag{A.7}$$

for $l = 1, 2, ...$ and $l\omega_p \leqslant (N-1)/2$. From this it can be seen that D_p takes on a value between 0 and 1. $l\omega_p$ is an integer and accounts for all the multiples of ω_p—the harmonics of ω_p.

One way of determining the size of N, is to define it to be free of interference up to order M if N satisfies,

$$N = 2M\omega_{max} + 1, \tag{A.8}$$

where M is typically taken to be 4 or 6 and ω_{max} is the largest frequency that has been assigned [74, 134]. This means that there will be little or no interference up to the M-th harmonics for the chosen frequencies. If $M = 4$ and $\omega_{max} = 23$ then $N = 185$. This choice of N allows the search function to take on values of 0 or 1 for certain frequencies. In itself this is not a problem, but it does mean that if a normal distribution is used then $\mathrm{cdf}^{-1}(0) \to -\infty$ and $\mathrm{cdf}^{-1}(1) \to \infty$, which is a problem. The number of runs is therefore incremented by 2. For $N = 187$, sensitivity of $f(s)$ to variations in p and the response coefficients to p are given in Table A.1. The sensitivity indices take on values in the interval, $[0, 1)$. As N becomes larger,

Table A.1: The sensitivity of $f(p)$ to p. Included for comparison in the two right hand columns, are the response coefficients calculated from a metabolic control analysis.

p	D_J	D_a	R_p^J	R_p^a
V_1	0.896	0.447	1.000	3.000
V_2	0.002	0.441	0.000	-2.999
k_x	0.088	0.037	-0.333	-1.000
k_a	0.003	0.066	0.000	1.000

the sum of the sensitivities approach unity [79]. Inspection of Table A.1 will show that the sum of sensitivity indices is marginally less than one. However, as implied above, if N is too large then interference increases.

Cukier *et al.* [74] noted that N can be chosen to be even smaller. If there are n oscillating parameters then the number of model runs required is given by $N \approx 2.6n^{2.5}$ [74]. This approximation is used for the modelling in Chapters 3 and 4.

Sensitivities have a purely statistical interpretation, in other words they lack the clear operational interpretation of response coefficients. If a parameter is allowed to vary in the defined range, then its contribution to the variation in the model output is given by the sensitivity. The parameters are therefore ranked according to their contribution to the model variance.

Biologically, this means that of all the possible factors in a set, such as a group of kinetic parameters, that could possibly affect behaviour, such as homoeostasis, then those with the highest sensitivity indices will have the greatest effect. Another way of interpreting sensitivity indices, modified from Saltelli *et al.* [86], could be as follows. Suppose it is desirable that a certain model output is minimised (or maximised), then the first parameters that should to be changed, for the greatest effect, are the ones with the highest sensitivity index.

The absolute value of the response coefficients can be ranked in the same order as the sensitivities. Intuitively this can be explained by both coefficients quantifying similar effects, i.e. the propagation of a parameter perturbation through to model output. FAST sensitivities do not carry a sign like response coefficients, but a ranking according to absolute value should give the same order. A rigorous mathematical comparison of the two approaches is left for future work.

Appendix B

Comparison of maximal activities

The behaviour of a biochemical reaction kinetic model is sensitive to the choice of maximal activities of the enzymes. Therefore, building a model using parameter values obtained from the literature requires care in the selection of maximal activities. It is not sufficient that a particular value is correct, the whole set of values needs to be internally and mutually consistent.

It is not uncommon to find that two assays of the same enzyme activity give two different results. This is not surprising since enzyme concentration is subject to genetic regulation and is supposed to be able to change. It is for this reason that databases such as BRENDA [114, 115, 135] report catalytic activity values (k_{cat}) instead of maximal activity values that depend on enzyme concentration (V_{max}).

To obtain an accurate picture of all the enzyme profiles at any point in time, the following criteria should be adhered to. Measurements should preferably be made from the same tissue sample, in one laboratory, at the same time and by the same investigators.

Enzyme isoforms are the norm rather than the exception in plants. This complicates matters even further, since the apparent maximal activity of an enzyme is the weighted average of its respective isoforms. This makes it even more important that all the enzymes are measured together.

There are two sets of maximal activity data for sugarcane that come close to satisfying the criteria given above. The first set is published, but is missing SPS [136]. The second set is complete, but is unpublished (Botha, F.C., private communication). This presents somewhat of a conundrum. Uys *et al.* [33] used the first set to model sucrose accumulation, while "borrowing" the value for SPS from the unpublished data. However, it has subsequently emerged that the same model, using all the unpublished data, gives predictions more in line with experiment.

A comparison of the two models is given in Figure B.1. In general, the unpublished activities provide steady-state values that vary over a smaller range across the internodes. In other words, there is a smoother transition from mature to immature internodes. In this work the

unpublished data were used for the sake of internal consistency. The comparison is shown here for completeness.
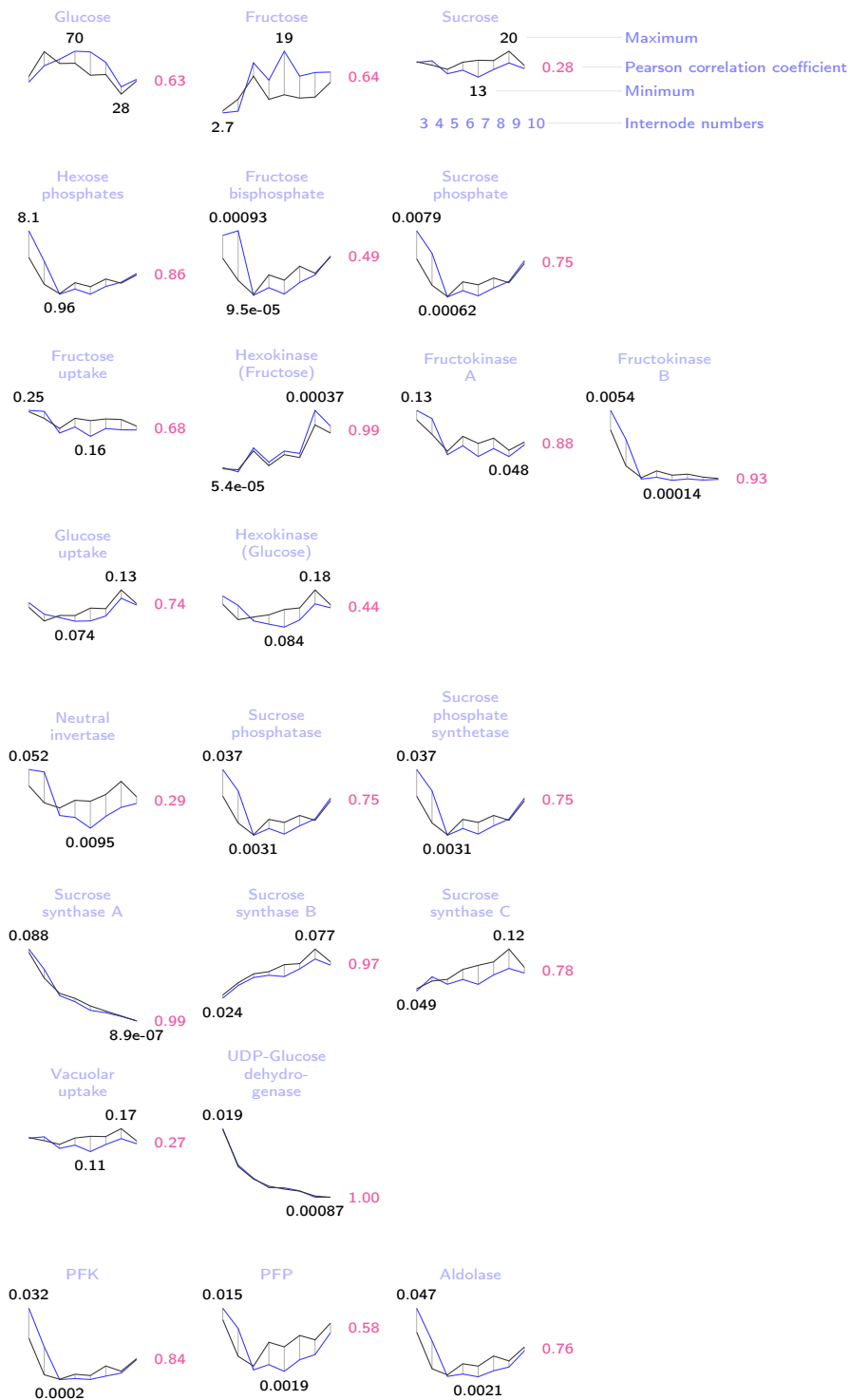
Figure B.1: Comparison of two model runs differing in the choice of maximal activity data sets. The blue lines are the data from [136] as used in [33] and the black lines are unpublished data. Vertical lines indicate internodes 3—10. A key to the values are in the top right hand corner.

Bibliography

[1] Kitano, H.: Computational systems biology. *Nature*, vol. 420, pp. 206–210, 2002.

[2] Palsson, B.O.: *Systems biology — Properties of reconstructed networks.* Cambridge University Press, 2006.

[3] Heinrich, R. & Schuster, S.: *The Regulation of Cellular Systems.* Chapman & Hall, New York, 1996.

[4] Hofmeyr, J.-H.S.: Metabolic control analysis in a nutshell. In: Yi, T.-M., Hucka, M., Morohashi, M. & Kitano, H. (eds.), *Proceedings of the 2nd International Conference on Systems Biology*, pp. 291–300. Omnipress, Madison, WI, USA, 2001.

[5] Fell, D.A.: *Understanding the Control of Metabolism.* Portland Press, London, 1996.

[6] Cornish-Bowden, A.: *Fundamentals of Enzyme Kinetics.* Portland Press, London, 1995.

[7] Hofmeyr, J.H.S. & Westerhoff, H.V.: Building the cellular puzzle - control in multi-level reaction networks. *J. Theor. Biol.*, vol. 208, pp. 261–285, 2001.

[8] Hofmeyr, J.-H.S. & Cornish-Bowden, A.: Regulating the cellular economy of supply and demand. *FEBS Lett.*, vol. 476, pp. 47–51, 2000.

[9] Kacser, H. & Burns, J.A.: The control of flux. *Symp. Soc. Exp. Biol.*, vol. 27, pp. 65–104, 1973.

[10] Heinrich, R. & Rapoport, T.A.: A linear steady-state treatment of enzymatic chains. general properties, control and effector strength. *Eur. J. Biochem.*, vol. 42, pp. 89–95, 1974.

[11] Morgan, J.A. & Rhodes, D.: Mathematical modeling of plant metabolic pathways. *Metab. Eng.*, vol. 4, no. 1, pp. 80–89, 2002.

[12] Rios-Estepa, R. & Lange, B.M.: Experimental and mathematical approaches to modeling plant metabolic networks. *Phytochemistry*, vol. 68, pp. 2351–2374, 2007.

[13] Moore, P.H. & Maretzki, A.: Sugarcane. In: Zamski, E. & Schaffer, A.A. (eds.), *Photoassimilate Distribution in Plants and Crops: Source-Sink Relationships*, pp. 643–669. Marcel Dekker Inc., New York, 1996.

[14] Komor, E.: The physiology of sucrose storage in sugarcane. In: Gupta, A.K. & Kaur, N. (eds.), *Carbohydrate Reserves in Plants - Synthesis and Regulation*, pp. 35–54. Elsevier Science, Amsterdam, 2000.

[15] Komor, E.: Source physiology and assimilate transport: the interaction of sucrose metabolism, starch storage and phloem export in soure leaves and the effect on sugar status in phloem. *Aust. J. Plant. Physiol*, vol. 27, pp. 497–505, 2000.

[16] Van Bel, A.: Strategies of phloem loading. *Annu. Rev. Plant Phys.*, vol. 44, no. 1, pp. 253–281, 1993.

[17] Walsh, K., Sky, R. & Brown, S.: The anatomy of the pathway of sucrose unloading within the sugarcane stalk. *Funct. Plant. Biol.*, vol. 32, pp. 367–374, 2005.

[18] Bull, T. & Glasziou, K.: The evolutionary significance of sugar accumulation in saccharum. *Aust. J. Biol. Sci.*, vol. 16, pp. 737–742, 1963.

[19] Alexander, A.G.: *Sugarcane Physiology*. Elsevier scientific publishing Co. Amsterdam-London-New York, 1973.

[20] van Dillewijn, C.: *Botany of sugarcane*. Waltham Co. Mass. USA, 1952.

[21] Ming, R., Liu, S.C., Moore, P.H., Irvine, J.E. & Paterson, A.H.: QTL analysis in a complex autopolyploid: genetic control of sugar content in sugarcane. *Genome Res.*, vol. 11, no. 12, pp. 2075–84, 2001.

[22] Wendler, R., Veith, R., Dancer, J., Stitt, M. & Komor, E.: Sucrose storage in cell suspension cultures of *Saccharum* sp. (sugarcane) is regulated by a cycle of synthesis and degradation. *Planta*, vol. 183, pp. 31–39, 1990.

[23] Komor, E.: Regulation by futile cycles: the transport of carbon and nitrogen in plants. In: Schulze, E.D. (ed.), *Flux Control in Biological Systems*, pp. 153–201. Academic Press, San Diego, 1994.

[24] Whittaker, A. & Botha, F.C.: Carbon partitioning during sucrose accumulation in sugarcane internodal tissue. *Plant Physiol.*, vol. 115, pp. 1651–1659, 1997.

[25] Zhu, Y.J., Komor, E. & Moore, P.H.: Sucrose accumulation in the sugarcane stem is regulated by the difference between the activities of soluble acid invertase and sucrose phosphate synthase. *Plant Physiol.*, vol. 115, pp. 609–616, 1997.

[26] Rohwer, J.M. & Botha, F.C.: Analysis of sucrose accumulation in the sugar cane culm on the basis of *in vitro* kinetic data. *Biochem. J.*, vol. 358, pp. 437–445, 2001.

[27] Lemoine, R.: Sucrose transporters in plants: update on function and structure. *BBA-Biomembranes*, vol. 1465, no. 1-2, pp. 246–262, 2000.

[28] Rae, A.L., Perroux, J.M. & Grof, C.P.L.: Sucrose partitioning between vascular bundles and storage parenchyma in the sugarcane stem: a potential role for the ShSUT1 sucrose transporter. *Planta*, vol. 220, no. 6, pp. 817–25, 2005.

[29] Reinders, A., Sivitz, A.B., Hsi, A., Grof, C.P.L., Perroux, J.M. & Ward, J.M.: Sugarcane ShSUT1: analysis of sucrose transport activity and inhibition by sucralose. *Plant Cell Environ.*, vol. 29, no. 10, pp. 1871–1880, 2006.

[30] Uys, L.: *Computational systems biology of sucrose accumulation in sugarcane.* Master's thesis, University of Stellenbosch, 2006.

[31] Schäfer, W.E., Rohwer, J.M. & Botha, F.C.: Protein-level expression and localization of sucrose synthase in the sugarcane culm. *Physiol. Plantarum*, vol. 121, pp. 187–195, 2004.

[32] Bosch, S.: *Trehalose and carbon partitioning in sugarcane.* Ph.D. thesis, University of Stellenbosch, 2005.

[33] Uys, L., Botha, F., Hofmeyr, J.-H. & Rohwer, J.: Kinetic model of sucrose accumulation in maturing sugarcane culm tissue. *Phytochemistry*, vol. 68, pp. 2375– 2392, 2007.

[34] Thompson, M.V.: Phloem: the long and the short of it. *Trends Plant Sci.*, vol. 11, no. 1, pp. 26–32, 2006.

[35] Van Bel, A.: The phloem, a miracle of ingenuity. *Plant Cell Environ.*, vol. 26, pp. 125–149, 2003.

[36] van Bel, A.J.E., Ehlers, K. & Knoblauch, M.: Sieve elements caught in the act. *Trends Plant Sci.*, vol. 7, no. 3, pp. 126–132, 2002.

[37] Thompson, M.: Scaling phloem transport: Elasticity and pressure-concentration waves. *J. Theor. Biol.*, vol. 236, pp. 229–241, 2005.

[38] Bieleski, R.: The bigger picture - phloem seen through horticultural eyes. *Aust. J. Plant Physiol.*, vol. 27, pp. 615–624, 2000.

[39] Münch, E.: Über Dynamik der Saftströmungen. *Ber. Deut. Bot. Ges.*, vol. 44, pp. 68–71, 1926.

[40] Münch, E.: Versuche über den Saftkreislauf. *Ber. Deut. Bot. Ges.*, vol. 45, pp. 340–356, 1927.

[41] Münch, E.: *Die Stoffbewegungen in der Pflanze.*, vol. 45. Jena: Gustav Fischer, 1930.

[42] Daudet, F., Lacointe, A., Gaudillére, J.P. & Cruiziat, P.: Generalized münch coupling between sugar and water fluxes for modelling carbon allocation as affected by water status. *J. Theor. Biol.*, vol. 214, pp. 481–498, 2002.

[43] Lampinen, M.J. & Noponen, T.: Thermodynamic analysis of the interaction of the xylem water and phloem sugar solution and its significance for the cohesion theory. *J. Theor. Biol.*, vol. 224, no. 3, pp. 285–298, 2003.

[44] Hölttä, T., Vesala, T., Sevanto, S., Perämäki, M. & Nikinmaa, E.: Modeling xylem and phloem water flows in trees according to cohesion theory and münch hypothesis. *Trees-Struct. Funct.*, vol. 20, no. 1, pp. 67–78, 2006.

[45] Gould, N., Thorpe, M.R., Koroleva, O. & Minchin, P.E.H.: Phloem hydrostatic pressure relates to solute loading rate: a direct test of the Münch hypothesis. *Funct. Plant Biol.*, vol. 32, pp. 1019–1026, 2005.

[46] Thompson, M. & Holbrook, N.: Application of a single-solute non-steady-state phloem model to the study of long distance assimilate transport. *J. Theor. Biol.*, vol. 220, pp. 419–455, 2003.

[47] Thompson, M. & Holbrook, N.: Scaling phloem transport: water potential equilibrium and osmoregulatory flow. *Plant Cell Environ.*, vol. 26, pp. 1561–1577, 2003.

[48] Henton, S., Greaves, A., Piller, G. & Minchin, P.: Revisiting the münch pressure-flow hypothesis for long-distance transport of carbohydrates: modelling the dynamics of solute transport inside a semipermeable tube. *J. Exp. Bot.*, vol. 53, no. 373, pp. 1411–1419, 2002.

[49] Thompson, M. & Holbrook, N.: Scaling phloem transport: information transmission. *Plant Cell Environ.*, vol. 27, pp. 509–519, 2004.

[50] Beek, W., Mutzall, K. & van Heuven, J.: *Transport Phenomena.* John Wiley & sons, Ltd., 1999.

[51] Bear, J.: *Dynamics of fluids in porous media.* Elsevier, 1972.

[52] Atkins, P. & de Paulo, J.: *Atkins' Physical Chemistry.* Oxford University Press, 2002.

[53] Hofmeyr, J.-H.S. & Cornish-Bowden, A.: The reversible Hill equation: how to incorporate cooperative enzymes into metabolic models. *Comp. Appl. Biosci.*, vol. 13, pp. 377–385, 1997.

[54] Hanekom, A.J.: *Generic kinetic equations for modelling multisubstrate reactions in computational systems biology.* Master's thesis, Stellenbosch University, 2006.

[55] Rohwer, J.M., Hanekom, A.J. & Hofmeyr, J.-H.S.: A universal rate equation for systems biology. In: Hicks, M.G. & Kettner, C. (eds.), *Experimental Standard Conditions of Enzyme Characterizations. Proceedings of the 2nd International Beilstein Workshop*, pp. 175–187. Beilstein-Institut zur FÃűrderung der Chemischen Wissenschaften, Frankfurt, 2007.

[56] Lacointe, A. & Minchin, P.E.H.: Modelling phloem and xylem transport within a complex architecture. *Funct. Plant Biol.*, vol. 35, pp. 772–780, 2008.

[57] Quereix, A., Dewar, R.C., Gaudillere, J.-P., Dayau, S. & Valancogne, C.: Sink feedback regulation of photosynthesis in vines: measurements and a model. *J. Exp. Bot.*, vol. 52, no. 365, pp. 2313–2322, 2001.

[58] Wheeler, D., Guyer, J.E. & Warren, J.A.: *FiPy: User's Guide.* Metallurgy Division and the Center for Theoretical and Computational Materials Science, Materials Science and Engineering Laboratory, NIST, 1st edn.

[59] Guyer, J.E., Wheeler, D. & Warren, J.A.: Fipy: Partial differential equations with python. *Comput. Sci. Eng.*, vol. 11, pp. 6–15, 2009.

[60] McCormick, A.J., Cramer, M.D. & Watt, D.A.: Sink strength regulates photosynthesis in sugarcane. *New Phytol.*, vol. 171, no. 4, pp. 759–770, 2006.

[61] McCormick, A.J., Cramer, M.D. & Watt, D.A.: Changes in photosynthetic rates and gene expression of leaves during a source-sink perturbation in sugarcane. *Ann. Bot.*, vol. 101, pp. 89–102, 2008.

[62] Michel, B.: Solute potential of sucrose solutions. *Plant. Physiol*, vol. 50, pp. 196–198, 1972.

[63] Botha, C. & Van Bel, A.: Quantification of symplastic continuity as visualised by plasmodesmograms: diagnostic value for phloem-loading pathways. *Planta*, vol. 187, pp. 359–366, 1992.

[64] Hofmeyr, J.-H.S. & Cornish-Bowden, A.: Quantitative assessment of regulation in metabolic systems. *Eur. J. Biochem.*, vol. 200, pp. 223–236, 1991.

[65] Beevers, H.: Metabolic compartmentation in plant cells. In: Huang, A.H.C. & Taiz, L. (eds.), *Molecular Approaches to Compartmentation and Metabolic Regulation.* The American Society of Plant Physiologists, 1991.

[66] Kruger, N.J., Le Lay, P. & Ratcliffe, R.G.: Vacuolar compartmentation complicates the steady-state analysis of glucose metabolism and forces reappraisal of sucrose cycling in plants. *Phytochemistry*, vol. 68, 2007.

[67] Rae, A., Grof, C., Casu, R. & Bonnett, G.: Sucrose accumulation in the sugarcane stem: pathways and control points for transport and compartmentation. *Field Crop. Res.*, vol. 92, pp. 159–168, 2005.

[68] Welbaum, G. & Meinzer, F.: Compartmentation of solutes and water in developing sugarcane stalk in tissue. *Plant Physiol.*, vol. 93, pp. 1147–1153, 1990.

[69] Dancer, J., Veith, R., Feil, R., Komor, E. & Stitt, M.: Independent changes of inorganic pyrophosphate and the ATP/ADP or UTP/UDP ratios in plant cell suspension cultures. *Plant Sci.*, vol. 66, pp. 59–63, 1990.

[70] Cloutier, M., Chen, J., Tatge, F., McMurray-Beaulieu, V., Perrier, M. & Jolicoeur, M.: Kinetic metabolic modelling for the control of plant cells cytoplasmic phosphate. *J. Theor. Biol.*, vol. 259, no. 1, pp. 118 – 131, 2009.

[71] Bindon, K. & Botha, F.: Carbon allocation to the insoluble fraction, respiration and triose-phosphate cycling in the sugarcane culm. *Physiol. Plant.*, vol. 116, pp. 12–19, 2002.

[72] Moore, P.H.: Temporal and spatial regulation of sucrose accumulation in the sugarcane. *Aust. J. Plant Physiol.*, vol. 22, pp. 661–679, 1995.

[73] Thom, M. & Komor, E.: Electrogenic proton translocation by the ATPase of sugarcane vacuoles. *Plant Physiol.*, vol. 77, pp. 329–334, 1985.

[74] Cukier, R.I., Fortuin, C.M., Shuler, K.E., Petschek, A.G. & Schaibly, J.H.: Study of the sensitivity of coupled reaction systems to uncertainties in rate coefficients. I theory. *J. Chem. Phys.*, vol. 59, no. 8, pp. 3873–3878, 1973.

[75] Cukier, R.I., Schaibly, J.H. & Shuler, K.E.: Study of the sensitivity of coupled reaction systems to uncertainties in rate coefficients. III. analysis of the approximations. *J. Chem. Phys.*, vol. 63, no. 3, pp. 1140–1149, 1975.

[76] Cukier, R.I., Levine, H.B. & Shuler, K.E.: Nonlinear sensitivity analysis of multiparameter model systems. *J. Comput. Phys.*, vol. 26, no. 1, pp. 1–42, 1978.

[77] Schaibly, J.H. & Shuler, K.E.: Study of the sensitivity of coupled reaction systems to uncertainties in rate coefficients. II applications. *J. Chem. Phys.*, vol. 59, no. 8, pp. 3879–3888, 1973.

[78] Fang, S., Gertner, G.Z., Shinkareva, S., Wang, G. & Anderson, A.: Improved generalized Fourier amplitude sensitivity test (FAST) for model assessment. *Stat. Comput.*, vol. 13, no. 3, pp. 221–226, 2003.

[79] Saltelli, A. & Bolado, R.: An alternative way to compute Fourier amplitude sensitivity test (fast). *Comput. Stat. Data An.*, vol. 26, no. 4, pp. 445–460, 1998.

[80] Xu, C. & Gertner, G.Z.: Extending a global sensitivity analysis technique to models with correlated parameters. *Comput. Stat. Data An.*, vol. 51, pp. 5579–5590, 2007.

[81] Xu, C. & Gertner, G.Z.: A general first-order global sensitivity analysis method. *Reliab. Eng. Syst. Saf.*, vol. 93, pp. 1060–1071, 2007.

[82] Koda, M., Dogru, A.H. & Seinfeld, J.H.: Sensitivity analysis of partial differential equations with application to reaction and diffusion processes. *J. Comput. Phys.*, vol. 30, no. 2, pp. 259–282, 1979.

[83] Koda, M., Mcrae, G.J. & Seinfeld, J.H.: Automatic sensitivity analysis of kinetic mechanisms. *Int. J. Chem. Kinet.*, vol. 11, no. 4, pp. 427–444, 1979.

[84] Marino, S., Hogue, I.B., Ray, C.J. & Kirschner, D.E.: A methodology for performing global uncertainty and sensitivity analysis in systems biology. *J. Theor. Biol.*, vol. 254, no. 1, pp. 178–196, 2008.

[85] Saltelli, A., Tarantola, S. & Campolongo, F.: Sensitivity anaysis as an ingredient of modeling. *Stat. Sci.*, vol. 15, no. 4, pp. 377–395, 2000.

[86] Saltelli, A., Ratto, M., Tarantola, S. & Campolongo, F.: Sensitivity analysis for chemical models. *Chem. Rev.*, vol. 105, pp. 2811–2828, 2005.

[87] Zádor, J., Zsély, I. & Turányi, T.: Local and global uncertainty analysis of complex chemical kinetic systems. *Reliab. Eng. Syst. Saf.*, vol. 91, no. 10-11, pp. 1232–1240, 2006.

[88] Hanekom, A.J., Hofmeyr, J.-H.S., Snoep, J.L. & Rohwer, J.M.: Experimental evidence for allosteric modifier saturation as predicted by the bi-substrate hill equation. *IEE Proc.-Syst. Biol.*, vol. 153, no. 5, pp. 342–345, 2006.

[89] Rohwer, J.M., Hanekom, A.J., Crous, C., Snoep, J.L. & Hofmeyr, J.-H.S.: Evaluation of a simplified generic bi-substrate rate equation for computational systems biology. *IEE Proc.-Syst. Biol.*, vol. 153, pp. 338—341, 2006.

[90] Braun, D.M. & Slewinski, T.L.: Genetic control of carbon partitioning in grasses: Roles of sucrose transporters and tie-dyed loci in phloem loading. *Plant Physiol.*, vol. 149, no. 1, pp. 71–81, 2009.

[91] Wu, L. & Birch, R.G.: Doubled sugar content in sugarcane plants modified to produce a sucrose isomer. *Plant Biotechnol. J.*, vol. 5, pp. 109–117, 2007.

[92] Plewa, T., Linde, T. & Weirs, V.G. (eds.): *Adaptive Mesh Refinement - Theory and Applications*, vol. 41 of *Lecture Notes in Computational Science and Engineering*. Springer, 2003.

[93] Artschwager, E.: Anatomy of the vegetative organs of sugarcane. *J. Agric. Res.*, vol. 30, pp. 197–230, 1925.

[94] Alberty, R.A.: Calculation of standard transformed Gibbs energies and standard transformed enthalpies of biochemical reactants. *Arch. Biochem. Biophys.*, vol. 353, pp. 116–130, 1998.

[95] Alberty, R.A.: Thermodynamic properties of oxidoreductase, transferase, hydrolase, and ligase reactions. *Arch. Biochem. Biophys.*, vol. 435, pp. 363–368, 2005.

[96] Cardini, C.E., Leloir, L.F. & Chiriboga, J.: The biosynthesis of sucrose. *J. Biol. Chem.*, vol. 214, no. 1, pp. 149–155, 1955.

[97] Avigad, G.: Sucrose-uridine diphosphate glucosyltransferase from Jerusalem artichoke tubers. *J. Biol. Chem.*, vol. 239, no. 11, pp. 3613–3618, 1964.

[98] Delmer, D.P.: The purification and properties of sucrose synthetase from etiolated phaseolus aureus seedlings. *J. Biol. Chem.*, vol. 247, no. 12, pp. 3822–3828, 1972.

[99] Morell, M. & Copeland, L.: Sucrose synthase of soybean nodules. *Plant Physiol.*, vol. 78, no. 1, pp. 149–154, 1985.

[100] Schäfer, W.E., Rohwer, J.M. & Botha, F.C.: A kinetic study of sugarcane sucrose synthase. *Eur. J. Biochem.*, vol. 271, pp. 3971–3977, 2004.

[101] Huber, S.C. & Huber, J.L.: Role and regulation of sucrose-phosphate synthase in higher plants. *Annu. Rev. Plant Phys.*, vol. 47, pp. 431–444, 1996.

[102] Hoepfner, S.W. & Botha, F.C.: Expression of fructokinase isoforms in the sugarcane culm. *Plant Physiol. Biochem.*, vol. 41, pp. 741–747, 2003.

[103] Turner, W. & Botha, F.C.: Purification and kinetic properties of UDP-glucose dehydrogenase from sugarcane. *Arch. Biochem. Biophys.*, vol. 407, no. 2, pp. 209–16, 2002.

[104] Veech, R., Raijman, L., Dalziel, K. & Krebs, H.: *Biochem J.*, vol. 115, p. 837, 1969.

[105] Alberty, R.A.: *Thermodynamics of Biochemical Reactions*. Wiley-Interscience, 2003.

[106] Alberty, R.A. & Cornish-Bowden, A.: The pH dependence of the apparent equilibrium constant, K', of a biochemical reaction. *Trends Biochem. Sci.*, vol. 18, pp. 288–291, 1993.

[107] Goldberg, R., Tewari, Y. & Bhat, T.: Thermodynamics of enzyme-catalyzed reactions - a database for quantitative biochemistry. *Bioinformatics*, vol. 20, pp. 2874—2877, 2004.

[108] Dèjardin, A., Rochat, C., Maugenest, S. & Boutin, J.P.: Purification, characterization and physiological role of sucrose synthase in the pea seed coat (*Pisum sativum L.*). *Planta*, vol. 201, no. 2, pp. 128–137, 1997.

[109] Guynn, R.W., Veloso, D., Lawson, J.W.R. & Veech, R.L.: The concentration and control of cytoplasmic free inorganic pyrophosphate in rat liver in vivo. *Biochem. J.*, vol. 140, pp. 369–375, 1974.

[110] Titus, C.: *Sucrose transporters and sucrose uptake mechanisms in sugarcane*. Master's thesis, University of Stellenbosch, 2005.

[111] Botha, F.C. & Black, K.G.: Sucrose phosphate synthase and sucrose synthase activity during maturation of internodal tissue in sugarcane. *Aust. J. Plant Physiol.*, vol. 27, pp. 81–85, 2000.

[112] Schäfer, W.E., Rohwer, J.M. & Botha, F.C.: Partial purification and characterisation of sucrose synthase in sugarcane. *J. Plant Physiol.*, vol. 162, pp. 11–20, 2005.

[113] Hoepfner, S.W. & Botha, F.C.: Purification and characterisation of fructokinase from the culm of sugarcane. *Plant Sci.*, vol. 167, pp. 645–654, 2004.

[114] Schomburg, I., Chang, A., Hofmann, O., Ebeling, C., Ehrentreich, F. & Schomburg, D.: BRENDA: a resource for enzyme data and metabolic information. *Trends Biochem. Sci.*, vol. 27, no. 1, pp. 54–6, 2002.

[115] Schomburg, I., Chang, A. & Schomburg, D.: BRENDA, enzyme data and metabolic information. *Nucleic Acids Res.*, vol. 30, no. 1, pp. 47–9, 2002.

[116] Valli, A.M.P., Carey, G.F. & Coutinho, A.L.G.A.: Control strategies for timestep selection in finite element simulation of incompressible flows and coupled reaction-convection-diffusion processes. *Int. J. Numer. Meth. Fluids*, vol. 47, pp. 201–231, 2005.

[117] Altet, F., Vilata, I., Prater, S., Mas, V., Hedley, T., Valentino, A. & Whitaker, J.: *PyTables User's Guide.* Cárabos Coop. V., 2007.

[118] Heroux, M.A., Bartlett, R.A., Howle, V.E., Hoekstra, R.J., Hu, J.J., Kolda, T.G., Lehoucq, R.B., Long, K.R., Pawlowski, R.P., Phipps, E.T., Salinger, A.G., Thornquist, H.K., Tuminaro, R.S., Willenbring, J.M., Williams, A. & Stanley, K.S.: An overview of the Trilinos project. *ACM Trans. Math. Softw.*, vol. 31, no. 3, pp. 397–423, 2005.

[119] Heroux, M., Bartlett, R., Hoekstra, V.H.R., Hu, J., Kolda, T., Lehoucq, R., Long, K., Pawlowski, R., Phipps, E., Salinger, A., Thornquist, H., Tuminaro, R., Willenbring, J. & Williams, A.: An Overview of Trilinos. Tech. Rep. SAND2003-2927, Sandia National Laboratories, 2003.

[120] Morris, M.D.: Factorial sampling plans for preliminary computational experiments. *Technometrics*, vol. 33, pp. 161—174, 1991.

[121] Storn, R. & Price, K.: Differential evolution - a simple and efficient heuristic for global optimization over continuous spaces. *J. Global. Optim.*, vol. 11, pp. 341–359, 1997.

[122] Allen, M.T., Prusinkiewicz, P. & DeJong, T.M.: Using L-systems for modeling source-sink interactions, architecture and physiology of growing trees: the L-PEACH model. *New Phytol.*, vol. 166, pp. 869–880, 2005.

[123] Mündermann, L., Erasmus, Y., Lane, B., Coen, E. & Prusinkiewicz, P.: Quantitative modeling of arabidopsis development. *Plant Physiol.*, vol. 139, pp. 960—968, 2005.

[124] Prusinkiewicz, P., Allen, M., Escobar-Gutiérrez, A. & Dejong, T.: *Numerical methods for transport-resistance source-sink allocation models*, chap. 11, pp. 123—137. Springer, 2007.

[125] Génard, M., Dauzat, J., Franck, N., Lescourret, F., Moitrier, N., Vaast, P. & Vercambre, G.: Carbon allocation in fruit trees: from theory to modelling. *Trees-Struct. Funct.*, vol. 22, no. 3, pp. 269–282, 2008.

[126] Ward, J.P., King, J., Koerber, A.J., Williams, P., Croft, J.M. & Sockett, R.E.: Mathematical modelling of quorum sensing in bacteria. *Math. Med. Biol.*, vol. 18, no. 3, pp. 263–292, 2001.

[127] Dockery, J. & Keener, J.: A mathematical model for quorum sensing in *Pseudomonas aeruginosa*. *Bull. Math. Biol.*, vol. 63, no. 1, pp. 95–116, 2001.

[128] Duddu, R., Chopp, D.L. & Moran, B.: A two-dimensional continuum model of biofilm growth incorporating fluid flow and shear stress based detachment. *Biotechnol. Bioeng.*, vol. 103, no. 1, pp. 92–104, 2009.

[129] Janakiraman, V., Englert, D., Jayaraman, A. & Baskaran, H.: Modeling growth and quorum sensing in biofilms grown in microfluidic chambers. *Ann. Biomed. Eng.*, vol. 37, no. 6, pp. 1206–1216, 2009.

[130] Hunter, P.J. & Borg, T.K.: Integration from proteins to organs: The physiome project. *Nature*, vol. 4, pp. 237—243, 2003.

[131] Coletti, F., Macchietto, S. & Elvassore, N.: Mathematical modeling of three-dimensional cell cultures in perfusion bioreactors. *Ind. Eng. Chem. Res.*, vol. 45, no. 24, pp. 8158–8169, 2006.

[132] Stitt, M.: Fructose-2,6-bisphosphate as a regulatory molecule in plants. *Annu. Rev. Plant Phys.*, vol. 41, pp. 153–185, 1990.

[133] Höfer, T. & Heinrich, R.: A second-order approach to metabolic control analysis. *J. Theor. Biol.*, vol. 164, pp. 85–102, 1993.

[134] Saltelli, A., Tarantola, S. & Chan, K.-S.: A quantitative model-independent method for global sensitivity analysis of model output.(statistical data included). *Technometrics*, vol. 41, no. 1, pp. 39–, 1999.

[135] Schomburg, I., Chang, A., Ebeling, C., Gremse, M., Heldt, C., Huhn, G. & Schomburg, D.: BRENDA, the enzyme database: updates and major new developments. *Nucleic Acids Res.*, vol. 32, no. Database issue, pp. D431–3, 2004.

[136] Botha, F.C., Whittaker, A., Vorster, D.J. & Black, K.G.: Sucrose accumulation rate, carbon partitioning and expression of key enzyme activities in sugarcane stem tissue. In: Wilson, J.R., Hogarth, D.M., Campbell, J.A. & Garside, A.L. (eds.), *Sugarcane: Research Towards Efficient and Sustainable Production*, pp. 98–101. CSIRO division of Tropical Crops and Pastures, Brisbane, 1996.